LBNL-45463

RECENT RESEARCH ON INDOOR AIR QUALITY: A COMPILATION IN MEMORY OF JOAN DAISEY

Indoor Environment Department
Lawrence Berkeley National Laboratory
Berkeley, CA 94720

Papers Presented at Indoor Air 99
Edinburgh, Scotland
August 1999

PREFACE

This compilation of papers was initiated by Joan Daisey as a broad overview of the indoor air research being conducted at Lawrence Berkeley National Lab. We have completed this report as a tribute to Joan's 13 year leadership of the Indoor Environment Department and to her vision for the department and its research.

Rich Sextro, April 2000

OVERVIEW

This LBNL report is a compilation of the 24 papers presented by Indoor Environment Department researchers and our collaborators at other institutions at the 8th International Conference on Indoor Air Quality & Climate (Indoor Air '99), held in Edinburgh, Scotland, August 8-13, 1999. These papers represent a cross-section of a substantial part of the ongoing research in the department. For information on other recent publications, please see our web site at http://eetd.lbl.gov/IEP/IEP.html.

Joan M. Daisey, Head
Indoor Environment Department

Acknowledgements

The authors thank all of the reviewers of these papers for their helpful comments and suggestions. We also thank the sponsors of the research represented in these papers:

California Environmental Protection Agency, Office of Environmental Health Hazard Assessments

California Tobacco-Related Disease Research Program

National Heart Lung and Blood Institute, Public Health Service, Department of Health and Human Services

U.S. Department of Energy, Office of Energy Efficiency and Renewable Energy, Office of Building Technology, State and Community Programs

U.S. Department of Energy, Chemical and Biological Nonproliferation Program, Office of Research and Development, Office of Nonproliferation and National Security

U.S. Environmental Protection Agency, National Exposure Research Laboratory

Table of Contents

The volume and page number for each paper in the IA'99 Conference Proceedings is provided in parenthesis (volume: first page). The citation for the proceedings is *Indoor Air 99*, G. Raw, C. Aizlewood, P. Warren, eds., Construction Research Communications, London 1999.

I. VOLATILE ORGANIC COMPOUNDS: EMISSIONS AND CONTROLS

CONCENTRATIONS AND SOURCES OF FORMALDEHYDE AND VOLATILE ORGANIC COMPOUNDS IN FOUR NEW MANUFACTURED HOUSES

A.T. Hodgson[1], D. Beal[2] and S. Chandra[2]

[1]E.O. Lawrence Berkeley National Laboratory, USA
[2]Florida Solar Energy Center, USA

ABSTRACT

The concentrations of formaldehyde, individual volatile organic compounds (VOCs) and total VOCs (TVOC) were measured in four new manufactured houses on three occasions over nine months following construction. Ventilation rates were also measured. A mass-balance model was used to calculate area-specific emission rates of the target analytes. Formaldehyde concentrations were all less than a guideline value of 50 ppb. One-half of the 58 target VOCs had median concentrations at or below 1 ppb. The most abundant VOCs were terpene hydrocarbons, ethylene glycol, hexanal, 2-butanone and acetic acid. Concentrations of hexanal, other aldehydes and acetic acid often exceeded their odor thresholds. The median TVOC concentration was 1.6 mg m^{-3}. In general, there were no large decreases in the emission rates of individual VOCs or TVOC over the course of the study. The data suggested that wood products were a dominant source of VOCs in all houses.

INTRODUCTION

Indoor sources of volatile organic compounds (VOCs) and building ventilation are important determinants of indoor air quality (IAQ) in houses. Many materials used to construct and finish houses emit VOCs and some emit formaldehyde. The trend in new house construction is to make building envelopes tighter. Consequently, ventilation rates are often relatively low. Elevated sources of indoor contaminants in combination with low ventilation rates create a potential for degraded IAQ that may affect occupant health and comfort. Prior to this study, there were no published VOC data for contemporary manufactured houses in the USA.

The objectives of the study were to: 1) quantify concentrations of total VOCs (TVOC), individual VOCs, and formaldehyde in four new manufactured houses over nine months following construction; 2) compare the concentrations to typical values and to odor thresholds; 3) document temporal changes in emission rates; and 4) evaluate the effectiveness of several ventilation and source modifications for reducing concentrations of VOCs.

METHODS

The four, two-section houses were constructed at a single manufacturing plant in Florida, USA. They were produced and set up at an adjacent model center during July and August 1997. All houses were equipped with a heating, ventilating and air conditioning (HVAC) system and a central occupant-controlled exhaust fan. The HVAC systems were operated daily. One of the houses had supplemental mechanical ventilation. Material substitutions were made in several of the houses either during the manufacturing or set up phases. The houses were decorated and fully furnished, but unoccupied. Air samples for the analysis of VOCs and formaldehyde were obtained in September and November 1997 and May 1998.

On each occasion, the samples were collected at a central location in each house and at a nearby outdoor location. Formaldehyde samples were collected on cartridges treated with 2,4-dinitrophenylhydrazine. Samples for TVOC and VOCs were collected on Tenax®-TA sorbent tubes. Ventilation rates were measured concurrently with the collection of air samples by tracer-gas decay using sulfur hexafluoride as the tracer gas.

Formaldehyde samples were analyzed by high-performance liquid chromatography following U.S. EPA Method TO-11. Sorbent tubes were analyzed for TVOC and individual VOCs by thermal desorption gas chromatography/mass spectrometry (GC/MS) using a modification of U.S. EPA Method TO-1. For the analysis of TVOC, a GC/MS total-ion-current chromatogram was integrated over a retention-time range bounded by n-heptane and n-heptadecane. The area response was calibrated with a mixture of ten common alkane and aromatic hydrocarbons. 58 target VOCs were selected for analysis. Some of the compounds are indicative of specific indoor sources. Others have low odor thresholds or are strong sensory irritants. 42 of the compounds are among the 63 target VOCs recommended to be included in an analysis of TVOC [1]. The concentration data for the target VOCs were also summarized as ΣVOC (*i.e.*, the sum of the individually measured VOC concentrations).

A steady-state mass-balance model was used to calculate area-specific emission rates with indoor and outdoor concentrations, ventilation rates and house volumes and areas as inputs.

RESULTS

The house specifications are given in Table 1. House M2 had supplemental mechanical ventilation provided by an outside air duct connected to the HVAC return duct and operated intermittently by a FanRecycler™ control device [2]. Low-VOC paints were used in House M2, and a low-emitting carpet assembly was installed in Houses M2 and M4.

Table 1. Specifications for the four houses.

Parameter	M1	M2	M3	M4
Floor area, m^2	112	169	141	131
Volume, m^3	273	412	344	320
Supplemental vent.	No	Yes	No	No
Ventilation rate, h^{-1}	0.57 - 0.78	0.53 - 0.71	0.35 - 0.36	0.35 - 0.50
Carpet area, m^2	72	128	94	96
Sheet vinyl area, m^2	0	29	29	21
Low-VOC paint	No	Yes	No	No
Low emitting carpet	No	Yes	No	Yes

The concentrations of TVOC and ΣVOC in the four houses are shown in Figures 1 and 2, respectively. TVOC concentrations ranged from 0.81-3.0 mg m^{-3} with a median value of 1.6 mg m^{-3}. TVOC concentrations in Houses M2 and M4 were relatively constant over time. For House M3 only, there was a substantial decrease in TVOC concentration from the 1st to the 2nd sampling period. For House M1, the TVOC concentration in the final sampling period was distinctly lower than concentrations in the 1st and 2nd periods. ΣVOC concentrations ranged from 44-100% of the TVOC concentrations. Typically, the individual VOCs accounted for ~70% of the TVOC values. The median ΣVOC concentration was 1.2 mg m^{-3}.

Five target VOCs, n-propylbenzene, isopropyl acetate, trichloroethene, tetrachoroethene and 1,4-dichlorobenzene, were not detected. 14 target VOCs had concentrations that were consistently at or below 1 ppb in all houses and sampling periods. These were benzene,

ethylbenzene, 1,3,5-trimethylbenzene, naphthalene, 4-phenylcyclohexene, n-pentadecane, n-hexadecane, propylcyclohexane, butylated hydroxytoluene, methyl isobutyl ketone, 1-phenylethanone, ethyl acetate, butyl acetate, and benzothiazole. About one-half of the target VOCs had median concentrations at or below 1 ppb. The concentrations (ppb) of 23 selected VOCs are listed in Table 2. These were either the dominant or most odorous compounds. The uncertainty for sampling and analysis of most VOCs was about 10% relative standard deviation. The relative uncertainty for the glycol ethers and acetic acid was 35% or more. Seven VOCs were among the most-abundant compounds in all four houses. These were α-pinene, β-pinene, 3-carene, ethylene glycol, hexanal, 2-butanone, and acetic acid. Acetic acid was the dominant compound.

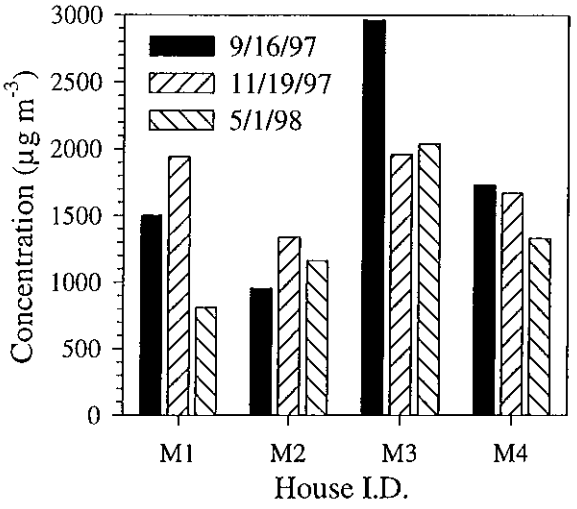

Figure 1. TVOC concentrations.

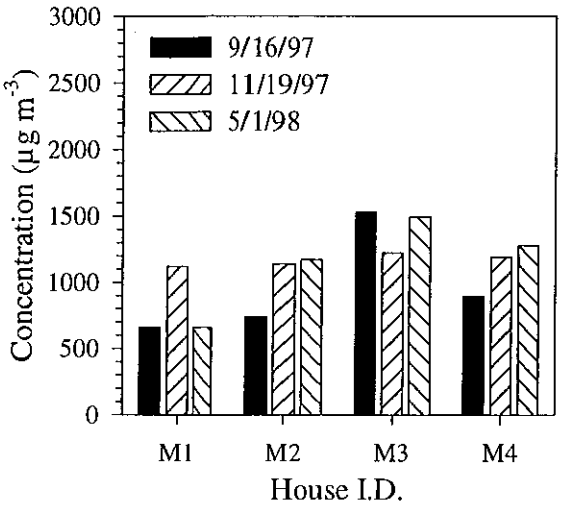

Figure 2. ΣVOC concentrations.

The formaldehyde concentrations are shown in Figure 3. The median formaldehyde concentration was 37 ppb, and all concentrations were less than 50 ppb.

The ranges of ventilation rates measured in the houses are shown in Table 1. Houses M1 and M2 had the highest ventilation rates, while House M3 had consistently lower rates. All of the values meet or exceeded the ASHRAE minimum ventilation standard of 0.35 h^{-1}.

The area-specific emission rates of TVOC are shown in Figure 4. The median TVOC emission rate was 1.6 mg m^{-2} h^{-1}. There was no obvious trend of TVOC (or ΣVOC) emission rates decreasing with time throughout the study. However, for Houses M1, M3 and M4, the TVOC emission rate in the final sampling period was less than the emission rate in the 1st sampling period. The TVOC emission rate in House M2 was constant over time. In the final sampling period, acetic acid accounted for 44-56% of the ΣVOC (mg m^{-2} h^{-1}) emission rates in the four houses.

There was also no general trend in the temporal profiles of the area-specific emission rates of the target VOCs. Among the dominant VOCs reported in Table 2, the emission rates of only n-decane, n-undecane, α-pinene, and 2-butanone decreased from the 1st to the final sampling period in all four houses. On the other hand, the emission rates of 1-octanol, 2-butoxyethanol, nonanal and acetic acid increased from the 1st to the final sampling period in all houses. The acetic acid emission rate increased by a factor of two to ten.

Table 2. Concentrations (ppb) of selected individual VOCs in the four houses on three sampling dates.

Compound	Chemical Class	M1 9/97	M1 11/97	M1 5/98	M2 9/97	M2 11/97	M2 5/98	M3 9/97	M3 11/97	M3 5/98	M4 9/97	M4 11/97	M4 5/98	Med.* Conc.
Toluene	AromaticHC	2	3	1	6	3	2	4	2	2	3	3	2	2
n-Decane	AlkaneHC	16	14	1	1	1	<1	8	4	2	2	1	1	1
n-Undecane	AlkaneHC	7	7	2	<1	<1	<1	3	2	1	1	1	<1	1
n-Dodecane	AlkaneHC	1	1	1	2	3	2	10	8	6	5	4	3	3
n-Tridecane	AlkaneHC	1	1	1	6	7	6	21	17	12	12	10	7	7
n-Tetradecane	AlkaneHC	1	1	1	4	4	5	13	10	11	6	6	5	5
α-Pinene	TerpeneHC	13	19	5	9	31	10	35	32	15	23	25	9	17
β-Pinene	TerpeneHC	3	6	2	2	7	3	11	8	5	7	6	3	5
3-Carene	TerpeneHC	3	6	2	1	5	2	15	11	7	9	10	4	5
d-Limonene	TerpeneHC	2	3	1	1	3	2	7	5	4	5	5	3	3
1-Butanol	Alcohol	2	6	3	3	4	1	4	4	5	3	4	4	4
1-Octanol	Alcohol	1	1	1	1	1	2	2	1	3	1	1	3	1
Phenol	Alcohol	1	1	1	2	2	4	4	4	6	3	3	4	3
Ethylene glycol	Glycol	32	39	12	41	44	17	<11	<10	21	<9	44	21	21
1,2-Propanediol	Glycol	<3	12	4	<3	5	<3	<4	<3	<3	<3	4	3	<3
2-Butoxyethanol	Glycol	1	2	1	3	5	5	2	2	3	3	6	6	3
Hexanal	Aldehyde	8	20	8	10	19	12	26	22	17	25	25	16	18
Heptanal	Aldehyde	1	2	1	1	1	1	2	2	3	2	2	2	2
Octanal	Aldehyde	1	2	2	2	2	2	3	3	4	3	3	3	3
Nonanal	Aldehyde	2	2	2	2	3	3	3	3	4	4	3	4	3
2-Butanone	Ketone	6	8	2	16	28	6	7	4	4	8	7	5	6
Acetic acid	Acid	25	102	142	80	122	264	123	120	267	53	126	275	122
Texanol®	Ester	2	7	3	2	2	2	2	1	2	2	2	2	2

*Median Concentration.

The area-specific emission rates of formaldehyde ranged from 24-68 $\mu g\ m^{-2}\ h^{-1}$ with a median value of 41 $\mu g\ m^{-2}\ h^{-1}$. The values for each house varied by less than a factor of two, and there was no consistent trend with time. The hexanal emission rates ranged from 45-137 $\mu g\ m^{-2}\ h^{-1}$ with a median value of 85 $\mu g\ m^{-2}\ h^{-1}$. For Houses M1, M2 and M4, the highest hexanal emission rates occurred in the 2nd sampling period. In the final sampling period, the rates were in a narrow range of 56-65 $\mu g\ m^{-2}\ h^{-1}$. The formaldehyde and hexanal emission rates were not correlated with each other (r = 0.54).

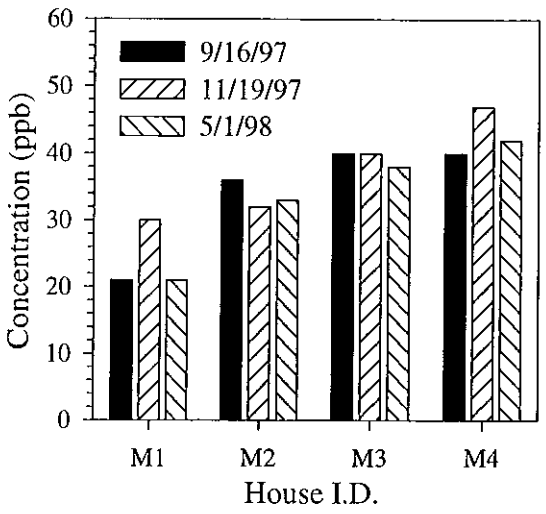

Figure 3. Formaldehyde concentrations.

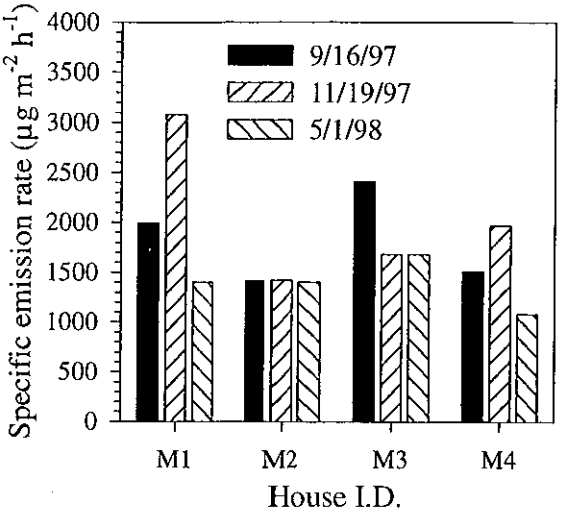

Figure 4. TVOC specific emission rates.

DISCUSSION

TVOC concentrations in various indoor environments are frequently about 1,000 $\mu g\ m^{-3}$, or lower [3]. One study of a probability-based sample of ~200 occupied houses of all ages recorded a median TVOC concentration of 700 $\mu g\ m^{-3}$ [4]. The TVOC concentration in House M3 during the 1st sampling period was about four times higher than this value while the median TVOC concentration in the four houses over the course of the study was only about twice this value. Supplemental mechanical ventilation may have contributed to the consistent, and generally low, TVOC concentrations in House M2.

In the past, formaldehyde concentrations in manufactured houses were frequently in excess of 100 ppb [5]. Guidelines for formaldehyde concentrations in buildings are now established at relatively low levels. The formaldehyde concentrations in the four houses were all lower than the most restrictive guideline in the USA of 50 ppb [6]. The low formaldehyde concentrations are probably due to the exclusive use of gypsum board panels for walls and ceilings and the relatively low emissions of formaldehyde from current wood products.

Indoor air concentration data for a number of VOCs have been summarized from the literature [3]. Compounds that had notably elevated concentrations in the study houses relative to these data included the alkane and terpene hydrocarbons, n-decane, n-undecane, n-dodecane, n-tetradecane, α-pinene and β-pinene. Other compounds in the houses with elevated concentrations relative to the literature were 1-butanol, hexanal, nonanal, and 2-butanone.

A number of alcohols, aldehydes and carboxylic acids produce objectionable odors at low concentration [7]. The hexanal concentrations in the houses frequently were near or exceeded

the hexanal odor threshold of 14 ppb. The odor thresholds for octanal and nonanal are 1 and 2 ppb, respectively. The concentrations of octanal and nonanal consistently were at or slightly exceeded these values. The odor threshold for acetic acid of 140 ppb was approached in all houses during the 2nd sampling period and was exceeded in all houses during the final period. Thus, while the concentrations of TVOC and VOCs in the houses were, in general, not abnormally elevated, it is expected that some occupants would be able to detect objectionable odors due to elevated concentrations of aldehydes and acetic acid.

The data suggest that IAQ in the houses was primarily impacted by a few dominant VOC sources. Phenol and at least a portion of the normal alkane hydrocarbons, such as n-tridecane and n-tetradecane, may have originated from the sheet vinyl flooring used only in Houses M2, M3 and M4. Wood and engineered wood products emit terpene hydrocarbons, such as α-pinene, β-pinene and d-limonene. Engineered wood products also emit hexanal and other aldehydes including heptanal, octanal and nonanal. It is likely that the terpene hydrocarbons and aldehydes originated from engineered wood products used in the construction and finishing of the houses. The possible sources include cabinetry, plywood floor decking and oriented-strand-board roof decking. The primary source of acetic acid is uncertain.

The effects of the two source substitution treatments were difficult to evaluate. House M2 with the low-VOC paints had some of the highest concentrations of ethylene glycol that is used as a solvent in many latex paints. It is possible that conventional latex paints were used in the house during the decorating phase or for touch up. The concentrations of specific VOCs typically emitted by carpets and carpet cushions were low in all four houses, suggesting that contemporary carpet materials are a relatively minor source of VOCs.

ACKNOWLEDGEMENT

Sponsored by the U.S. Depart. Of Energy, Assist. Secretary for Energy Efficiency and Renewable Energy, Office of Building Technology, State and Community Programs.

REFERENCES

1. ECA-IAQ. 1997. Report No. 19. Total volatile organic compounds (TVOC) in indoor air quality investigations. Report EUR 17775 EN, European Collaborative Action, Indoor Air Quality & Its Impact on Man.
2. Florida Solar Energy Center, www.fsec.ucf.edu/~eeih/fanrec/specs.html.
3. Brown, S.K., M.R. Sim, M.J. Abramson and C.N. Gray. 1994. Concentrations of volatile organic compounds in indoor air – A review. *Indoor Air* **4**: 123-134.
4. Wallace, L., E. Pellizarri and C. Wendel. 1991. Total volatile organic concentrations in 2700 personal, indoor, and outdoor air samples collected in the US EPA Team studies. *Indoor Air* **1**: 465-477.
5. Sexton, K., K.-S. Liu and M.X. Petreas. 1986. Formaldehyde concentrations inside private residences: a mail-out approach to indoor air monitoring. *J. Air Pollution Control Assoc.* **36**: 698-704.
6. CARB. 1991. *Indoor Air Quality Guideline No. 1: Formaldehyde in the Home.* California Air Resources Board, Research Division, Sacramento, CA.
7. Devos, M., F. Patte, J. Rouault, et al. 1990. *Standardized Human Olfactory Thresholds.* Oxford University Press, New York, NY.

TECHNIQUES FOR REDUCING EXPOSURES TO VOLATILE ORGANIC COMPOUNDS ASSOCIATED WITH NEW CONSTRUCTION AND RENOVATION

A.T. Hodgson[1] and D.A. Shimer[2]

[1]E.O. Lawrence Berkeley National Laboratory, USA
[2]California Environmental Protection Agency, Air Resources Board, USA

ABSTRACT

Chamber experiments were conducted with a combination of latex paints and new carpet and vinyl flooring assemblies. The first objective was to characterize the emissions of volatile organic compounds (VOCs) from the assemblies at simulated residential conditions. The second objective was to evaluate the effectiveness of techniques that homeowners and building managers might employ during new construction or renovation to reduce concentrations of VOCs and exposures to these VOCs. The techniques included: increased ventilation for three days following installation (each source); airing out of materials for two days prior to installation (carpet and vinyl flooring); and mild heating for three days following installation (combined sources). Short-term ventilation typically reduced VOC concentrations in room air only during the period of increased ventilation. Airing out of materials generally reduced the emissions of VOCs from carpet materials but was ineffective for VOCs emitted by vinyl flooring. Heating applied after materials were installed had mixed results.

INTRODUCTION

Paints and many materials used to finish the interiors of houses and other buildings emit volatile organic compounds (VOCs), including toxic air contaminants (TACs). These emissions result in exposures to occupants. The California Air Resources Board (ARB) is required to consider such indoor exposures in assessing risks from TACs to public health. Thus, it is necessary for the ARB to identify indoor sources of VOCs and to characterize their emissions. The ARB also provides information to the public regarding ways to reduce both indoor and outdoor exposures to TACs.

Numerous techniques for reducing occupant exposures to indoor sources of VOCs have been proposed. The California Department of Health Services developed guidelines for reducing exposures to VOCs from construction materials used in office buildings [1]. Tichenor and Sparks employed an indoor air quality model to predict occupant exposures for different source scenarios, building parameters and occupant activity patterns [2]. The current study was designed to evaluate selected exposure reduction techniques in environmental chambers. Emphasis was placed on practical techniques that homeowners and building managers might use to reduce occupant exposures to VOCs associated with new construction or renovation. The study is fully described in a recent report [3].

METHODS

A variety of interior latex paints, carpets, carpet cushions, and vinyl floor installation materials widely used by California homeowners were selected for study. Newly manufactured specimens of 24 materials were individually screened for emissions of VOCs in

small-scale environmental chambers following standard practice [4]. VOCs emitted by the materials were identified, and the emission rates of selected VOCs were determined.

In the 2nd phase, 13 large-scale experiments were conducted with realistic assemblies of new materials that were selected based on the screening results. The chamber facility with dual, 25-m^3 compartments was designed and operated to simulate a residential room environment. The walls and ceiling of each compartment were painted gypsum board. The floor was either carpeted or covered with sheet vinyl; and furnishings (*i.e.*, two upholstered chairs and a drapery panel) were installed to mimic typical "sink" effects. The study materials were installed following construction industry practice. For experiments with paint, a fast-drying latex primer sealer (LPS) was first applied to gypsum board and plywood substrates. This was followed by a flat latex paint (FLP) applied to 14.9-m^2 of gypsum board and a semi-gloss latex paint (SGLP) applied to 1.1-m^2 of plywood. The carpet and vinyl flooring assemblies were installed to cover the entire 10.4-m^2 floor area of a compartment. For the two experiments with the combined source assemblies, the paints were applied three days prior to the installation of the flooring materials, which consisted of two-thirds carpet and one-third sheet vinyl. Air samples for the analysis of VOCs and aldehydes were collected from a compartment throughout the first day of an experiment, daily over the next nine days and finally on day 14 following installation of the materials.

The exposure reduction techniques that were investigated included: additional ventilation for three days following installation (each source assembly); additional air mixing combined with additional ventilation (paint combination); airing out of materials for two days prior to installation (carpet and vinyl flooring assemblies); and room heating to 33° C for three days after painting and installing the flooring materials (combined source assemblies). The results for the treatment experiments were compared to the results for base-case experiments conducted at standardized conditions for ventilation, air mixing and temperature. For the base-case experiments, the ventilation rate was held at 2 h^{-1} during material installation and for the next two hours. Then it was reduced to 0.5 h^{-1} and held at that condition. For experiments with additional ventilation, the rate during material installation and the next two hours was 5 h^{-1}. The rate was then reduced to 2 h^{-1} and held at that condition until 72-h elapsed time when it was further reduced to 0.5 h^{-1}.

Air samples for VOCs were collected on Tenax®-TA sorbent tubes. These were analyzed for VOCs by thermal desorption GC/MS using a modification of U.S. EPA Method TO-1. Emission rates of the target VOCs were calculated by a steady-state mass-balance model [4].

Predicted exposure was calculated for two different time periods or scenarios. The 1st scenario was for an occupant who was present during the first 48 hours following installation. The 2nd scenario was for a full-time occupant who vacated the residence during the first 48 hours and then returned. Occupancy for 20 hours per day (*i.e.*, an occupancy factor of 0.83) was assumed for both scenarios. The cumulative exposure for a target VOC was calculated as the product of the concentration profile, the exposure time in hours, and the occupancy factor.

RESULTS

The screening measurements generated a large amount of qualitative and quantitative data. The VOC emissions from conventional latex paints principally consisted of a solvent component (ethylene glycol and/or propylene glycol) and the Texanol® coalescing aid. The 96-h emission rates of SigmaVOC (*i.e.*, the sum of the rates for individual VOCs) from eight conventional and two non-VOC latex paints are compared in Figure 1. The LPSs and FLPs were applied to gypsum board. The SGLPs were applied to plywood. The two non-VOC

paints, FLP4 and SGLP4, had substantially lower emission rates than did the conventional paints. These emissions consisted of small amounts of oxidized compounds. Paints LPS2, FLP3 and SGLP3 were selected for use in the large-scale experiments.

Approximately 3.6 kg of the combined paints was applied in each large-scale experiment. Ethylene glycol (EG) and Texanol® were the dominant emitted compounds (Table 1). Other compounds included acetaldehyde, propylene glycol and di(ethylene glycol)butyl ether. The maximum concentrations of the target compounds occurred within the first few hours after paint application. The experiments were compared over elapsed time periods of only 240 h since one experiment was terminated early. There were ~98% reductions in the concentrations of EG over this period. For all cases, 60% of the total cumulative exposures to this compound occurred within the first 48 h. The concentrations of Texanol® decreased by a factor of ~3.5 over the course of the experiments. The use of additional initial ventilation resulted in small decreases in exposures to EG and Texanol® over both the 0- to 48- and the 48- to 240-h time periods (Table 1). The small effect in the initial period was due to increased emission rates in response to additional ventilation. Additional air mixing created with two oscillating fans pointed at the painted surfaces in combination with additional ventilation resulted in somewhat greater exposure reductions relative to the base-case condition.

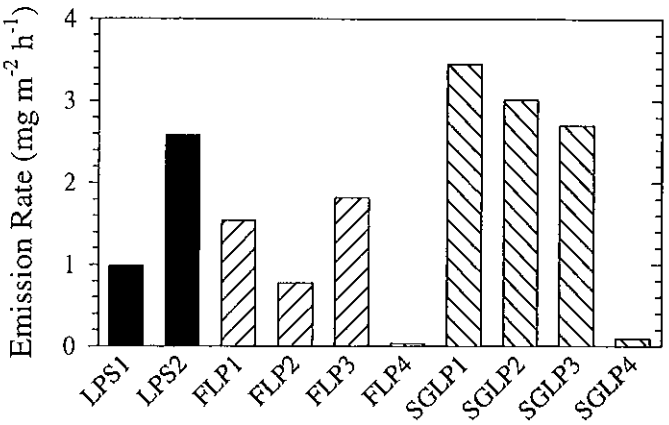

Figure 1. Specific emission rates of SigmaVOC at 96 h in screening measurements of latex paints.

The carpet assembly selected for the large-scale experiments consisted of a carpet with olefin face fibers and a bonded urethane carpet cushion. This assembly had substantially lower emissions of VOCs than the paint and vinyl flooring. (Note that the concentrations and exposures for the carpet and vinyl flooring assemblies are presented in ppb and ppb-h units.) The carpet emitted styrene, 4-ethenycyclohexene, 4-phenylcyclohexene (4-PCH), isomers of di(propylene glycol)methyl ether (DPGME) and N,N-dimethylacetamide. The cushion emitted butylated hydroxytoluene (BHT), 2,2'-azobisisobutryonitrile and a complex mixture of unsaturated hydrocarbons. Data for 4-PCH, DPGME and BHT are shown in Table 2. There were five-fold or more reductions in the concentrations of DPGME over the course of the experiments. The concentrations of 4-PCH only decreased by a factor of two or less while the concentrations of BHT increased with time. The concentrations of the individual VOCs at the ends of the experiments were ~1 ppb or less. The use of additional initial ventilation resulted in decreases in the exposures to most VOCs over 0-48 h (Table 2). However, the 48- to 336-h exposures to most VOCs were affected by less than 10% due to use of higher initial ventilation. Airing out of the carpet and cushion in a well-ventilated space for two days prior to installation substantially reduced the exposures to all VOCs in both time periods relative to the base-case experiment.

The vinyl flooring assembly selected for the large scale experiments consisted of residential "no-wax" sheet vinyl, low-VOC full-spread adhesive, liquid seam sealer, rubber cove base and cove base adhesive. Use of the seam sealer produced high (ppm) initial concentrations of tetrahydrofuran (THF) and cyclohexanone. The full-spread adhesive emitted toluene. The

dominant compounds emitted by the sheet vinyl were n-tridecane (n-C13), other alkane hydrocarbons, 1,2,4-trimethylbenzene, benzyl alcohol, phenol and TXIB® plasticizer. The cove base emitted benzothiazole. Data for n-C13, toluene, THF and phenol are shown in Table 3. There were rapid 100-fold or more reductions in the THF and cyclohexanone concentrations over the course of the experiments. There were also substantial rapid reductions in the toluene concentrations in all experiments. The use of additional initial ventilation clearly reduced the exposures to most VOCs over 0-48 h (Table 3). However, the apparent emission rates of benzyl alcohol, phenol, TXIB® and benzothiazole, all relatively low volatility compounds, increased in response to additional ventilation. Thus, the exposure to TXIB® was only reduced by 22% and the exposures to the other three compounds were affected by less than 10% during the initial period. The 48- to 336-h exposures to most VOCs were affected by less than 10% as the result of additional ventilation during the first 72 h. The most impacted compounds were toluene, THF and phenol with 16-30% reductions. Airing out of the sheet vinyl and cove base reduced the 0- to 48-h exposures to most VOCs by 25% or less. The most impacted compounds were phenol and benzothiazole with ~40% reductions. This treatment was less effective for reducing exposures over the longer period.

Heating the compartment to 33° C for three days following the installation of combined assemblies resulted in increases in the chamber concentrations of most VOCs during the heating period. At the onset of heating, there were rapid, typically three-fold concentration increases, which declined over the 72-h heating period. When the heat was turned off, the concentrations typically returned to values similar to the base-case values. Texanol® was a notable exception. Subsequent to heating, the concentrations of Texanol® were lower relative to the reference case. The cumulative exposures to selected VOCs in the heating and base-case experiments are compared in Figure 2. Occupancy was assumed to begin after the compartment temperature returned to normal. There was an increase in the exposure for THF and a more than two-fold decrease in the exposure for Texanol® due to heating.

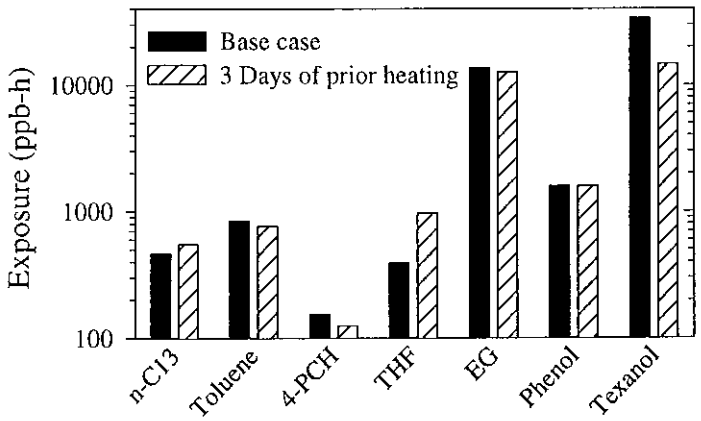

Figure 2. Cumulative exposures to selected VOCs over 96-336 hours in experiments with combined sources.

DISCUSSION AND CONCLUSIONS

A moderate increase in building ventilation during and for a short period following the installation of an indoor VOC source is probably the most accessible and practical exposure reduction technique for consumers. VOC concentrations were reduced during the period of additional ventilation; however, the reductions were frequently not directly proportional to the magnitude of the ventilation increase. VOC concentrations following the termination of additional ventilation often quickly returned to base-case values. An alternative exposure reduction technique is to select materials for new construction and renovation that have low emissions of VOCs. However, the informed selection of low-emitting materials is frequently a complex and difficult task.

The results of the investigation have been generalized to formulate the following practices that homeowners and building managers can employ to reduce VOC concentrations and decrease cumulative exposures to VOCs for occupants of houses and other buildings.

1) Materials that emit lower amounts of toxic or odorous VOCs should be selected whenever possible. Lower emitting materials should reduce occupant exposures and decrease the need for subsequent control strategies. The substitution of non-VOC latex paints for conventional latex paints appears to be one viable choice for reducing exposures.

2) The most effective way to reduce occupant exposures to the dominant VOCs emitted by conventional latex paints is to delay occupancy for several days following painting. This strategy may also be effective for reducing exposures due to sheet vinyl installations.

3) Although carpets and carpet cushions are relatively low sources of VOCs, exposures to VOCs emitted by these materials can be reduced by airing them out in a well-ventilated, clean, dry environment for several days prior to their installation.

4) High mechanically induced ventilation rates should be used during the application or installation of high emitting materials such as paints and vinyl seam sealers to protect the installers and any occupants that are present.

5) Additional ventilation should be maintained for periods longer than three days to more effectively lower occupant exposures. The ventilation rate should be maximized since, in many cases, the beneficial effects of ventilation, are not in direct proportion to the increase in the ventilation rate.

ACKNOWLEDGEMENT AND DISCLAIMER

Sponsored by the California Environmental Protection Agency, Air Resources Board under Contract No. 95-302 and by the U.S. Depart. Of Energy, Assist. Secretary for Energy Efficiency and Renewable Energy, Office of Building Technology, State and Community Programs under Contract No. DE-AC03-76SF00098. The statements and conclusions herein are those of the authors and not necessarily those of the sponsoring agencies. The mention of commercial products or their use in connection with material reported herein is not to be construed as actual or implied endorsement of such products.

REFERENCES

1. Alevantis, L.E. 1996. Reducing occupant exposure to volatile organic compounds (VOCs) from office building construction materials: Non-binding guidelines. California Department of Health Services Report released July, 1996, 46 p.
2. Tichenor, B.A. and L.E. Sparks. 1996. Managing exposure to indoor air pollutants in residential and office environments. *Indoor Air* **6**: 259-270.
3. Hodgson, A.T. 1999. Common Indoor Sources of Volatile Organic Compounds: Emission Rates and Techniques for Reducing Consumer Exposures. Final Report to California Environmental Protection Agency, Air Resources Board, Contract No. 95-302.
4. ASTM. 1997. *ASTM Standard D 5116-97, Standard Guide for Small-Scale Environmental Chamber Determinations of Organic Emissions from Indoor Materials/Products*. American Society for Testing and Materials, Philadelphia, PA.

Table 1. Effects of additional initial ventilation and air mixing on concentrations and exposures to selected VOCs emitted by latex paints.

Compound	Added Vent. (Yes/No)	Air Mixing (Yes/No)	Max. Conc. 1-48 h (ppm)	Conc. @ 240 h (ppm)	Exposure 0-48 h (ppm-h)	Exposure 48-240 h (ppm-h)
EG	No	No	6.7	0.148	72	37
	Yes	No	6.5	0.129	59	38
	Yes	Yes	4.0	0.118	45	28
Texanol®	No	No	0.48	0.138	14.1	36
	Yes	No	0.63	0.179	12.4	31
	Yes	Yes	0.49	0.164	10.8	26

Table 2. Effects of additional initial ventilation and airing out of materials on concentrations and exposures to selected VOCs emitted by carpet assembly.

Compound	Added Vent. (Yes/No)	Airing Out (Yes/No)	Max. Conc. 1-48 h (ppb)	Conc. @ 336 h (ppb)	Exposure 0-48 h (ppb-h)	Exposure 48-336 h (ppb-h)
4-PCH	No	No	1.9	0.9	70	320
	Yes	No	1.5	1.1	53	300
	No	Yes	1.4	0.8	46	260
DPGME	No	No	4.2	0.5	111	198
	Yes	No	3.2	0.6	66	187
	No	Yes	0.9	<0.5	32	<109
BHT	No	No	0.7	0.9	14	152
	Yes	No	0.8	1.2	17	220
	No	Yes	0.4	0.8	10	122

Table 3. Effects of additional initial ventilation and airing out of materials on concentrations and exposures to selected VOCs emitted by vinyl flooring assembly.

Compound	Added Vent. (Yes/No)	Airing Out (Yes/No)	Max. Conc. 1-48 h (ppb)	Conc. @ 336 h (ppb)	Exposure 0-48 h (ppb-h)	Exposure 48-336 h (ppb-h)
n-Tridecane	No	No	27	6.1	420	1,720
	Yes	No	11.3	6.8	220	1,620
	No	Yes	23	7.6	370	1,820
Toluene	No	No	60	8.2	870	2,800
	Yes	No	11.2	8.2	196	2,100
	No	Yes	44	8.8	580	2,200
THF	No	No	2,600	2.7	7,300	2,000
	Yes	No	330	3.4	1,400	1,400
	No	Yes	2,200	5.8	8,900	2,400
Phenol	No	No	32	16.9	930	4,700
	Yes	No	21	15.9	730	3,900
	No	Yes	18.7	15.9	510	4,000

EFFECT OF REVERSIBLE, DIFFUSION-CONTROLLED SINKS ON VOC CONCENTRATIONS IN BUILDINGS

D. Y. Zhao[1], J. Rouques[2], J. C. Little[1] and A. T. Hodgson[2]

[1]Department of Civil & Environmental Engineering, Virginia Tech, USA
[2]E. O. Lawrence Berkeley National Laboratory (LBNL), USA

ABSTRACT

This paper evaluates the impact of reversible, diffusion-controlled sinks on indoor air contaminant concentrations. Four typical scenarios are considered, each involving a variable mass flow rate entering a room containing an idealized sink with realistic properties. The four scenarios include a sinusoidal source, a double-exponential decaying source, an episodic introduction of a volatile compound, and a constant source with varying ventilation rates. Using a source/sink diffusion model developed in earlier work, the evolving indoor-air concentrations are predicted. A parametric study, with respect to the material/air partition coefficient (K) and the material-phase diffusion coefficient (D), shows that equilibrium dominates the source/sink effect for a wide range of volatile organic compounds commonly found indoors. D only becomes important for compounds with low vapor pressures.

KEYWORDS: diffusion, mass balance model, sink, sorption, VOC

INTRODUCTION

Diffusion is an important mechanism governing the source/sink behavior of certain indoor materials [1]. Although several empirical or semi-empirical models have been proposed to describe diffusion-controlled emission processes [2], predictions for conditions not covered by the experimental data are often uncertain, and such models provide little insight into the controlling mechanisms. Little et al. [3] developed a source model for predicting emissions of volatile organic compounds (VOCs) from new carpets. An analytical solution was obtained assuming that the influent air was free of VOCs. Later, Little and Hodgson [1] extended the model to allow predictions to be made with a transient forcing function. This model permits the evaluation of the source/sink behavior of homogeneous, diffusion controlled indoor materials based solely on a knowledge of relevant properties such as the material-air partition coefficient (K) and the material-phase diffusion coefficient (D). This paper applies the sink model developed by Little and Hodgson [1] to cases where a room is subject to a time-varying contaminant source. Model predictions for four VOC source scenarios are demonstrated. Also, to gain insight into the expected behavior, a parametric study is conducted with respect to the key model parameters, K and D.

THE MODEL

Consider a room, which contains a homogeneous sink in the form of a thin slab. Transient diffusion through the slab can be described using the one-dimensional diffusion equation

$$\frac{\partial C}{\partial t} = D\frac{\partial^2 C}{\partial x^2} \qquad (1)$$

where C(x, t) is the concentration of the contaminant in the slab, t is time, and x is distance from the base of the slab. Only one surface of the slab is exposed to the air in the room. Equilibrium is assumed to hold between the VOC concentration in the surface layer of the slab and the indoor air, or

$$K = \frac{C|_{x=L}}{y} \tag{2}$$

where y is the air-phase concentration. Further assuming that the sink is initially free of contaminant, and that there is no flux through the base of the slab, the following analytical solution is obtained [1]

$$C(x,t) = \frac{2Q}{AK}\sum_{n=1}^{\infty}\left\{\frac{\exp(-Dq_n^2 t)(q_n^2)\cos(q_n x)}{\left[L(h-kq_n^2)^2 + q_n^2(L+k) + h\right]\cos(q_n L)} \cdot \int_0^t \exp(Dq_n^2\tau)\cdot K \cdot y_{in}(\tau)d\tau\right\} \tag{3}$$

where

$$h = \frac{Q}{ADK} \tag{4}$$

and

$$k = \frac{V}{AK} \tag{5}$$

The q_n's are the positive roots of

$$q_n \tan(q_n L) = h - kq_n^2 \tag{6}$$

A is the exposed surface area of the slab, V the volume of well-mixed air within the room, Q the volumetric flow rate of air, L the thickness of the slab, and τ is a dummy variable.

Once the source function, $y_{in}(t)$ is defined, equation (3) can be used to predict C(x, t) the contaminant concentration in the slab. The concentration of a VOC in the air y(t) is obtained by first finding the concentration at the slab surface C(x=L, t) and then applying the equilibrium condition defined by equation (2).

MODEL PARAMETERS

Styrene and naphthalene are used as example VOCs with a sink represented by a carpet with a 2mm thick Styrene Butadiene Rubber (SBR) backing. The surface area (A) is assumed to be 9 m^2 and the volume (V) of the room is 20 m^3. A ventilation rate of 1 air change per hour is assumed, which results in an air flow rate (Q) of 20 m^3/h. Values of K and D, estimated using appropriate correlation equations [4], are 330 and 1.6×10^{-12} m^2/s for SBR-styrene, and 270,000 and 1.6×10^{-12} m^2/s for SBR-naphthalene, respectively.

RESULTS AND DISCUSSION

Four scenarios are now considered. In each case, air enters a single room either from the outside or from a connected room. Either the concentration or the flow rate of the air entering the room varies as a function of time. The previously described model is used to predict the resulting contaminant concentration within the target room, a calculation that implicitly includes the effect of the hypothetical sink. The VOCs used in the calculations (styrene and naphthalene) cover a wide range in volatility and illustrate the impact of this parameter on the predicted concentrations.

Scenario 1

The first scenario involves a constant Q and a sinusoidal variation in concentration. A practical example of this type of source is benzene from motor vehicle exhaust in outdoor air in Los Angeles, as described by Harley and Cass [5]. The following source function was inferred from that data

$$y_{in}(t) = 10 \cdot \mathrm{Sin}\left(\frac{\pi}{12} t\right) + 20 \tag{7}$$

Figure 1 compares the source concentration profile defined by equation (7) to that predicted using the model. For naphthalene, whose K value is orders of magnitude higher than that of styrene, a significant depression in concentration is evident. For both compounds, the indoor material shows alternating sink and source behavior. As the source concentration rises the SBR functions as a sink ($y < y_{in}$). As the source strength decreases the SBR acts as a source ($y > y_{in}$). In both cases, the periodicity of the output function remains the same as that of the source despite a discernable lag time.

Scenario 2

The second scenario again involves a constant Q but with a slowly depleting VOC source, such as a new carpet, in the connected room. The decaying source function was obtained from a double exponential relationship for emission of styrene from carpet as reported by Hodgson et al. [6]

$$y_{in}(t) = 793 \cdot e^{-0.15t} + 139 \cdot e^{-0.022t} \tag{8}$$

Figure 2 plots the source function as well as the resulting concentrations predicted for styrene and naphthalene. The concentrations peak about four hours after initialization of the source and naphthalene is again substantially reduced as a result of the sink effect.

Scenario 3

The third scenario simulates the intermittent use of a volatile consumer product such as an aerosol spray in the connected room. The air flow rate Q remains constant. It is assumed that the product is used twice a day (once at 9 a.m. and again at 1 p.m.), that initial values for both spikes are 500 ppb, and that the parameters for styrene are applicable. A mass balance yields the following source functions on a daily basis.

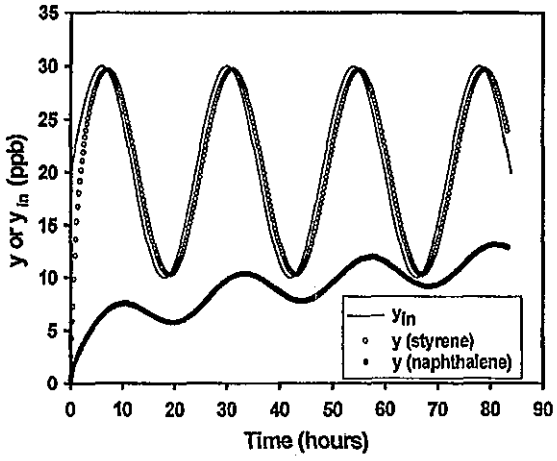

Figure 1. Sink effect on indoor VOC concentrations responding to a sinusoidal source.

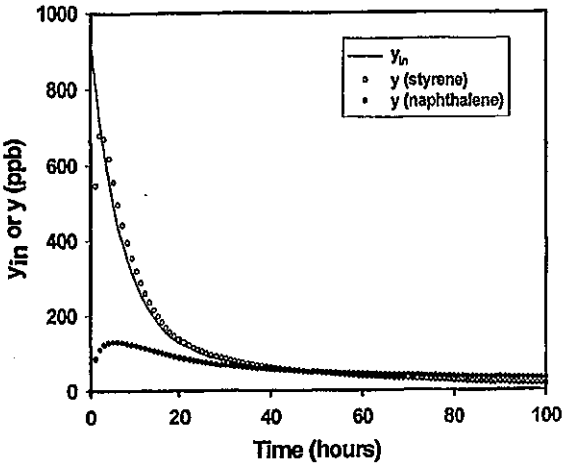

Figure 2. Sink effect on indoor VOC concentrations responding to a double-exponential decaying source.

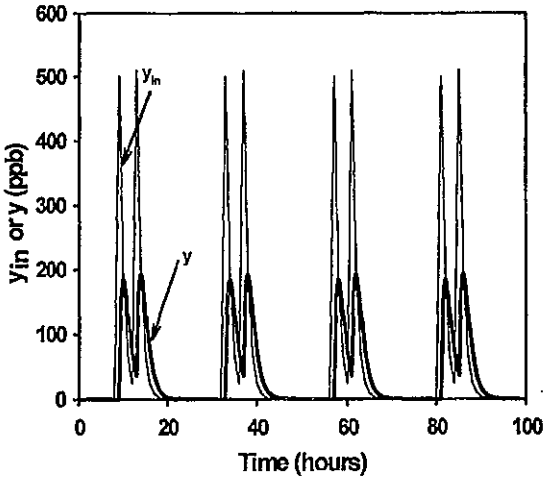

Figure 3. Sink effect on indoor concentrations following an episodic input of a volatile compound.

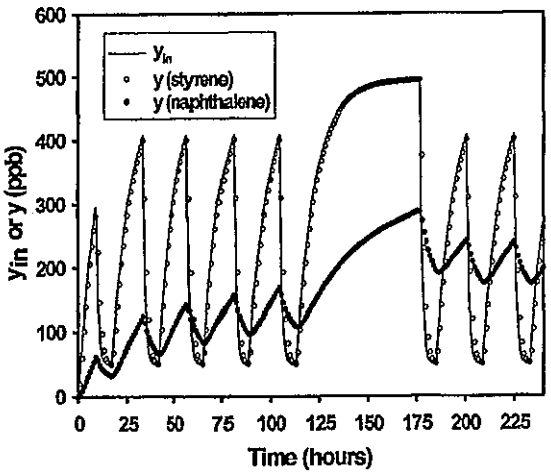

Figure 4. Effect of sink and daily change in ACH on indoor air concentrations responding to a constant source.

$$y_{in}(t) = 0 \qquad 0 \le t < 9 \qquad (9)$$

$$y_{in}(t) = \frac{500}{e^{-9\cdot\frac{Q}{V}}} \cdot e^{-\frac{Q}{V}t} \qquad 9 \le t < 13 \qquad (10)$$

$$y_{in}(t) = \frac{500}{e^{-9.\frac{Q}{V}}} \cdot \{e^{-\frac{Q}{V}(t-4)} + e^{-\frac{Q}{V}t}\} \qquad 13 \leq t < 24 \qquad (11)$$

where midnight is taken as the starting point. It is assumed that releases from the previous day will not affect the indoor air concentration on the following day. However, the impact of the first release is added to the second release on the same day as shown in equation (11). Figure 3 shows the transient concentrations induced by these releases with and without the sink effect.

Scenario 4

The fourth scenario utilizes an unspecified source emitting a VOC at a constant rate. A ventilation rate of 1.0 air change per hour is assumed between 9 a.m. and 5 p.m. from Monday through Friday, while it is reduced to 0.1 air changes per hour during nights and weekends. A mass balance approach similar to that taken in scenario 3 is used to define the appropriate source functions. Figure 4 presents the concentration histories for styrene and naphthalene, respectively, in the presence of the hypothetical sink.

Parametric analysis

The model allows the influence of the key parameters on the predicted concentrations to be examined. For illustrative purposes, a constant y_{in} of 500 ppb is considered in equation (3). Figures 5 and 6 provide plots of y(t) for values of D varying between 0.01×10^{-12} and 100×10^{-12} m^2/s, while K is fixed at 1000 and 100,000, respectively. Figure 5 demonstrates that for a K value of ~1000, which is typical for several VOC/indoor material combinations, a variation in D does not alter the y(t) profiles considerably. However, D becomes important when K is large as shown in Figure 6.

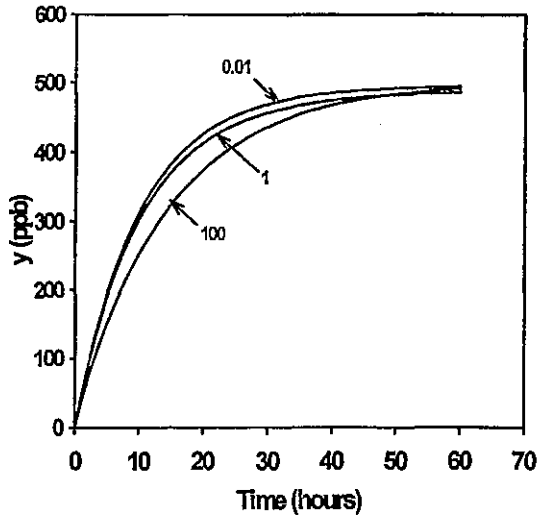

Figure 5. Plots of y(t) for D varying between 0.01×10^{-12} and 100×10^{-12} m^2/s at a constant K of 1000 and y_{in} of 500 ppb.

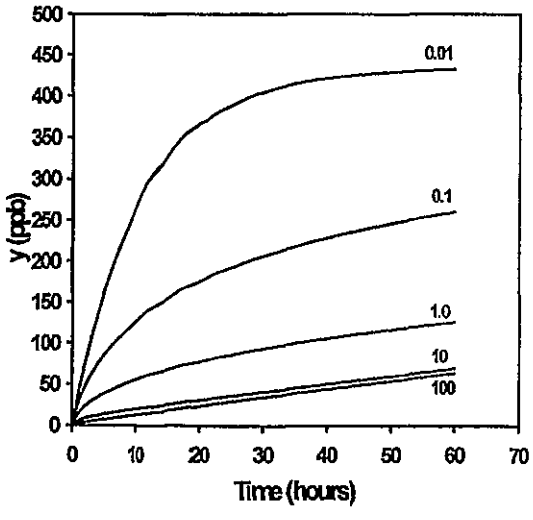

Figure 6. Plots of y(t) for D varying between 0.01×10^{-12} and 50×10^{-12} m^2/s at constant K of 100,000 and y_{in} of 500 ppb.

ACKNOWLEDGEMENTS

Work at Virginia Tech was supported by the National Science Foundation (NSF) through a NSF CAREER Award to J. C. Little (Grant No. 9624488) and the Center for Indoor Air Research (CIAR) through a CIAR Postdoctoral Fellowship Award to D. Y. Zhao. Work at LBNL was sponsored by the U.S. Department of Energy, Assistant Secretary for Energy Efficiency and Renewable Energy, Office of Building Technology, State and Community Programs under Contract No. DE-AC03-76SF00098.

REFERENCES

1. Little J. C. and Hodgson A. T. 1996. A strategy for characterizing homogeneous, diffusion-controlled, indoor sources and sinks. *Standard Technical Publication* 1287, American Society for Testing and Materials, 294-304.

2. Mathews T. G., Hawthorne A. R. and Thompson C. V. 1987. Formaldehyde sorption and desorption characteristics of gypsum wallboard. *Environmental Science & Technology*, 21, 629-634.

3. Little J. C., Hodgson A. T., and Gadgil A. J. 1994. Modeling emissions of volatile organic compounds from new carpets. *Atmospheric Environment* 28, 227-234.

4. Zhao D. Y., Cox S. S., and Little J. C. 1999. Source/sink characterization of homogeneous, diffusion-controlled building materials. Paper in preparation.

5. Harley R. A. and Cass G. R. 1994. Modeling the concentrations of gas-phase organic air pollutants: direct emissions and atmospheric formation. *Environmental Science & Technology*, 28, 88-98.

6. Hodgson, A. T., Wooley, J. D. and Daisey, J. M. 1992. Volatile Organic Chemical Emissions from Carpets. Final report to the U.S. Consumer Product Safety Commission under Contract CPSC-IAG-90-1256. Lawrence Berkeley Laboratory Report LBL-31916.

EMISSIONS OF ODOROUS OXIDIZED COMPOUNDS FROM CARPET AFTER OZONE EXPOSURE

G C Morrison and W W Nazaroff
Civil and Environmental Engineering
University of California, Berkeley, USA

ABSTRACT

We have conducted laboratory experiments on ozone interactions with carpets, measuring the ozone loss rate and changes in the emissions of volatile organic compounds that result from ozone exposure. Four different samples of residential and commercial grade carpet were aged in ventilated chambers for greater than 12 months ("airing"). After airing, we exposed them to 100 ppb ozone in 10.5-L stainless steel chambers for 48-120 h. The rate of ozone uptake on the carpet was continuously monitored and the gaseous organic compounds emitted were periodically sampled. In addition to the whole-carpet studies, we separately measured ozone uptake and oxidized-organic compound release for carpet backing and for carpet fibers. Three of the carpets released relatively small amounts of oxidized products. However, from one residential carpet we measured cumulative emissions of 186 mg m^{-2} of normal C4-C11 aldehydes and 73 mg m^{-2} of 2-nonenal. Aldehydes have low odor thresholds and 2-nonenal has an especially low threshold of 0.8 μg m^{-3}. We predict that occupants could smell these compounds for years after installation of this carpet in a typical home.

INTRODUCTION

Ozone is a very strong oxidant and can react with many surfaces. This results in reduced indoor ozone concentrations and can increase the gas phase concentration of reaction products, such as aldehydes. The emissions of a number of aldehydes and organic acids have been detected over carpet and painted surfaces upon ozone exposure [1,2]. Indoor aldehyde concentrations have also been correlated with ozone concentrations [3].

In this study, we revisited ozone interactions with carpeting to better understand the source of oxidized products and the impact on indoor environments. We aired out 4 different carpets in separate ventilated chambers for 12 to 15 months to reduce the emissions of volatile compounds. These carpets were then subjected to a controlled atmosphere containing ozone. We measured the release rates, and time-integrated releases of the oxidized products of ozone reactions with these surfaces. From this information, along with assumptions about the geometry and ventilation conditions of typical homes, we can predict how these ozone/surface interactions influence indoor concentrations of odorous compounds. The dynamic pattern of emissions also reveals information about the form of the precursor surface species.

METHODS

Four carpets were chosen for this study. Carpets CP1 and CP3 are residential, nylon fiber, cut pile carpets; CP2 and CP4 are commercial, olefin fiber, loop carpets. These were prepared by cutting squares (232 cm^2) from newly manufactured rolls, and placing them in 19 L chambers. Filtered air was allowed to ventilate the chambers at 10 L min^{-1} for greater than 6 months. This allowed most of the volatile compounds to be released from the carpet samples, thus simulating carpet emissions long after installation. Ozone induced emissions were measured from whole carpet, carpet backing and carpet fibers taken from each carpet sample.

The experimental set-up was as follows. A 10.5-L electropolished stainless steel reaction chamber was placed inside a temperature-controlled cabinet along with spargers for humidifying the air in the chamber. The sample material was placed in a Teflon frame so that only the upper surface was exposed and this assemblage was placed on a Teflon shelf inside

the reaction chamber. Ozone was generated in the reactor inlet stream using ultraviolet light. A portion of the vented exhaust was sampled by a UV photometric ozone analyzer. An electromechanical 3-way valve was used to direct the air stream from the inlet to the ozone analyzer so that either supply air or chamber air ozone concentrations could be measured. The chamber was maintained at 23 ± 0.5°C and 50 ± 5% relative humidity based on an initial calibration using a Vaisala temperature and humidity probe. During the experiments, the chamber was continuously ventilated with a total of 1.2 ± 0.05 L min^{-1} air. A feedback control loop was used to control the concentration of ozone in the chamber so that it remained at 100 ppbv throughout the entire experiment, unless otherwise indicated.

A different reactor was used to measure emissions of VOCs from carpet fibers separated from the backing. We cut fibers from the carpet backing and randomized them with wool carders. These were then weighed and packed into a 15-cm long Teflon fixed-bed reactor with an inner diameter of 1.75 cm. For the fixed-bed experiments, the flowrate was 1.2 L min^{-1}. The upstream ozone concentration was maintained at about 100 ppbv. The downstream concentration was continuously measured.

Gas samples for the analyses of individual volatile organic compounds (VOCs), were collected from the reactor exhaust stream at average elapsed times of 0, 24 and 48 hours. Intermediate samples were also obtained at various times as necessary, especially during the first 5 hours of ozone exposure. The 0-hour samples were collected in the absence of ozone after the chamber containing the sample had been ventilated for 0.5 hours. Samples for most VOCs were collected on Tenax-TA sorbent tubes and were analyzed by thermal desorption gas chromatography/mass spectrometry. Details of this technique have been previously reported [4]. Individual VOCs were quantified using pure standards. Formaldehyde, acetaldehyde and propionaldehyde were collected on treated dinitrophenylhydrazine cartridges and analyzed by high-performance liquid chromatography [5]. An ozone denuder, constructed of tubing internally coated with potassium iodide, was used to eliminate interferences due to ozone in the sampling and analysis of C1 through C3 n-aldehydes[6].

The emission rate of an analyte from either whole carpet or backing samples was calculated by the following equation assuming that all environmental variables were constant, the reactor atmosphere was well mixed, and the emission rate was at steady state:

$$E = \frac{(C - C_0) \cdot Q}{A} \qquad (1)$$

where E is the emission rate of the analyte per unit area of material, Q is the volumetric flow rate of the gas stream, C is the concentration of the analyte in the chamber exhaust, C_0 is the chamber background concentration, and A is the exposed cross-sectional area of the carpet face. These assumptions are not strictly valid for the fixed-bed reactor because the ozone concentration decreases with distance down the bed of fibers. However, equation 1 was used to estimate of the average emission rate for the whole bed where A is replaced by A_F, the fiber surface area. The average measured fiber diameters, d_F, (by light microscope) and fiber mat height, H_F, can be found in Table 1.

RESULTS

We found that ozone-induced emissions of aldehydes from most carpets were relatively low. However, one residential carpet, CP3, was found to release very large quantities of n-aldehydes. The emissions consisted primarily of n-nonanal, 2-nonenal, n-heptanal, and n-octanal. The emission rates of all n-aldehydes from C1 through C14, 2-octenal and 2-nonenal increased upon exposure to ozone. The time-integrated mass emissions, M_T, of aldehydes for each carpet is shown in Table 1. For carpets CP1, CP2, and CP4, M_T is

calculated based on the whole carpet experiment, typically using 1, 4, 24 and 48-h average data to calculate a midpoint Riemann sum. For carpet CP3, M_T is calculated by integrating the emissions from the carpet backing and the fibers,

$$M_T = M_B + R_F M_F \quad (2)$$

where M_B is the time integrated mass emissions from carpet backing, M_F is the time integrated mass emissions from carpet fibers, and R_F is the fiber surface area per superficial area of carpet. Also shown in Table 1 are the mean emission rates ($\overline{E}$) of aldehydes for each carpet. Mean emission rate values for CP1, CP2 and CP4 are simply based on the integrated mass emissions (M_T) divided by 48 hours. For sample CP3, $\overline{E}$ is based on a 120-h, whole carpet experiment (shown in Figure1a). Values for R_F for all carpets are shown in Table 1. Mass emission and emission rate values have an error range of approximately ± 10%. The results for carpet CP3 are discussed in more detail below.

Table 1. Carpet characteristics and emission results [a]

Carpet sample	d_F (μm)	H_F (cm)	R_F [b]	M_T (mg m^{-2})	$\overline{E}$ (μg $m^{-2} h^{-1}$)
CP1	60 ± 5	9.4 ± 0.3	66 ± 7	0.9	19
CP2	70 ± 5	5.5 ± 0.6	33 ± 3	5.9	123
CP3	80 ± 5	9.9 ± 0.3	46 ± 3	263	490
CP4	70 ± 5	3.7 ± 0.6	30 ± 3	4.2	88

[a] d_f = fiber diameter; H_F = fiber mat height; R_F = normalized fiber area; M_T = total emissions of aldehydes; $\overline{E}$ =mean emission rate of aldehydes. [b] Fibers assumed to be cylindrical.

In Figure 1, we show how the emissions of specific aldehydes from CP3 evolve during exposure to ozone. The emissions profile from whole carpet and fibers are given as stacked area plots (a) and (b), respectively. The area between the curves represents the total emissions of the given compound over the period of the experiment. The label "other aldehydes" refers to the sum of the emissions of C4-C6, C10, C11 n-aldehydes and 2-octenal. Note that for the whole carpet experiment ozone was shut off after an elapsed time of 72 h, for a period of 22 h, then turned on briefly and shut off again. This was done to measure aldehyde decay in the absence of ozone, as well as the short-term increase in aldehyde emissions upon re-exposure to ozone.

Nonanal and 2-nonenal are released in larger amounts than any other compound. Only 0.5 h after initiation of ozone exposure, n-nonanal is emitted at a high rate of 158 μg m^{-2} h^{-1} that increases to a maximum of 247 μg m^{-2} h^{-1} by 51 h. In contrast, 2-nonenal has a barely detectable initial emission rate of 2 μg m^{-2} h^{-1} that rises more slowly to reach a maximum of 235 μg m^{-2} h^{-1} at 75.5 h. The emissions from fibers show similar trends. In addition to aldehydes, small amounts of C4-C10 2-ketones were detected as secondary emission products from CP3. In the period between 72 and 94 hours, when the ozone concentration is zero, the aldehyde emissions drop relatively slowly. The emission rate of 2-nonenal drops slower than any other aldehyde. The emission rate of the summed aldehydes drops by approximately 50% over this period in which about 150 air changes take place.

DISCUSSION

Carpet CP3 emits a large quantity of aldehydes. We believe that the bulk of the emissions are coming from fibers. While the backing also emits compounds at a high rate, the tested backing samples are not completely separated from fibers. The fibers were sheared off level with the top of the carpet backing, but the fibers left below the surface could not be removed. However, we measure large emissions of aldehydes from the fibers, which can be completely separated from the backing.

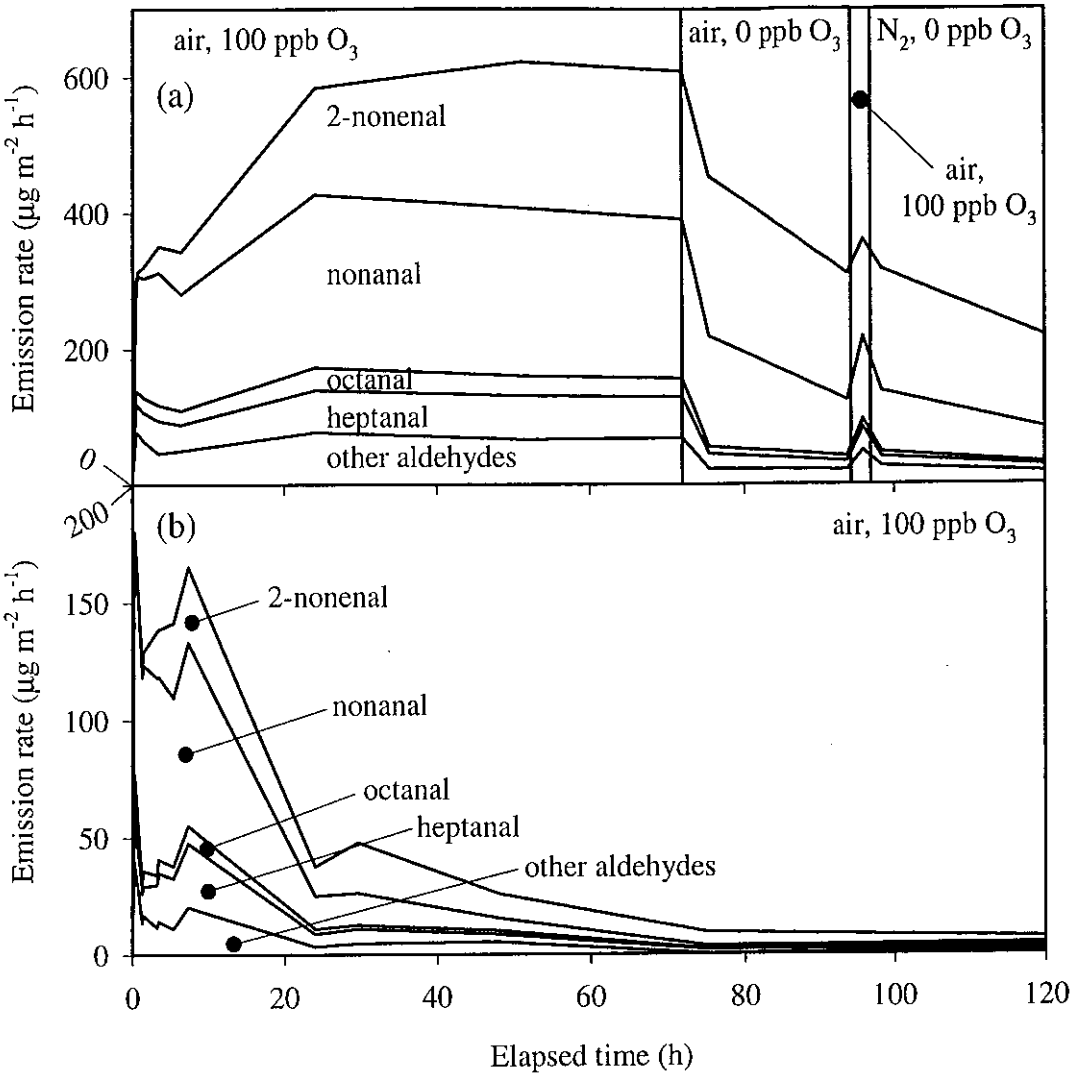

Figure 1. Stacked plot of aldehyde emission rates for carpet CP3: (a) whole carpet (emission rate per area of carpet); (b) carpet fibers (emission rate per area of fibers). "Other aldehydes" include n-hexanal, n-octenal, n-decanal, and n-undecanal.

In general, the dynamic emission profiles of n-aldehydes correlate well with each other (mean correlation coefficient, r = 0.78). On the other hand, the profile of 2-nonenal only correlates with n-heptanal (r = 0.7). This is to be expected if further oxidation of the 2-nonenal produces n-heptanal or if a single precursor compound produces both of these compounds. Based on typical gas-phase reaction rates of ozone with alkenes, little of the gaseous 2-nonenal should be oxidized during the plug flow reactor experiments with fibers. However, oxidation of 2-nonenal adsorbed on the surface is a strong possibility. Based on the slow reduction in the emission rate of 2-nonenal in the absence of ozone, 2-nonenal may strongly adsorb to carpet elements. If these compounds derive from a single precursor compound on the fiber surface, it should have a pair of conjugated double bonds at the 7 and 9 carbon positions counting from the free end of a straight carbon chain. Other aldehydes should similarly come from unsaturated straight-chain compounds with the double bond in a different location. Weschler, et al.[1] suggested that carpets could be coated with vegetable oils which commonly consist of multiply unsaturated fatty acid esters.

The pattern of compounds released from this carpet can be used to predict what oil may be

present, and in what quantities. Castor oil is a commonly used vegetable oil, but does not contain conjugated double bonds. However, castor oil can be dehydrated so that conjugated double bonds form, thus changing the properties of the oil [7]. Based on the ratio of compounds released, dehydrated castor oil (or a mixture of castor oil with other vegetable oils) is a likely candidate as a precursor species. For a given unsaturated fatty acid ester, only one volatile aldehyde would be released upon ozone oxidation (not including di-aldehydes). Other products of the ozone/double-bond reaction are likely to be much less volatile and would not be measured in this analysis. Making the assumption that a single aldehyde is derived from a single fatty-acid ester, we estimate that castor oil may present on the carpet at greater than 0.5 g m^{-2}. This leads to an oil thickness of about 10 nm on the fibers. Other possible precursors include isomerized sunflower, isomerized linseed oil, and unmodified tung oil.

The large quantities of unsaturated surface oils could adversely impact indoor air in locations where ozone concentrations are elevated. We can make an estimate of the indoor concentration of a given species based on the emission rate measured under laboratory conditions and extrapolation to conditions in indoor environments. In this estimate, the aldehyde emissions are assumed to be directly proportional to the rate of ozone removal at the surface of the carpet. For example, in the experiment shown in Figure 1(b), the molar ratio of 2-nonenal released to ozone reacted is 0.11 and for all quantified aldehydes is 0.39 mol aldehydes per mol ozone. The flux, F, of ozone to a flat indoor surface can be parameterized by the deposition velocity, v_d,

$$F = v_d C_{ozone} \tag{3}$$

where, C_{ozone} is the spatial average concentration of ozone indoors (usually measured at the center of a room). The concentration of ozone indoors can be estimated from a completely mixed flow reactor (CMFR) at steady-state [8],

$$C_{ozone} = \frac{\lambda C^{o}_{ozone}}{\lambda + \overline{v}_d \frac{S_T}{V}} \tag{4}$$

where C^{o}_{ozone} is the outdoor concentration of ozone, λ is the air exchange rate, $\overline{v}_d$ is the area-averaged deposition velocity, S_T is the total indoor surface area, and V is the indoor volume.

Under average conditions in Los Angeles, the annual average ozone value ranges from 20 to 54 ppb [9]. We will take a middle value of 37 ppb, and combine this with an estimated surface area to volume ratio of 3 m^{-1}, an air exchange rate of 1 h^{-1} and a mean deposition velocity of 1.4 m h^{-1}. The resulting indoor ozone concentration is 7.1 ppb. Using these values, we can estimate the flux of ozone to carpet and multiply this by the aldehyde emission ratio to obtain an estimated emission rate, E_i (moles per carpet area per time), for compound *i*. The concentration of compound *i* indoors is then calculated using the same CMFR analysis as above,

$$C_i = \frac{E_i S_C}{\lambda V} \tag{5}$$

where S_C is the area of the carpet. To derive this equation we assumed that outdoor air is free of compound *i*, and that there is no net loss of compound *i* from indoor air, e.g., by surface deposition. The indoor concentrations were estimated assuming $S_C/V = 0.4$ m^{-1} and $\lambda = 1$ h^{-1}. The indoor concentrations for 2-nonenal and nonanal from carpet CP3 are estimated to be 2.6 and 3.5 μg m^{-3}. Odor thresholds for 2-nonenal and nonanal are 0.8 μg m^{-3} and 13 μg m^{-3} [10].

We estimate that these levels would be maintained for over a year if the emission rate is constant. Under conditions where the average indoor ozone concentration is somewhat lower (2.2 ppb), the concentration of 2-nonenal could be maintained at the odor threshold for greater than six years. These estimates are based on total emissions from the carpet elements over a limited experimental time period. Ultimately, the total emissions from the carpet could be higher and the odor may persist for an even longer period.

We noted that the emission rate of aldehydes drops relatively slowly after the ozone concentration drops to zero. This is probably due to strong adsorption of aldehydes to the surface of the carpet fibers and backing. Using the CMFR model, the concentration of aldehydes should drop to about 5% of the 72 h value in only 0.4 h, if the emissions of these aldehydes are a direct result of ozone reactions, and there is no significant adsorption to the carpet and chamber surfaces. In experiments not reported here, we found minimal aldehyde adsorption to chamber surfaces. Thus, it appears that, carpets can act as a large reservoir of these odorous compounds, even in the absence of ozone. Outdoor and indoor ozone concentrations tend to follow a strong diurnal pattern, with the highest ozone concentrations occurring midday. Aldehyde emissions will also follow a diurnal pattern since they are formed by ozone reactions. However, the temporal emissions pattern might be smoothed, as the carpet stores aldehydes during the day, and releases them at night.

ACKNOWLEDGEMENTS

The authors thank Al Hodgson and Joan Daisey for guidance. This research was funded through a grant from the U.S. Environmental Protection Agency STAR Fellowship Program and by the Assistant Secretary for Energy Efficiency and Renewable Energy, U.S. Department of Energy, under contract No. DE-AC03-76SF00098.

REFERENCES

1. Weschler, C.J.; Hodgson, A.T.; Wooley, J.D.; *Environmental Science and Technology* **1992** *26*, 2371-2377.
2. Reiss, R.; Ryan, P.B.; Koutrakis, P.; Tibbetts, S.J; *Environmental Science and Technology* **1995**, *29*, 1906-1912.
3. Reiss, R.; Ryan, P.B.; Tibbetts, S.J.; Koutrakis, P.; *J. Air and Waste Management Assoc.* **1995** *45*, 811-822.
4. Hodgson, A.T.; Girman, J.R.; *Design and Protocol for Monitoring Indoor Air Quality, ASTM STP 1002*, N.L. Nagda and J.P. Harper, Eds., American Society for Testing and Materials, Philadelphia, 1989, 244-256.
5. Fung, K.; Grosjean, D.; *Analytical Chemistry* **1981** *53*, 168-171.
6. Kleindienst T.E.; Corse E.W.; Blanchard F.T.; Lonneman W.A.; *Environmental Scence and Technology*, **1998**, *32*, 124-130.
7. Gunstone F.D.; Harwood J.L.; Padley F.B., Eds; *The Lipid Handbook*; Chapman and Hall Ltd.: London, 1986.
8. Weschler C.J.; Shields H.C.; Naik D.V.; *JAPCA: The Journal of the Air and Waste Management Association*, **1989**, *39*:1562-1568.
9. Cass G.R.; Nazaroff W.W.; Tiller C.; Whitmore P.M. *Atmospheric Environment*, **1991**, *25A*, 441-451.
10. Devos M.; Patte F.; Rouault J.; Laffort P. Van Gemert L.J., Eds.; *Standardized Human Olfactory Thresholds*; Oxford University Press: Oxford, 1990.

II. ENVIRONMENTAL TOBACCO SMOKE

DYNAMIC BEHAVIOR OF POLYCYCLIC AROMATIC HYDROCARBONS IN ENVIRONMENTAL TOBACCO SMOKE: EFFECTS OF AGING AND TEMPERATURE VARIATION ON PHASE AND SIZE DISTRIBUTIONS

L.A. Gundel[1], K. Mahanama[2], M.G. Apte[1], S.V. Hering[3], M.D. Van Loy[1] and J.M. Daisey[1]

[1]Environmental Energy Technologies Division, Lawrence Berkeley National Laboratory, University of California, Berkeley, CA, USA
[2]Department of Chemistry, University of Colombo, Sri Lanka
[3]Aerosol Dynamics, Berkeley, CA, USA

ABSTRACT

The purpose of the study is to improve understanding of the dynamic behavior of the polycyclic aromatic hydrocarbons (PAH) in environmental tobacco smoke (ETS) as it ages. Gas/particle phase distributions of PAH were measured in ETS using a diffusion-based sampler. Simultaneously, the size distributions of particulate PAH were determined with a microslot impactor. Experiments were conducted in an environmental chamber (20 m^3, $16 \leq T \leq 25$ °C) for two hours after smoking ceased. The particulate PAH fractions were significantly higher for ETS than for ambient indoor particles. Both gas/particle partitioning and depositional losses to chamber surfaces were highly dependent on PAH vapor pressures. The least volatile particulate PAH were associated with particles with mass median with aerodynamic diameters (MMAD) of less than 0.1 μm. The more volatile PAH were distributed among particles up to 1.7 μmeter in diameter.

INTRODUCTION

The purpose of the study is understanding the dynamic behavior of polycyclic aromatic hydrocarbons (PAH) in ETS sufficiently well to predict their behavior in realistic indoor environments. This work is part of a larger effort to improve exposure assessment by considering aging and deposition of semi-volatile components of ETS onto indoor surfaces. We examined gas/particle partitioning and particle size distributions of ETS components because they influence lung dosimetry. Gas-phase species deposit more efficiently than particles, and they impact the upper airways of the respiratory system where they are quickly cleared. ETS particles of 0.1 to 0.5 μm diameter penetrate deeply into the lung and clear more slowly. Although the dosimetry of particulate organic compounds depends on their particle-size distributions, very little data exists for specific classes such as PAH in ETS. Even less is known about the behavior of the size distributions of PAH as the smoke dilutes and ages.

METHODS

Simulated ETS was generated in two environmental chambers (stainless steel, 20 m^3 and painted wallboard, 36 m^3) using an Arthur D. Little smoking machine with an attached 12-port programmable auto-igniting and extinguishing cigarette holder. Mainstream smoke was ventilated outside the chamber, while the sidestream smoke was emitted directly into the

room. In each experiment, two Kentucky reference type 1R4F cigarettes were smoked sequentially at one 35 mL puff per minute using a standard puff profile. The chamber was sealed, and the air exchange rate was monitored continuously by following the concentration of the tracer gas SF_6. Five experiments were conducted at temperatures between 16 and 25 °C. Integrated PAH measurements were made for 45-min sampling periods. Sampling began 10 min after the cigarettes were extinguished. In two experiments conducted in the stainless steel chamber at 18°C and 25°C, respectively, a second set of integrated PAH measurements were made starting 2.5 hr after smoking. In one experiment at 24°C in the 36 m^3 chamber PAH were determined over four sampling intervals from 30 to 60 min, starting about an hour after smoking.

Gas and particulate phase concentrations of PAH were determined from separate extracts of each of the components of the Integrated Organic Vapor Particle Sampler (IOVPS), a diffusion-based air sampler that minimizes the artifacts associated with sampling semi-volatile organic compounds [1]. The IOVPS operated at 10 L min^{-1}. PAH were determined using high performance liquid chromatography with selective fluorescence detection [2,3]. The relative precision at the 95% confidence level averaged 20% for particulate PAH [3].

Size distributions of twelve PAH were measured using a new impactor, the Size-Segregated Environmental Tobacco Smoke Sampler (SSETS) [4] that was co-located with the IOVPS. The SSETS has cutpoints at 0.10, 0.38, 0.84, 1.7 and 3.5 μm at a flow rate of 36 L min^{-1}. The SSETS uses microslots, 100 μm to 1.4 mm in width, that concentrate the sample and eliminate interferences between jets. The small orifice widths achieve a 0.1 μm cutpoint without using low pressures, thus avoiding volatilization losses. The pressure drops for the smallest stage is 8 kPa [4]. Gravimetric mass and PAH were determined for each stage and for the afterfilter. The mass size distribution of ETS was also measured with a quartz crystal microbalance impactor in some experiments.

RESULTS

Gas/particle phase distribution. The particulate PAH fractions were significantly higher for ETS than those measured for ambient aerosol in indoor air [1]. This characteristic suggests that ETS is especially prone to the sampling artifact problems with semi-volatile species (especially "blow off" of PAH from particles) that the IOVPS has been designed to avoid. Higher particulate PAH fractions are probably due to differences in the nature and age of the particles. Chamber-generated ETS is a relatively fresh, liquid aerosol, compared to ambient particulate matter which usually contains insoluble solid carbonaceous material in addition to sorbed organic and inorganic species.

Phase distributions of semi-volatile organic compounds (SVOC) in ambient airborne particles at equilibrium have been described by Yamasaki [5] and Pankow [6]. They define a partition coefficient, K_p, as

$$(1) \qquad K_p = F / (A \cdot P)$$

where F is the semivolatile organic compound (SVOC) particulate phase concentration in ng m^{-3} (determined from a filter), P is the concentration of total suspended particulate matter in

$\mu g\ m^{-3}$, and A is the SVOC vapor-phase concentration in $ng\ m^{-3}$, determined from an adsorbent (here, the IOVPS denuder). Temperature is an important factor in determining the phase distribution. The temperature dependence of K_p for PAH in ambient air as formulated by Yamasaki [5] is

$$(2) \qquad \log K_p = m/T + b$$

where m and b are the slope and intercept of the Yamasaki plots, respectively, for each PAH. The value of m reflects the enthalpy of volatilization. Plots of - log K_p vs. T^{-1} for three PAH in ETS from our chamber studies at temperatures ranging from 16.1 to 25.1 °C are linear (Figure 1), demonstrating that the Yamasaki relationship can be used to predict PAH phase distributions and exposures to ETS over a range of temperatures. The data illustrated in Fig. 1 were based on sampling during the first hour after smoking ended, for five separate experiments, three of which were conducted in the 36 m^3 chamber. The other two took place in the 20 m^3 chamber.

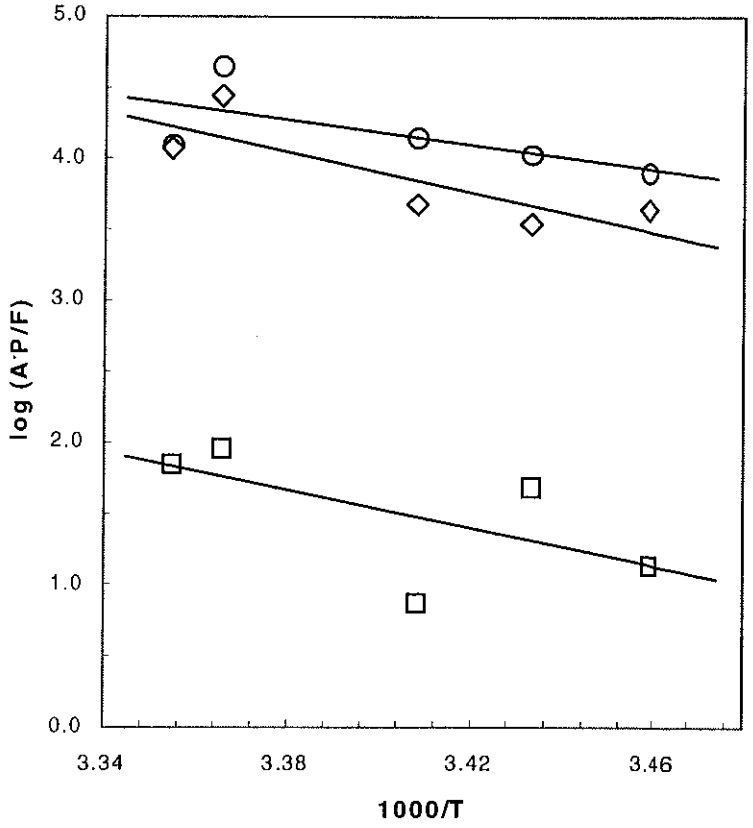

Figure 1. Arrhenius plots (-log K_p vs. $1000 \cdot T^{-1}$) for gas-particle partitioning in ETS over the temperature range 16-25°C. Data from five experiments: phenanthrene, circles o; pyrene, diamonds <>; and benz[a]anthracene, squares . The solid lines are linear least squares regression lines.

Aging of PAH in ETS. To investigate further the dynamic behavior of PAH in ETS, the phase distributions of several PAH were measured at half-hour intervals over a 3-hour period in the 36 m^3 environmental chamber under static conditions (air exchange rate = 0.04 hr^{-1}). Within the experimental uncertainties of the measurement, particulate PAH losses via deposition to

surfaces were similar to those measured for ETS particles. Deposition losses of the vapor-phase semi-volatile PAH were highly dependent upon vapor pressure - more rapid losses were observed for the higher molecular weight PAH. Phenanthrene, pyrene and benz(a)anthracene exhibited much faster decay in gas phase concentration than the more volatile species such as naphthalene and its methyl derivatives, as shown in Figure 2. The effect of these differential deposition rates is to change the relative proportions of the different vapor-phase PAH in ETS and thereby, the overall chemical composition of ETS. The values of K_p also increased over time due to more rapid losses of vapor- than particulate-phase PAH.

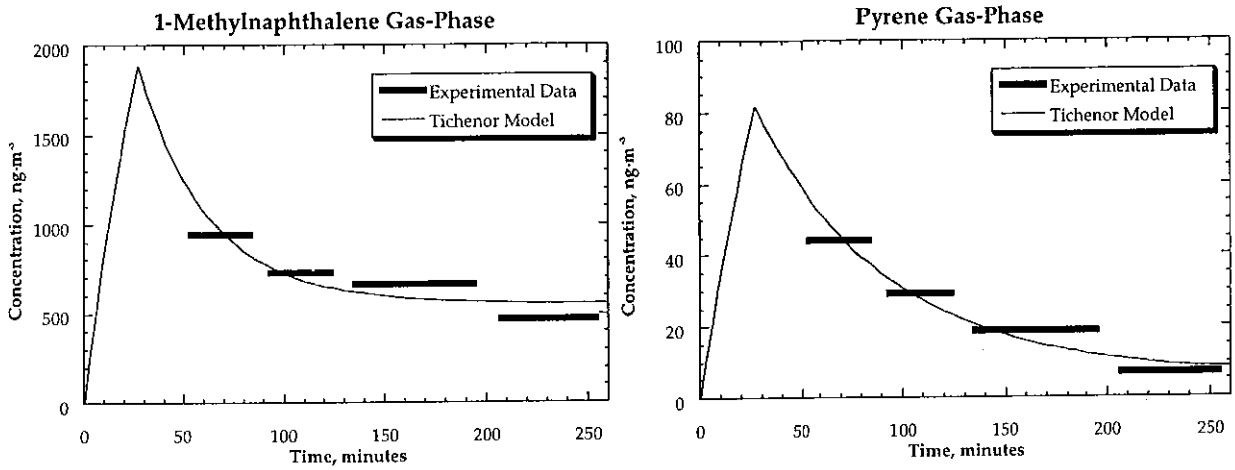

Figure 2. Decay of 1-Methylnaphthalene and pyrene in ETS, measured with the IOVPS in the 36 m^3 environmental chamber.

We applied the Tichenor model [7] to the concentrations of vapor and particle phase PAH measured over time. For the model, we used the sidestream smoke yields reported by Eatough [8] for the 1R4F cigarette to provide an estimate of the total (initial) emissions from the cigarettes. The dynamic behavior of some of the vapor-phase PAH appeared to fit this model, *i.e.*, there was an initial rapid deposition to the chamber surfaces, and then concentrations reached a quasi-steady state over the three hour period of the experiment, as shown in the figure.

Table 1. Size distribution of PAH in ETS at 18.3 °C

size range, µm PAH, ng/m^3 (18-62 min)	< 0.1 Filter	0.1-0.38 Stage 5	0.38-0.84 Stage 4	0.84-1.7 Stage 3	< 1.7 Sum
Phenanthrene	4.63	2.0	3.7	1.0	11.3
Anthracene	0.12	0.27	0.55	0.04	0.98
Fluoranthene	3.4	5.2	10.4	1.0	20.0
Pyrene	3.4	5.3	12.4	0.9	22.0
Benz(a)anthracene	9.9	3.8	9.5	0.2	23.4
Benzo(b)fluoranthene	10.2	1.7	5.4	≤0.2	17.5
Benzo(k)fluoranthene	2.8	0.60	1.3	≤0.03	4.7
Benzo(a)pyrene	3.2	1.3	2.2	≤0.1	6.8
Mass, µg/m^3 (18-62 min)	560	112	249	12	933
Mass, µg/m^3 (149-194 min)	304	61	256	18	639

Size distributions. Apparent bimodal size distributions were observed for the particulate PAH and mass at the temperatures shown in Tables 1 and 2. The mass measured with the quartz crystal microbalance did not show bimodal distributions. More recent measurements with the Hering impactor did not show bimodal mass distributions, and we suspect that the gap for stage 5 was smaller than intended for the data reported in Tables 1 and 2, thus possibly skewing the size cuts for stages 4 and 5. Nevertheless, the higher the MW of the PAH the more they were associated with smaller particles. The reported MMAD for ETS particle mass is ~ 0.2 μm [5]. At 25 °C, the concentrations of particulate PAH < 0.8 μm were significantly lower than at 18 °C, and the vapor-phase concentrations were higher at 25 °C.

Table 2. Size distribution of PAH in ETS at 25.1°C

size range, μm PAH, ng/m^3 (23-68 min)	< 0.1 Filter	0.1-0.38 Stage 5	0.38-0.84 Stage 4	0.84-1.7 Stage 3	< 1.7 Sum
Phenanthrene	10.6	1.1	3.8	≤0.5	15.5
Anthracene	0.22	0.02	0.29	≤0.02	0.53
Fluoranthene	1.9	1.1	3.2	1.2	7.4
Pyrene	2.0	2.0	4.7	0.7	9.4
Benz(a)anthracene	3.6	1.7	3.0	≤0.1	8.3
Benzo(b)fluoranthene	5.8	0.8	2.8	≤0.2	9.4
Benzo(k)fluoranthene	1.6	0.48	0.72	≤0.03	2.8
Benzo(a)pyrene	1.2	0.39	1.0	≤0.1	2.6
Mass, μg/m^3 (23-68 min)	356	170	219	12	757
Mass, μg/m^3 (155-200 min)	237	97	231	44	609

DISCUSSION

Semi-volatile PAH in fresh ETS followed the general features of gas/particle partitioning equilibrium theory. However, as the smoke aged, depositional losses to interior surfaces depleted the gas phase more rapidly than the particulate phase semi-volatile PAH. Depositional losses of the vapor-phase PAH were highly dependent on the PAH vapor pressure. The effect of these differential deposition rates is to change the relative proportions of vapor-phase PAH in ETS and thereby, the overall chemical composition of ETS. The values of the measured partitioning constant K_p also increased over time due to more rapid losses of vapor- than particulate-phase PAH.

Particle mass size distributions measured in recent experiments in our laboratory [9] do not show a dip in mass between 0.1 and 0.4 μm, as do the some of the data collected with the SSETS. We suspect that the apparent bimodal distribution in mass and PAH size distribution may be an experimental artifact. However, if the distribution proves to be bimodal after further investigation, the results would suggest that lung deposition for particulate PAH, such as benzo(a)pyrene, may be greater than predicted from ETS particle mass alone, and that previous lung dosimetry calculations for ETS might underestimate the doses of the biologically active components.

ACKNOWLEDGEMENTS

This work was supported by the National Heart Lung and Blood Institute, Public Health Service, Department of Health and Human Services, and by the Tobacco-Related Disease Research Program, University of California, through the U. S. Department of Energy, under Contract No. DE-AC03-76SF00098.

REFERENCES

1. Gundel, L A, Lee, V C, Mahanama, K R R, Stevens, R K and Daisey, J M. 1995. Direct determination of the phase distributions of semi-volatile polycyclic aromatic hydrocarbons using annular denuders, *Atmos. Environ.* Vol. 29, pp 1719-1733.

2. Mahanama, K R R, Gundel, L A, Daisey, J M. 1994. Selective fluorescence detection of polycyclic aromatic hydrocarbons in environmental tobacco smoke and other airborne particles, *Intern. J. Environ. Anal. Chem.* Vol. 56, pp 289-309.

3. Gundel, L A, Mahanama, K R R, Daisey J M. 1995. Semi-volatile and particulate polycyclic aromatic hydrocarbons in environmental tobacco smoke: Cleanup, speciation and emission factors, *Environ.Sci. Technol.* Vol. 29, pp 1607-1614.

4. Hering, S, Gundel, L and Daisey, J M. 1997. A microslot impactor for organic aerosol sampling, *J. Aerosol Sci.* Vol. 28, 1283-1290.

5. Yamasaki H, Kuwata K and Miyamoto H. 1987. Effects of ambient temperature on aspects of airborne polycyclic aromatic hydrocarbons. *Environ. Sci. Technol.* Vol. 16, pp 189-194.

6. Pankow, J F, Isabelle, L M, Buchholz, D A, *et al.* 1994. Gas/particle partitioning of polycyclic aromatic hydrocarbons and alkanes to environmental tobacco smoke. *Environ. Sci. Technol.* Vol. 28, pp 363-365.

7. Tichenor, B A, Guo, Z, Dunn, J E *et al.* 1991. The interaction of vapour phase compounds with indoor sinks. *Indoor Air*, Vol. 1 pp 23-35.

8. Eatough, D J, Benner, C L, Bayona, J M *et al.*, 1989. Chemical composition of environmental tobacco smoke, *Environ. Sci. Technol.*, Vol. 23, pp 679-687.

9. Apte, M G, Gundel, L A, Singer, B C et al., 1999. Indoor transport of ETS particles and tracers, Indoor Air 99, Eighth International Conference on Indoor Air Quality and Climate, Edinburgh, 8-13 August.

CHARACTERIZING ETS EMISSIONS FROM CIGARS: CHAMBER MEASUREMENTS OF NICOTINE, PARTICLE MASS, AND PARTICLE SIZE

N E Klepeis[1], M G Apte,[2] L A Gundel,[2] W W Nazaroff,[2,3] and R G Sextro[2]

[1]Environmental Health Sciences, School of Public Health, University of California at Berkeley USA. [2]Indoor Environment Program, Lawrence Berkeley National Laboratory, Berkeley, CA USA. [3]Department of Civil and Environmental Engineering, University of California at Berkeley USA.

ABSTRACT

We measured the environmental tobacco smoke (ETS) emissions (diluted sidestream plus mainstream tobacco smoke) from three types of cigars: regular, small plastic-tipped, and large premium. Fifteen experiments (nine using cigars and six using cigarettes) were conducted in a well-mixed 20 m^3 chamber with stainless steel walls. The cigars and cigarettes were both smoked by machine at a rate of two 35-ml puffs a minute. For each experiment, we collected filter samples to obtain total particle mass concentration. Integrated nicotine samples were collected on Tenax sorbent tubes, and nicotine analyses were performed using thermal desorption followed by GC-FID. Size-resolved particle measurements were made using a differential mobility particle sizer with a 0.01 - 0.5 μm diameter range. Emission factors for nicotine and total particle mass (for either milligrams emitted per gram of tobacco smoked or milligrams emitted per minute) were up to 6 times larger for cigarettes than for cigars.

INTRODUCTION

The characterization of emissions from sources of indoor air pollution is important in the fields of indoor air quality, exposure assessment, risk assessment, and epidemiology. A critical attribute of sources is the mass of pollutant emissions per unit of fuel consumed or per unit time. The latter is called the emission rate. Smoke exhaled by smokers and emitted from the burning end of a tobacco product, commonly called second-hand smoke or environmental tobacco smoke (ETS), is a major source of indoor pollution.

ETS emission data have been reported for cigarettes by a number of researchers (*1*). However, the available information on cigar ETS emissions appears limited to three studies. Two investigators have reported cigar ETS emission factors for carbon monoxide (*2*) and total particle mass (TPM) (*2, 3 as cited in 4*) and another investigator has reported concentrations for several compounds emitted from cigars that were smoked in an unventilated chamber (*5*). The need for more emissions data for cigars motivates the current study.

We conducted a series of controlled chamber experiments for the specific purpose of generating TPM and nicotine ETS emission data for three different types of cigars (premium, regular, and small). We measured the size distribution of ETS particles, since particle size is crucial in determining both the regional lung deposition and the dynamic behavior of particles in indoor air. All cigar results are compared to results for cigarettes smoked under identical conditions.

METHODS

Chamber Experiments. We conducted nine cigar (premium, regular, and cigarillo) and six cigarette (regular and lights) smoking experiments in an unventilated 20 m^3 chamber (< 0.1 air changes per hour). The chamber's interior surfaces consisted entirely of stainless steel.

In addition, two 4' x 8' sheets of upright gypsum wallboard (a total of 12 m^2 of exposed surface area) were placed vertically in the center of the chamber. The cigars were smoked by machine (ADL/II, Arthur D. Little, Inc., Cambridge, MA) at a rate of two 35-ml puffs per minute. Both sidestream and mainstream tobacco smoke were freely emitted into the chamber where they were mixed thoroughly by 6 small fans. For each experiment, we collected TPM on Teflon-coated glass fiber filters (sampling at ~18 liters/min), after smoking stopped over a sampling time period of between 30 and 60 min. Although nicotine in ETS is mostly in the vapor phase (*6*), we collected both particle and vapor-phase nicotine on a single Tenax sorbent tube (sampling at ~100 cm^3/min) just after smoking stopped for sampling time periods similar to those for the filters. The nicotine samples were analyzed by thermal desorption onto a GC with a flame ionization detector.

We determined TPM concentration gravimetrically by weighing the accumulated mass on each filter using a Cahn 25 precision electrobalance. Semi-continuous particle size measurements were made using a differential mobility particle sizer (TSI, Inc., St. Paul, MN), which scanned over 34 size bins in the range of approximately 0.01 to 0.5 μm in diameter.

Calculation of Nicotine and TPM Emission Factors. Our goal is to calculate apparent emission factors for nicotine and TPM. Emission factors are defined as the mass of pollutant emitted per unit mass of tobacco smoked [mg/g] or per unit of time [mg/min]. We use a well-mixed reactor model with terms for source emission, pollutant removal by ventilation, and pollutant removal by deposition:

$$V\frac{dC(t)}{dt} = E - AC(t) - KC(t) \qquad (1)$$

where V is the volume of the chamber [m^3], $C(t)$ is the pollutant concentration in the chamber at time t [mg/m^3], E is the pollutant emission rate [mg/min], A is the ventilation rate [m^3/min], and K is the deposition rate [m^3/min], which can be related to the deposition velocity, v_d [cm/s]. While ETS particles adhere to surfaces and are well described by the linear model in Equation 1, nicotine has been described by Van Loy et al. (*7*) using a nonlinear, reversible sorption model. They observed the nicotine concentration to decrease rapidly immediately following smoking, and subsequently begin a slower decay. Since Equation 1 neglects this initial, rapid nicotine loss, we expect our results for ETS to underestimate total nicotine emissions (see additional discussion below).

Since E, A, and K in Equation 1 are taken to be constant, the mass emitted, q, can be written as follows (for either TPM or nicotine):

$$q = E[t_2 - t_1] = V[C(t_2) - C(t_1)] + [A + K]\int_{t_1}^{t_2} C\,dt \qquad (2)$$

where $t = t_1$ is the time that smoking begins and $t = t_2$ is the time that smoking ends. In our case, we have $t_1 = 0$ and $C(0) = 0$, so that $C(t_2)$ is the peak pollutant concentration, C_{max}. In addition, the integral on the right-hand side of Equation 2 is equal to the average pollutant concentration, $\overline{C}$, between $t = t_1 = 0$ and $t = t_2$ multiplied by $t_2 - t_1 = t_2$. With an elapsed smoking time $t = t_2$:

$$q = VC_{max} + [A + K]\,\overline{C}\,t_2 \qquad (3)$$

Dividing q by the mass of tobacco smoked gives the mass-normalized emission factor [mg/g]. Dividing q by the source duration gives the emission rate [mg/min]. If the total removal rate ($A + K$) is fairly low, the concentrations determined from our integrated samples (taken immediately after smoking) are approximately equal to C_{max}, and the second term on the right-hand side of Equation 3 is likely to be small. We have included this term in our calculations by using half of the peak concentration, ½ C_{max}, to represent the mean pollutant concentration during smoking, $\overline{C}$, since the increase in C during the smoking episode is nearly linear.

RESULTS

The smoking times and calculation of the mass of tobacco smoked are summarized in Table 1. We determined the mass of tobacco smoked on a length basis (i.e., we multiplied the length smoked by the mass of tobacco per unit length of tobacco in the fresh product) to eliminate errors produced by changes in density of the unsmoked tobacco column. Estimates of the measurement uncertainty for concentrations of TPM and nicotine are 3% and 5%, respectively. The total removal rate $A+K$, as determined by exponential decay constants (first order), ranged from 0.04 to 0.08 m^3/min (mean of 0.06 m^3/min) for TPM and 0.08 to 0.16 m^3/min (mean of 0.12 m^3/min) for nicotine.

Table 1. Smoking Time and Mass Smoked for the Cigars and Cigarettes Used in This Study

Tobacco Product (N) [a]	Smoking Time, Ave (SD) [min]	Original Mass, [b] Ave (SD) [g]	Original Length, [b] Ave (SD) [mm]	Mass per Length, Ave (SD) [g/mm]	Length Smoked, Ave (SD) [mm]	Mass Smoked, [c] Ave (SD) [g]
Regular Cigar (5)	12.6 (1.8)	6.2 (0.26)	133 (0.44)	0.047 (0.002)	34 (5.0)	1.6 (0.21)
Premium Cigar (1)	13.2 (0)	16.3 (0)	181 (0)	0.09 (0)	14 (0)	1.3 (0)
Cigarillo (3)	13.2 (2.7)	2.7 (0.39)	105 (0)	0.026 (0.004)	44 (12)	1.12 (0.21)
Cigarette (5)	6.4 (0.8)	0.74 (0)	80.9 (0)	0.009 (0)	79.3 (0.13)	0.72 (0.001)

[a] Regular cigar = Swisher Sweets regular, premium cigar = Macanudo, cigarillo = Tiparillo (aromatic or mild blend), cigarette = Marlboro regular or Camel light. [b] These columns contain statistics for the mass and length of tobacco only – not including filters or plastic tips. [c] The mass smoked is calculated by multiplying the length smoked by the mass of tobacco per unit length of fresh tobacco. Abbreviations: N, sample size (number of trials); Ave, average; SD, standard deviation.

Total Particle Mass (TPM) and Nicotine Emissions. The ETS TPM emissions per unit mass of tobacco smoked [mg/g] for premium cigars, regular cigars, and cigarillos are, on average, approximately 50% of those for cigarettes (see Table 2). The nicotine emissions (mostly vapor) per unit mass of tobacco smoked for regular cigars and cigarillos are, on average, about one third of those for the cigarettes, and about one fifth of cigarettes for the premium cigar. The TPM emission rates [mg/min] for cigars are, on average, about one third to two thirds of those for cigarettes and the nicotine emission rates are, on average, about one sixth to one third of those for cigarettes. Since cigars typically contain more tobacco mass than cigarettes (up to 16 g for cigars and under 1 g for cigarettes; see Table 1), the TPM and

nicotine emitted by a fully smoked cigar is expected to be greater than that emitted from a single cigarette. ETS particles are all in the respirable size range (< 2.5μm), so TPM can be considered equivalent to respirable suspended particle (RSP) measurements.

Particle Size Distributions. The fitted geometric mean of the ETS particle-size distribution (the median particle size) measured just after smoking appears to be slightly smaller (by 0.025 μm) for regular cigars than for cigarettes (see Table 3). Cigarettes and cigarillos appear to have comparable geometric means. These results are based on only three experiments and should be considered preliminary. All three distributions were approximately lognormal and had similar fitted geometric standard deviations (1.6 to 1.7). Both cigar and cigarette generated particles were observed to coagulate with time. The observed GM of their respective size distributions was seen to increase by about 0.05 μm during the two hours after smoking ceased.

Table 2. Total Particle Mass (TPM) and Nicotine Emission Factors

Tobacco Product (N_{tpm}, N_{nic}) [a]	TPM Emission Factors, [b] Ave (SD) [mg/g]	TPM Emission Factors, [b] Ave (SD) [mg/min]	Nicotine Emission Factors, [b] Ave (SD) [mg/g]	Nicotine Emission Factors, [b] Ave (SD) [mg/min]
Regular Cigar (5,4)	5.7 (1.5)	0.75 (0.23)	0.41 (0.25)	0.052 (0.032)
Premium Cigar (1,1)	4.3 (0)	0.40 (0)	0.26 (0)	0.024 (0)
Cigarillo (2,1)	4.1 (0.45)	0.33 (0.11)	0.42 (0)	0.027 (0)
Cigarette (3,2)	10.3 (1.7)	1.1 (0.11)	1.3 (0.25)	0.14 (0.0052)

[a] Regular cigar = swisher sweets, premium cigar = Macanudo, cigarillo = Tiparillo (aromatic or mild blend), cigarette = Marlboro regular or Camel light. [b] Emission factors have the units of milligrams emitted per gram of tobacco smoked and milligrams emitted per minute. Abbreviations: N_{tpm}, sample size for total particle mass (TPM) determinations (number of trials); N_{nic} sample size for nicotine determinations (number of trials); Ave, average; SD, standard deviation.

Table 3. Particle-Size Distribution Immediately After Smoking Stopped

Tobacco Product [a]	Particle Size [μm] Fitted GM [b]	Particle Size [μm] Fitted GSD [b]
Regular Cigar	0.075	1.7
Cigarillo	0.094	1.6
Cigarette	0.10	1.6

[a] Regular cigar = Swisher Sweets regular, cigarillo = Tiparillo (aromatic or mild blend), cigarette = Marlboro regular or Camel light. Distribution statistics represent measurements taken from a single experiment. [b] The statistics GM and GSD were obtained from the lognormal fit to binned particle count data. Abbreviations: GM, geometric mean; GSD, geometric standard deviation.

DISCUSSION

The emission factors reported in this paper can be used to model the ETS exposure that humans receive. Through knowledge of (1) source activity (i.e., when and how many

cigarettes or cigars are smoked), (2) source emission factors, such as those presented in this paper, (3) receptor proximity (i.e., when and where the exposed person is present during smoking), and (4) building characteristics, reasonable estimates of human exposure can be made. Since the smoking of cigars has recently become more popular (*4*), it is important to understand how ETS emissions from cigars and cigarettes differ. Rather than look at total emissions, in which case a single cigar would typically have greater emissions than a single cigarette, we use normalized quantities such as the amount of emissions per unit mass of tobacco smoked to compare the source strengths of different tobacco products. These quantities can be used to calculate the resulting emissions after an arbitrary portion of a cigar (or cigarette) has been smoked.

In the present study, we have smoked cigars and cigarettes in an identical manner and under identical room conditions. This methodology increases our confidence in making comparisons between the two different sources.

Calculations of apparent ETS nicotine emission factors that don't account for rapid sorption of nicotine, such as ours and those of Daisey et al. (*1*), underestimate nicotine emissions. For example, Daisey et al. (*8*) report total sidestream nicotine emissions of 5.35 mg/cigarette or about 7–9 mg/g (assuming 0.6–0.7 g of tobacco smoked per cigarette). However, while our apparent emission factors do not describe absolute nicotine emissions, they can still be useful for comparisons and predictions of exposure under conditions similar to those in our study.

Table 4. Comparison of Particle Mass and Nicotine Emissions to Those from Other Studies

Study	Source Type [b]	Particle Mass Emission Factor, [a] Ave (SD) [mg/g]	Nicotine Emission Factor, [a] Ave (SD) [mg/g]
This Study	3 Cigars	5.2 (1.4)	0.39 (0.20)
CPRT (*3*)	13 Cigars	10.3 (2.4)	0.13 (0.08)
Klepeis et al. (*2*)	2 Cigars	8.1 (0.14)	-
Nelson et al. (*5*) [c]	6 Cigars	6.4 (4.1)	-
This Study [d]	2 Cigarettes	10.3 (1.7)	1.3 (0.25)
Daisey et al. (*1*)	6 Cigarettes	12.4 (1.3)	1.4 (0.26)

[a] Emission factors in this table have the units of milligrams emitted per gram of tobacco smoked. [b] The number of different types of cigars or cigarettes used in the study. [c] Mass emission factor obtained from presentation slides (*5*). Nicotine emission factor unavailable. [d] Only 1 type of cigarette was used for nicotine statistics
Abbreviations: Ave, average; SD, standard deviation.

The normalized, apparent cigarette emission factors [mg/g] that we determined for both TPM and nicotine are comparable to those determined using a similar method by Daisey et al. (*1*) (see Table 4). The emission factors we determined for cigars are clearly much lower than those determined for cigarettes. The work by CPRT (*3*) suggests even lower nicotine emission factors for cigars than for cigarettes, but particle mass emission factors that are comparable to what has been obtained for cigarettes. In addition, Klepeis et al. (*2*) report particle mass emission factors for two premium cigars that are approximately 80% of those for cigarettes.

From the above comparisons between different studies, it appears as though cigar brand and/or smoking style (two principal variants within and/or between these studies) may be important factors in determining emissions of particles. While normalized nicotine emissions seem to always be lower for cigars than for cigarettes, particle mass emissions can range from being approximately equal to emissions for cigarettes to being half those of cigarettes.

ACKNOWLEDGMENTS

This work was supported with funds from the California Tobacco-Related Disease Research Program, Grant Number 6RT-0307, and by the Assistant Secretary of Conservation and Renewable Energy, Office of Building Technologies, Building Systems and Materials, Division of the U.S. Department of Energy (DOE) under Contract DE-AC03-76SF0098. We would like to express our appreciation for the invaluable technical assistance of D. Sullivan. S. Baker assisted with sample preparation and experimental procedure, and B. Singer assisted with sample analysis. A. Hodgson also contributed important knowledge and expertise.

REFERENCES

1. Daisey JM, Mahanama KRR, and Hodgson AT (1998) Toxic volatile organic compounds in simulated environmental tobacco smoke: emission factors for exposure assessment *J. Expos. Anal. Environ. Epidemiol.* 8(3): 313-334.
2. Klepeis NE, Ott WR, and Repace JL (in press) The effect of cigar smoking on indoor levels of carbon monoxide and particles *J. Expos. Anal. Environ. Epidemiol.*
3. CPRT Laboratories, Inc. (1990) Development of Methods for the Characterization of Toxic Constituents in Cigars, Pipe Tobacco, and Smokeless Tobacco. Tobacco Branch, Health Canada. SSC Contract #H4078-1-C230/01-SS. Cited on pages 169 and 178 in reference number 4.
4. NCI (1998) Cigars: Health Effects and Trends, Monograph 9, Bethesda: National Institutes of Health, National Cancer Institute.
5. Nelson PR, Kelly SP, and Conrad FW (1997) Generation of environmental tobacco smoke by cigars. Presented at the 51st Tobacco Chemists' Research Conference. Winston-Salem, NC, September 14-17, p. 15. Cited on page 102 in reference number 4.
6. Gundel LA and Lane DA (1998) Sorbent-Coated Diffusion Denuders for Direct Measurement of Gas/Particle Partitioning by Semi-Volatile Organic Compounds. Final Report LBNL-41278. Berkeley: Lawrence Berkeley National Laboratory, Environmental Energy Technologies Division.
7. VanLoy MD, Lee VC, Gundel LA, Daisey JM, et al. (1997) Dynamic behavior of semivolatile organic compounds in indoor air 1. Nicotine in a stainless steel chamber *Environ. Sci. Technol.* 31(9): 2554-2561.
8. Daisey JM, Mahanama KRR, and Hodgson AT (1994) Toxic Volatile Organic Compounds in Environmental Tobacco Smoke: Emission Factors for Modeling Exposures of California Populations. Final Report. Contract Number A133-186. LBL Report No. 36379. Sacramento: California Air Resources Board.

III. EXPOSURE AND HEALTH RISK ANALYSIS

VOCS AND "SICK BUILDING SYNDROME": APPLICATION OF A NEW STATISTICAL APPROACH FOR SBS RESEARCH TO U.S. EPA BASE STUDY DATA

M. G. Apte and J. M. Daisey

Indoor Environment Department, Lawrence Berkeley National Laboratory, Berkeley, CA, USA

ABSTRACT

Causal associations between "Sick Building Syndrome" (SBS) symptoms and specific environmental stressors were explored using a recently developed approach employing Principal Components Analysis (PCA) and Logistic Regression [1]. This approach was applied to data collected by the U.S. EPA from 1995 to 1996 in 28 large U.S. office buildings in the Building Assessment Survey and Evaluation study. PCA was used to apportion measurements of 13 VOC species and carbon monoxide into source-related vectors. A reduced set of four source-based exposure vectors, tentatively identified as photocopiers, automotive emissions, environmental tobacco smoke, and latex paints were derived from the data. Regression analyses indicate statistically significant associations between mucous membrane related symptoms and the PCA photocopier vector (odds ratio=1.2, p=0.04), after adjustment for age, gender, smoking status, presence of carpeting, and thermal exposure. Similar relationships (odds ratio=1.2, p=0.03) were found between sore throat symptoms and the PCA paint vector. Odds ratios are given per unit increase in PCA vector which range over 5-6 units.

INTRODUCTION

Causal associations between "Sick Building Syndrome" (SBS) symptoms and specific environmental stressors have been elusive. Although volatile organic compounds (VOCs) are suspected to be significant contributors to SBS, field studies to demonstrate this relationship have not generally proven successful. Ten Brinke, et al. [1] recently reported a new approach to develop exposure metrics for VOCs that were statistically significant predictors of SBS symptoms reported in the California Healthy Buildings Study. The method utilizes Principal Component Analysis (PCA) to group correlated VOCs into a reduced set of Principal Component vectors (PCs) that are associated with sources. The PCs are then used in a logistic regression analysis to estimate the association between SBS symptoms and these exposure metrics (the calculated PC scores), while adjusting for other building-environmental and occupant-related covariates. This approach has now been applied to a second set of VOC measurements and self-reported SBS symptom data, a subset of the Building Assessment Survey and Evaluation (BASE) study, collected by the U.S. EPA in 1995 and 1996 in 28 large U.S. office buildings.

METHODS

The data analyzed in this paper were collected in 28 large U.S office buildings in 1995 and 1996, a subset of 100 buildings studied from 1994-1998 by the U.S. EPA in the BASE study [2]. These 100 buildings were selected at random to be a representative sample of the nation's office building stock, however at the time that the analyses were conducted, only the '95-'96 data were available and suitable for this analysis. These 28 buildings are located in 11 states (AZ, CA, CO, FL, LA, NE, NV, PA, SC, TN, and TX). Their individual studies

were carried out during one-week periods of the winter, spring, or summer months. The BASE protocol includes the collection of an exhaustive database on the physical characteristics of the buildings' construction and HVAC systems; extensive indoor and outdoor environmental monitoring data from a selected space within each building. Data were also collected via questionnaire from all study space occupants within each building. The questionnaire collected information on the occupants' perceptions of their workplace environments, job characteristics, and health and well-being (including symptoms associated with SBS). The BASE study protocol is described in detail elsewhere [2].

VOC samples were collected over 9-hours in canisters and analyzed by gas chromatograph-mass spectrometry for 56 VOC species. Thirteen of the VOCs (Table 1) were selected for inclusion in the present analyses, based upon literature of indoor or outdoor sources common to office buildings, and their similarity to those used in the analyses of Ten Brinke et al. [1].

Nine-hour time-weighted-average (TWA) indoor VOC and indoor minus outdoor CO (ΔCO) concentrations were averaged across the three indoor measurement sites for the Wednesday measurements at each building. A value of half of the limit of detection (LOD) was used to replace values reported as below LOD for individual VOC species. A value of 0.5 ppm was applied to CO data reported below LOD. Table 1 summarizes the VOC and ΔCO data. Thermal exposure (°C-hours) was calculated for each building, as the integrated difference between 5-minute-average-temperature and 20°C, averaged over 3 indoor locations and 2 measurement heights, and normalized to 10-hours of exposure.

Table 1. The geometric mean and standard deviation (GM,GSD), minimum, and maximum 9-hr TWA indoor VOC concentrations for the 28 '95-'96 BASE buildings are shown. Common sources of these VOCs derived from the literature are listed.

Compound	CAS No.	GM (ppb)	GSD	Min (ppb)	Max (ppb)	Common Sources[a]
styrene	100-42-5	0.21	1.5	0.10	1.2	1,2,3,4,13
a-pinene	2437-95-8	0.19	2.5	0.05	0.7	5,6
2-butanone	78-93-3	1.4	2.5	0.23	9.0	7,11,12
1,4-dichlorobenzene	106-46-7	0.13	2.7	0.05	2.4	6,8
toluene	108-88-3	4.8	2.5	1.5	97	1,2,9,11
ethylbenzene	100-41-4	0.38	2.5	0.14	2.6	1,2,3,9
1,2,4-trimethylbenzene	95-63-6	0.63	2.3	0.12	4.7	1,2,4,9
m&p-xylenes	1330-20-7	1.6	2.7	0.24	8.2	3,9,11
n-undecane	1120-21-4	1.2	2.2	0.33	3.6	1,2,4,5,10,14
4-methyl-2-pentanone	108-10-1	0.38	3.2	0.10	15	11
butyl acetate	123-86-4	0.63	3.3	0.13	6.9	7,11,12,14
d-limonene	5989-27-5	0.66	2.6	0.08	6.3	2,5,6,13
ethyl acetate	141-78-6	0.70	2.7	0.11	7.1	7,14
ΔCO (indoor-outdoor, ppm)	630-08-0	0.02	5.7	0.00	4.3	9,13,16

[a]1=Carpet; 2=Undercarpet; 3=Photocopier; 4=Building Materials, 5=Cleaners; 6=Deodorants; 7=Solvent; 8=Air Fresheners; 9=Automotive sources; 10=Latex Paint; 11=Solvent-Based Paints; 12=Spray Paints; 13=Environmental Tobacco Smoke; 14=Adhesives; 15=Inks; 16=Unvented Combustion Sources.

The BASE Study occupant questionnaire was used to derive SBS symptom prevalences (Table 2). These include upper respiratory and mucous membrane (MM) irritation, including the eyes, nose, and throat; chest tightness, difficulty breathing, cough, or wheezing; fatigue;

headache; eye strain; and dry or itchy skin. SBS symptoms are those which are reported to occur when the occupants are in the building and decrease when they leave. In order to qualify as a SBS symptom, the occupant must have reported it to have occurred at least 1-3 days per-week during the month previous to the study.

Table 2. Sick Building Syndrome (SBS) symptoms and average prevalence across 28 BASE '95-96 buildings.

SBS Symptoms	Avg. Prevalence(%)
Mucous Membrane Symptoms (Combined)	30
dry, itching, or irritated eyes	22
sore or dry throat	8.3
stuffy or runny nose, sinus congestion	15
Chest Tightness or Difficulty Breathing	8.2
chest tightness	2.2
shortness of breath	2.3
cough	5.9
wheezing	2.4
Fatigue or Sleepiness	
unusual tiredness, fatigue, or drowsiness	17
Headache	18
Tired or strained eyes	5.1
Dry or itchy skin	5.0

The approach using PCA to derive exposure metrics has been discussed thoroughly by Ten Brinke et al. [1]. In brief, the object of PCA is to convert a set of highly correlated variables (i.e., measured VOC species in office buildings), into a reduced number of uncorrelated vectors which are linearized sums (principal components) of *standardized* individual variables (i.e., normalized between ±1). These PCs represent source types or building materials which emit VOCs, since species originating from the same types of sources tend to co-vary in concentration from one building to the next. Some VOC species can originate from more that one source, so it is possible that they will be associated with more than one PC. Thus, the PCA method is useful because it can apportion the VOC contributions from different source groups. It should be noted that since the PCs represent particular groups of sources, it is likely that they correlate with other (possibly unmeasured) compounds emitted from those sources. In these analyses, PCA correlation matrix eigenvalues of the PCs were used to determine the extent of the PCs interpretability, with a cutoff criterion of ≥ 1.0 used to determine the PCs to be kept in the analysis.

Multivariate logistic regressions (MLR) [3] were used to assess associations between SBS symptoms and both individual VOCs and the PCA-based exposure metrics. Both crude bivariate and multivariate models were adjusted for other risk potential risk factors and confounders. The SBS symptom/environmental exposure associations are presented as odds ratios (OR).

RESULTS AND DISCUSSION

The average (min-max) of informative physical and demographic characteristics needed for this paper follow. Further details for BASE '95-'96 can be found elsewhere [2]. Occupied floor area of buildings (m^2): 17,000 (1,700-54,000); typical building occupancy (persons): 1460 (95-7130); average cooling degree days (°C-days): 1000 (180-2200); average heating degree days (°C-days): 2000 (100-3500); gender of survey responders (% male): 29 (6-70); survey age group mode (years): 40-50; survey participants per building (N): 50 (23-123); RH (%): 33 (10-49); thermal exposure (°C-hours): 33 (7-49); overall prevalence of ever smokers (42.3%); overall prevalence of carpeted workspaces (21.1%). All of the buildings had at least some air-conditioned spaces. The prevalence of operable windows in the buildings was as follows: 60% had 0% operable, 28% had at least 50% operable, and 17% had 100% operable. Some smoking areas were allowed in 32% of the buildings, 1 (4%) building had no smoking

Table 3. Results of Principal Components Analysis on VOCs and Carbon Monoxide from the 28 '95-'96 BASE Study Buildings

Compounds	Principal Components 1	2	3	4	Communality
styrene	**0.91**	0.16	-0.08	-0.07	0.94
a-pinene	0.19	-0.04	0.18	-0.11	0.98
2-butanone	**0.83**	0.32	-0.18	-0.02	0.95
1,4-dichlorobenzene	0.18	-0.02	-0.04	0.03	1.00
toluene	**0.83**	**0.45**	0.07	0.00	0.94
ethylbenzene	**0.38**	**0.90**	0.11	-0.01	0.98
1,2,4-trimethylbenzene	**0.66**	**0.64**	0.25	-0.01	0.91
m&p-xylenes	**0.39**	**0.86**	0.15	-0.04	0.95
n-undecane	0.00	0.14	0.09	-0.08	0.99
4-methyl-2-pentanone	-0.07	-0.02	-0.05	**0.97**	0.97
butyl acetate	0.25	0.63	0.40	**0.52**	0.90
d-limonene	0.11	0.07	**0.94**	-0.01	0.93
ethyl acetate	**0.91**	0.22	0.19	0.05	0.94
Indoor – Outdoor CO (ΔCO)	-0.08	0.25	**0.91**	0.00	0.91
Variance (%)	30	21	16	9	Total=66%
Probable Identity of Source:	Photo-copier	Motor Vehicles	Tobacco Smoke	Paint	

restrictions, while smoking was observed in 3 (16%) of the buildings where it was prohibited.

Table 3 presents the results of the PCA analysis for the VOCs in Table 1. Based upon the PC loading patterns and source information from the literature (Table 2), the sources were identified as emissions from photocopiers, motor vehicles outdoors, indoor environmental tobacco smoke (ETS), and latex paints for PC#s 1-4, respectively. PC #1 may also include emissions from under-carpeting or other building materials. PC #3 was identified as environmental tobacco smoke because of the clear correlation between elevated indoor CO and d-limonene levels. The BASE database showed that the buildings with elevated ΔCO and d-limonene also either allowed smoking or had notations regarding observations of unsanctioned smoking activity.

Relative humidity (RH) was found to be significantly correlated ($r = 0.6$, $p = 0.0001$) with 1,2,4 trimethylbenzene (TMB) and PC#1. Humidity levels affect the rates of VOC emissions from materials. Also, due to the obvious dehydrating effects of low RH, especially on MM symptoms, humidity is likely an effect modifier in the VOC-symptom relationship. For these reasons it was deemed inappropriate to directly include RH in the statistical models. The various MLR analyses discussed below were conducted with RH < 20% excluded. The number of observations in these analyses averaged 820±18.

MLRs of individual VOCs against the individual and grouped BR symptoms, after controlling for age and gender, were conducted, and only TMB and 2-butanone (2BU) showed significant positive associations. The TMB associations, per ppb increase, were: grouped MM, OR = 1.14 (p=0.04); dry eyes, OR = 1.12 (0.08); wheezing, OR = 1.27 (0.1). 2BU was found to be associated with grouped MM, OR = 1.09 (0.03); and dry eyes, OR = 1.08 (0.09)).

MLRs were conducted to investigate the association between the SBS symptoms and the PCA source emissions vectors. The models included the 4 VOC vectors (PC #1-4), categorical age, gender, thermal exposure, ever smoker, and presence of carpet in workspace. Statistically

significant ($p \leq 0.1$) results are presented in Table 4. The photocopier source is associated with the MM symptoms (OR = 1.17, p = 0.01), especially those of dry and irritated eyes, and stuffy/runny nose and sinus congestion. The association between the photocopier source vector and MM symptoms is biologically plausible. This PC vector contains a number of constituents known to be highly irritating to the respiratory tract. The irritancy of styrene, ethyl acetate, TMB, and m&p-xylene, relative to toluene are 7.9, 7.6, 3.6, and 3.4, respectively [1].

The Latex Paint vector was found to be significantly associated with sore throat (OR = 1.22, p = 0.03), and with chest tightness (OR = 1.33, p = 0.08). Associations between the "Cleaning products & water-based paints" vector and these SBS symptoms was also observed in the Ten Brinke et al. analyses (Throat OR = 1.8, 95% CI = 1.1-3.1; Chest Tightness OR = 1.8, 95% CI = 0.8-4.0). The major component in this vector is butyl acetate, with irritancy relative to toluene being a factor of 6.3 greater.

Statistically significant "protective" associations (those with OR < 1) with a number of symptoms are observed for the ETS source vector. This may be due to some confounding effect or misidentification of the source. If the d-limonene vector actually represents cleaning and deodorizing agents, it is possible that the "protective" association may indicate a positive effect of cleaning activities in reducing overall symptoms. Finally, the analyses indicate an OR of 1.2 for the association between the "tired or strained eyes" symptom and the Motor Vehicle source metric.

Table 4. Association[1] between Principal Component-derived VOC Exposure Metrics and Sick Building Syndrome (SBS) Symptoms in the 28 '95-'96 BASE Study Buildings.

SBS	VOC Exposure Metric[2] [Odds ratio (95% Confidence Interval)]			
Symptom	1 (Photocopier)	2 (Motor Vehic.)	3 (ETS)	4 (Latex Paint)
MM Combined	1.17 (1.04-1.33)		0.84 (0.74-0.96)	
Dry eyes	1.13 (0.99-1.28)		0.83 (0.70-0.97)	
Sore Thrt.				1.22 (1.02-1.47)
Nose/sinus	1.15 (0.99-1.33)			
Chest/breath.				
Chest tight.				1.31 (0.97-1.77)
Short breath				
Cough				
Wheeze				
Fatigue			0.86 (0.73-1.02)	
Headache				
Tired eyes		1.22 (1.06-1.39)	0.82 (0.71-0.95)	
Dry/itchy Skin				

[1] Controlled for Age, Gender, Thermal Exposure, Tobacco User, and Carpet in Workspace. All buildings with average relative humidity ≥ 20%

[2]The listed VOC sources are tentative "best guesses" based on available information.

It should be noted that as with the individual VOC analyses, gender was almost always a significant parameter in the models, with females 1.5 to 6 times more likely to report the SBS symptoms. Thermal exposure was significantly associated with the MM and respiratory symptoms, indicating that symptoms were slightly reduced (OR range = 0.95 to 0.99, p always < 0.1) with exposures above 20°C.

The above results should be interpreted with caution. The OR is defined by the ratio of odds of having a symptom to the odds of not having it, *per unit change* in exposure or risk factor. For the individual VOC analyses the units are merely per- 1 ppb increase in TWA (i.e. the odds of perceiving symptoms increase by a factor of 1-OR per 1ppb exposure increase). For example the 95th percentile TMB concentration is 2.7 ppb, and the OR for wheezing increases from 1.3 to 1.9. In the case of the PCA-based exposure metrics where the unit change of the metric is a composite vector of standardized components, the interpretation is complicated. These vectors range over 5 to 6 units. A comparison with the magnitude of the ORs in the individual VOC analysis indicates that the unit change may be roughly of the same order for the PCA-based associations. Nonetheless, the associations observed help provide one line of evidence regarding specific VOC sources that may be factors in SBS symptoms.

CONCLUSIONS

The application of the new PCA-based technique for developing source-based exposure metrics was successfully applied to a second set of indoor VOC data. Four source-based exposure vectors, tentatively identified as photocopiers, automotive emissions, environmental tobacco smoke, and latex paints were derived from the data. These metrics, which collapsed data from 13 VOC species into four vectors, were useful in conducting logistic regression analyses to identify associations between exposure and SBS symptoms. The regressions indicate statistically significant associations between mucous membrane related symptoms and the PCA photocopier vector, after adjustment for age, gender, smoking status, presence of carpeting, and thermal exposure. Similar relationships were found between sore throat symptoms and the PCA paint vector. Although the PCA was able to apportion the measured VOC species into several meaningful vectors, exact source identification was difficult due to the wide use of organic materials in man-made environments. Further work in this area should include enlargement of the analyses to include all 100 of the BASE Study buildings, to apply irritancy factor weightings to the VOC analyses, and to further develop VOC source fingerprints for materials in order to better specify the identity of the exposure metrics.

ACKNOWLEDGEMENTS

We would like to thank Susan Womble and Laureen Burton, and the US EPA Office of Air and Radiation for making the data used in this study available. Thanks also go to Al Hodgson and to Olli Seppänen for their reviews of this work. This work was supported by the Assistant Secretary of Energy Efficiency and Renewable Energy, Office of Building Technologies, State and Community Programs, U.S. Department of Energy (DOE) under Contract DE-AC03-76SF00098.

REFERENCES

1. Ten Brinke, J., Selvin, S, Hodgson, A. T., Fisk, et al. 1998. Development of new VOC exposure metrics and their relationship to "Sick Building Syndrome" symptoms, *Indoor Air,* Vol. 8.
2. Womble, S. E., Ronca, E. L., Girman, J. R., and Brightman, H. S. 1996. Developing Baseline Information on Buildings and Indoor Air Quality (Base '95). In *IAQ 96/Paths to Better Building Environments/Health Symptoms in Building Occupants,* Atlanta: American Society of Heating Refrigeration and Air-conditioning Engineers, Inc.
3. SAS. 1989. *SAS/STAT user's guide, Version 6,* 4th ed., Cary NC: SAS Institute.
4. D G Kleinbaum, L L Kupper, H Morgenstern. 1982. *Epidemiologic research : principles and quantitative methods.* Belmont, CA: Lifetime Learning Publications.

INDOOR AIR QUALITY, VENTILATION AND HEALTH SYMPTOMS IN SCHOOLS: AN ANALYSIS OF EXISTING INFORMATION

Joan M. Daisey[1] and William J. Angell[2]

[1]Indoor Environment Department, MS: 90-3058, Lawrence Berkeley National Laboratory, Berkeley, CA 94720, U.S.A.
[2] Indoor Air Quality Project, Minnesota Extension Service, University of Minnesota, St. Paul, MN 55108, U.S.A.

ABSTRACT

Existing information on indoor air quality (IAQ), ventilation, and building-related health problems in schools was critically reviewed. Asthma and "sick building syndrome" (SBS) symptoms were the most commonly reported health symptoms reported in the literature. Although there is evidence that ventilation rates in many schools do not meet minimum standards, ventilation rates and CO_2 concentrations have generally proven to be poor surrogates for assessing exposure to the specific agents causing health symptoms. Studies to date indicate that exposures to volatile organic compounds (VOCs) and to molds and allergens in schools are related to asthma, SBS and other respiratory symptoms. However, there have been very few studies in which relations between symptoms and exposures to multiple pollutants were investigated.

INTRODUCTION

Existing information on IAQ, ventilation, and building-related health problems in schools were critically reviewed and analyzed, with emphasis on U.S. (California in particular), Canadian, and European schools. The objectives of this review were to:

1. Identify the most commonly reported building-related health symptoms for schools;
2. Assemble and evaluate existing measurement data on ventilation rates and CO_2 concentrations;
3. Evaluate evidence for causal relationships between indoor pollutant exposures and symptoms in schools.

A more detailed report on this review, with bibliography, is available upon request [1].

METHODS

Over 600 publications were identified through computer searches of bibliographic databases. About 450 publications were obtained and reviewed, including 77 Health Hazard Evaluation Reports (HHERs) from the National Institute for Occupational Safety and Health (NIOSH) on investigations on IAQ and health complaints in schools. Seventy reports on IAQ investigations in California schools were obtained through requests for information to state authorities.

RESULTS AND DISCUSSION

Building-Related Health Symptoms Reported in Schools

The types of health complaints cited in requests for school investigations in 53 NIOSH HHERs and 35 California school IAQ investigations were analyzed to identify the most common symptoms in complaint schools. Symptoms from the California school investigations were classified according to the NIOSH questionnaire. In general, the types of symptoms reported in the NIOSH HHERs and the California schools investigations were similar to those defined as SBS, *i.e.*, eye, nose, throat irritation, chest tightness, headaches, fatigue, dry or itchy skin. This may be partially due to the type symptom questionnaires used in the HHERs. Symptom complaints for many of the school studies reported in scientific journals were also similar to SBS symptoms. In addition, studies reported in the scientific journals were often conducted to elucidate the school-related causes of asthma and of SBS.

Ventilation Rates and CO_2 Concentrations

Although "inadequate" ventilation has often been suggested as a cause of SBS symptoms, outside air ventilation rates have rarely been measured in schools. A minimum ventilation rate of 7 L/s-person is recommended for classrooms, about 3 air changes per hour (ACH) for a typical classroom [2]. Carbon dioxide concentration is commonly used as a surrogate of the rate of outside air supply per occupant, with concentrations above ~1000 ppm CO_2 generally regarded as indicative of inadequate ventilation rates.

Nielsen [3] reported an average ventilation rate of 6.4 L/s-person with a range of 1.8 - 15.4 L/s-person in a random selection of 11 Danish schools in 1984. This study indicated that a ventilation rate of about 10 L/s-person is required for 80% of the pupils to describe the air quality as satisfactory. In 1989, Turk et al. [4] reported that two out of six non-complaint schools in the U.S. Pacific Northwest had *whole building* ventilation rates below the current recommended minimum. The largest set of ventilation rate measurements was for 14 California schools [5]. It is probably reasonably representative, although not a randomly selected set of schools. The median air change rate for these schools was 2.24 ACH and ranged from 0.6 to 7.49 ACH. Nine of the 14 schools had air change rates below 2.5 ACH. The schools built or retrofitted after 1987 had lower total air change rates (by an average of 30%) than those built or retrofitted before that year. Ventilation rates reported for U.S. schools with high radon concentrations are also generally below the recommended rate.

Concentrations of CO_2 have been measured more commonly than ventilation rates. Forty-four of the HHERs reported CO_2 measurements. In 32% (14/44) of these schools, half or more of the CO_2 measurements were greater than 1000 ppm. Twenty-one of the California school IAQ investigations reported CO_2 measurements, with a range of 300 ppm to 4,000 ppm CO_2, and one measurement of 11,500 ppm CO_2. The CO_2 concentrations were often in excess of 1000 ppm in portable classrooms that had no outdoor air intakes or had ventilation systems that were off, with windows and doors closed due to fan or outdoor noise. Smedje, *et al.* [6] reported the average and range of indoor CO_2 concentrations for 96 classrooms in 38 Swedish schools, randomly selected from 130 Uppsala public schools. Sixty-one percent of the schools had mechanical supply and exhaust systems; the remainder had natural ventilation. The average concentration of CO_2 for the 38 schools was 990 ppm. CO_2 concentrations were above 1000 ppm for 41% of the measurements, with a maximum concentration of 2,800 ppm.

Air Pollutants in Schools

The most commonly measured air pollutants in schools were volatile organic compounds (VOCs), including total VOCs (TVOC), formaldehyde and microbiological pollutants. Very few of these studies involved investigations of the relationships between symptoms and measured pollutant exposures. TVOC measurements were reported in 27 of 77 HHERs. Many of these were below the limits of detection or were similar to typical indoor concentrations in homes, about 0.5 mg/m^3. In a only a few HHERs were TVOC concentrations reported that were in the range in which SBS symptoms might be expected, i.e., $\geq$ 2-3 mg/m^3 [7]. For the California schools, there were only a few TVOC measurements; the highest TVOC concentration was 2.9 mg/m^3 for a portable classroom. Formaldehyde measurements were reported for only 15 of the 77 HHERs investigations. Of his set, < 20% exceeded 0.05 ppm. For 14 California schools, of the 57 measurements made using a method with an adequate lower limit of detection, only 4 were above 0.05 ppm; none was above 0.1 ppm.

Table 1 summarizes the averages and ranges of TVOC and formaldehyde concentrations reported in scientific journals for some *non-complaint* schools. The median TVOC concentration was surprisingly high for the Italian nurseries and kindergartens and might have induced SBS symptoms [7]. Although average formaldehyde concentrations in the Italian and French schools were generally near 0.05 ppm, concentrations in some schools were high enough to cause irritant symptoms.

Table 1. Some Measurements of TVOC and Formaldehyde Made in Non-Complaint Schools

Measurements made in:	**TVOC, mg/m^3**		**Formaldehyde, ppm**	
6 Swedish primary schools, 36 classrooms [8]	Average 0.13	Range of 6 averages 0.07 - 0.18	-	-
10 Italian schools [9]:	Medians:	Range:	Average:	Range:
Nurseries & kindergartens (16 samples):	3.6	0.28 - 11.3	0.065	0.008-.137
Primary & secondary (24 samples):	0.26	0.005 - 13.6	0.067	0.006 - 0.171
10 schools in Paris, 6 primary and 4 nursery schools [10]	Average: 1.0	Maximum: 1.7	Average: 0.049	Range: 0.005 - 0.20

The major classes of microbiological pollutants considered in this review were: (1) bacteria; (2) allergens, including house dust mite, cat and dog allergens, and (3) fungal spores. Commonly available sampling and analysis methods limit our ability to characterize exposures to these agents to adequately understand their influence on health outcomes.

One of the largest databases of measurements of airborne bacteria is for 150 classrooms in 40 California complaint schools [11]. The average airborne bacterial count for these classrooms when occupied was 2,345 colony forming units (CFU)/m^3, with a maximum of 18,432 CFU/m^3. These data suggest that these schools did not have the ventilation rates needed to remove and dilute the indoor concentrations of airborne bacteria and viruses that can cause infectious diseases.

Most studies of health symptoms and pollutant exposures in classrooms have used surrogates of exposure (*e.g.*, presence of molds on walls), have measured a single pollutant, or have assumed that whatever mitigation measures were taken were effective in reducing or eliminating symptoms. We found only three epidemiological studies in schools in which multiple logistical regression analysis was used to more rigorously examine relationships between health symptoms and measured exposures to more than one pollutant. Table 2 summarizes key features of these studies.

Table 2. School studies in which multiple regression analysis was used to investigate relations between health symptoms and pollutant exposures (statistically significant associations are shown in ***bold italicized*** print)

[Reference] Type of Study	Schools/Subjects	Health Symptoms	Pollutant exposures measured:
[12] Longitudinal	6 Swedish schools 129 school employees	SBS	Formaldehyde[1], ***VOCs[2], RSP*** [3]
[6] Cross-sectional	38 Swedish schools, 96 classrooms, 1410 school employees	Asthma	Formaldehyde[1], VOCs, NO_2, RSP, Total bacteria, Viable bacteria, ***Total molds,*** Viable molds, ***Microbial VOCs*** [4], Endotoxin in settled dust, Cat & dog allergens in settled dust
[13] Cross-sectional	11 Swedish secondary schools, 28 classrooms, 627 students	Asthma	***Formaldehyde[1], 14 VOCs (Sum)***, NO_2, RSP, Total & ***viable bacteria***, Total & ***viable molds,*** Endotoxin in settled dust, **Cat allergen** & Dog allergen in settled dust

[1] Formaldehyde concentrations all low. [2] VOCs = sum of concentrations of 15 VOCs, as well as subsets of these: aromatics, alkanes, terpenes, and butanols. [3] RSP = respirable dust in air
[4] 2-methyl-isoborneol, 3-methylfuran, 2-heptanone, 1-octen-3-ol

Chronic SBS symptoms in 129 Swedish school employees were found to be significantly related to exposures to VOCs and to previous wall-to-wall carpeting in the schools; the incidence of new SBS was related to RSP [12]. In a larger study of asthma symptoms in 1410 school employees, Smedje, *et al.* [6] found no statistically significant relationships between asthma and many commonly measured environmental factors, *e.g.*, CO_2, air exchange rates, humidity. Higher concentrations of molds and of 4 microbial VOCs were significantly related to asthma in the 1410 school employees, even after controlling for other factors, *i.e.*, allergies, stressful work situation and recent repainting of homes. More recently, Smedje, *et al.* [12] reported statistically significant relationships between current asthma in secondary school pupils and school exposures to formaldehyde, VOCs (sum of 14 compounds, 1 week sample), viable bacteria (in air), viable molds (in air) and cat allergen in settled dust. Evidence of a dose-response relationship with these variables was also reported.

In other studies, carpeting in schools has been associated with increased prevalences or severity of health symptoms [13,14]. Significantly higher contents of allergens per gram of dust were found for carpeted than smooth floors in 10 Norwegian schools [15], indicating a possible causal relationship between health symptoms and allergens. House dust mite allergens have also been found in floor dusts in Florida schools [16].

SUMMARY AND MAJOR CONCLUSIONS

Asthma and SBS were the most commonly reported building-related health symptoms investigated in schools. The few studies in which exposure and symptoms were simultaneously investigated indicate that exposures to VOCs, to molds and microbial VOCs, and to allergens and molds in floor dust in schools are related to asthma, SBS and other respiratory symptoms. The particular pollutants causing symptoms may differ among schools.

The available measurements of ventilation rates and CO_2 concentrations in schools suggest that many classrooms are not adequately ventilated. However, most studies have failed to show significant associations between SBS or asthma symptoms with ventilation rates or CO_2 concentrations, indicating that CO_2 is a poor surrogate for exposures to the actual agents causing the symptoms.

In general, there has been a dearth of studies in which relations between symptoms and *measured* exposures to multiple pollutants have been rigorously investigated. Furthermore, there is very little information on exposure-response relationships that would provide a sound basis for setting standards for schools or for insuring cost-effective mitigation measures. Improved methods for exposure measurements are also needed.

ACKNOWLEDGMENTS

This research was supported the California Environmental Protection Agency, Office of Environmental Health Hazard Assessments, Contract No. 94-E0076 and by the Office of Energy Efficiency and Renewable Energy, U.S. Department of Energy, Contract No. DE-AC03-76SF00098.

REFERENCES

1. Daisey, J.M. and Angell, W. J. 1998. A survey and critical review of the literature on indoor air quality, ventilation and health symptoms in schools. Report No. LBNL-41517. Lawrence Berkeley National Laboratory, Berkeley, CA.

2. ASHRAE. 1989. *Ventilation for Acceptable Indoor Air Quality, Standard 62-1989*, Atlanta: American Society for Heating, Refrigerating and Air Conditioning Engineers, Inc.

3. Nielsen O. 1984. Quality of air and the amount of fresh air in classrooms, In: *Indoor Air: Buildings, Ventilation and Thermal Climate*. B. Berglund, T. Lindvall, and J. Sundell, eds. Swedish Council for Building Research, Vol. 5, pp 221-226.

4. Turk, B.H., Grimsrud, D.T., Brown, J.T., *et al.* 1989. Commercial building ventilation rates and particle concentrations, *ASHRAE Transactions*, Vol. 95, pp 422-433.

5. Lagus Applied Technology. 1995. Air change rates in non-residential buildings in California, California Energy Commission, P400-91-034BCN.

6. Smedje, G., Norback, D., Wessen, B. and Edling, C. 1996. Asthma among school em - ployees in relation to the school environment. *Proceedings of the 7th International Conference on Indoor Air Quality and Climate - Indoor Air '96*, Vol. 1, pp. 611-616.

7. Molhave, L. 1990. Volatile organic compounds, indoor air quality and health, *Proceedings of the 5th International Conference on Indoor Air Quality and Climate - Indoor Air '90*, Vol. 5, pp 15-34.

8. Norback, D. 1995. Subjective indoor air quality in schools - the influence of high room temperature, carpeting, fleecy wall materials and volatile organic compounds. *Indoor Air*, Vol. 5, pp 237-246

9. Cavallo, D., Alcini, D., de Bortoli, M., *et al.* 1993. Chemical contamination of indoor air in schools and office buildings in Milan, Italy, *Proceedings of the 6th International Conference on Indoor Air Quality and Climate - Indoor Air '93*, Vol. 2, pp 45-49.

10. Laurent, A.M., Person, A., Petit-Coviaux, F., *et al.* 1993. Chemical characterization of indoor air quality inside schools in Paris, *Proceedings of the 6th International Conference on Indoor Air Quality and Climate- Indoor Air '93*, Vol. 3, pp 23-28.

11. Gallup, J.M., Zanolli, J. and Olson, L. 1993. Airborne bacterial exposure: preliminary results of volumetric studies performed in office buildings, schools, and homes in California, *Proceedings of the 6th International Conference on Indoor Air Quality and Climate - Indoor Air '93*, Vol. 4, pp 167-170.

12. Norback, D., Torgen, M. and Edling, C. 1990. Volatile organic compounds, respirable dust, and personal factors related to prevalence and incidence of sick building syndrome in primary schools. *British Journal of Industrial Medicine*, Vol. 47, pp 733-741.

13. Smedje, G., Norback, D., and Edling, C. 1997. Asthma among secondary school children in relation to the school environment. *Clinical and Experimental Allergy*, Vol. 27, pp 1270-1278.

14. Hansen, L., Bach, E., Kass Ibsen, K. and Osterballe, O. 1987. Carpeting in schools as an indoor pollutant, *Proceedings of 4th International Conference on Indoor Air Quality and Climate - Indoor Air '87*, Vol. 2, pp 727-731.

15. Dybendal, T., Vik, H. and Elsayed, S. 1989. Dust from carpeted and smooth floors. 2. Antigenic and allergenic content of dust vacuumed from carpeted and smooth floors in schools under routine cleaning schedules. *Allergy*, Vol. 44, pp 401-411.

16. Bates, J.M. and Mahaffy, D.J. 1996. Relationships of reported allergy symptoms, relative humidity and airborne biologicals in thirteen Florida classrooms. *Proceedings of the 7th International Conference on Indoor Air Quality and Climate - Indoor Air'96*, Vol., pp 551-556.

INHALATION TRANSFER FACTORS FOR ASSESSING HUMAN HEALTH RISKS FROM AIR POLLUTANT SOURCES

A C K Lai[1], T L Thatcher[1] and W W Nazaroff[1,2]

[1]Indoor Environment Dept., Lawrence Berkeley National Laboratory, Berkeley, CA, USA
[2]Dept. of Civil and Environmental Engineering, University of California, Berkeley, CA, USA

ABSTRACT

To facilitate routine health-risk assessments, we introduce the concept of an inhalation transfer factor (ITF). The ITF is defined as the pollutant mass inhaled per pollutant mass emitted. The concept is illustrated by computing the ITF for two pollutant release scenarios: (a) elevated (30 m) point-source emission to outdoor air and (b) indoor emission into a small (60 m^3) well-mixed apartment. For case (a), individual ITFs are less than 3×10^{-8}, and the cumulative population ITF is in the approximate range 10^{-6} to 10^{-3}, depending on atmospheric stability, wind speed, and population density. For case (b), the individual ITF was found to be in the range 0.002 to 0.057 for typical ventilation and pollutant deposition conditions. Thus, the individual ITF for release of pollutants into an apartment can exceed by a large factor even the population ITF for outdoor release from an elevated source.

INTRODUCTION

Quantitative health risk assessments are routinely used to support environmental policy decisions. For toxic air pollutants, an evaluation of the human health risk caused by pollutant release may be required as part of a permitting process [1]. Considerable attention has also been given to health-risk evaluations for indoor pollution sources, such as environmental tobacco smoke [2].

Health risk assessments that focus on the impact of a single source or source category involve several steps. For outdoor air releases, pollutant emissions are estimated, often as the product of an emission factor times the intensity of an activity. The emissions information is supplied along with meteorological data to a dispersion model to predict downwind concentrations. Then, some information on the downwind population is provided to predict exposure and inhalation dose. Finally, the health risk is estimated, often by multiplying the exposure or dose by a unit risk factor. For indoor air releases, a similar set of steps can be carried out. Emissions data are combined with an indoor air quality model to predict indoor air concentrations from which exposure, dose, and risk are evaluated.

For most primary pollutants, i.e. those emitted directly from sources (rather than formed, for example, by chemical reactions in the atmosphere), concentrations, exposures, and doses are each proportional to emissions. That is, if all other variables are held fixed, then doubling the rate of emissions leads to a doubling of the inhalation dose rate. An example for which proportionality applies well is benzene, which is emitted from combustion sources (motor vehicles and cigarettes, for example) and evaporation (gasoline and solvents). Benzene is not formed nor degraded to a substantial degree by atmospheric reactions on the residence time scale of air in an urban air basin or an indoor environment. On the other hand, the proportional relationship between emissions and dose would not apply for ozone, a secondary pollutant whose concentration depends in a complex, nonlinear manner on emissions of hydrocarbons and nitrogen oxides.

The linear relationship between emissions and dose for many pollutants suggested to us the idea of an *inhalation transfer factor* (ITF) to facilitate the conduct of routine or preliminary health risk assessments. We define the ITF to be the dimensionless ratio of pollutant mass inhaled to pollutant mass emitted. Multiplying an appropriate ITF by expected pollutant emissions would produce an estimate of inhaled presented dose. Armed with tables of ITF values that correspond to different release and exposure scenarios, an estimate of health risk could be obtained as the product of three terms: rate or amount of emissions × inhalation transfer factor × unit risk factor. The virtue of the ITF concept is that it simplifies the analysis of the relationship between pollutant emissions and inhaled dose.

In addition to introducing the ITF concept, the goal of this paper is to compute its value for a few sample cases. The results provide some insight into the importance of pollutant releases into indoor air.

METHODS

Inhalation transfer factor

The inhalation transfer factor (ITF) is the fraction of an emitted pollutant that is expected to be inhaled for a given release and exposure scenario. The mass inhaled accounts for presented dose only; lung deposition efficiency is not considered here. The ITF is defined both for individuals and for populations. The individual ITF is the fraction of the released pollutant that would be inhaled by a single person at a particular location, evaluated as

$$\mathrm{ITF} = \frac{\text{mass inhaled by an individual}}{\text{mass emitted}} = \frac{\int C(t) Q_B(t) dt}{\int E(t) dt} \qquad (1)$$

where $C(t)$ is the concentration of the pollutant caused by the particular source (g m^{-3}), $Q_B(t)$ is the breathing rate (m^3 s^{-1}), and $E(t)$ is the pollutant emission rate from the source (g s^{-1}). The breathing rate depends on the gender, age health condition and the activity level. For the present purposes, which focus on a magnitude comparison, the choice is not critical. In addition, it is easy to convert to a different breathing rate since the ITF is directly proportional to Q_B. For short-term pollutant release, the integrals would be carried out over a period sufficiently long for complete removal of the emitted pollutant from the environment in question. In an urban air basin this period might extend to a few days. For indoor environments, the typical integration period would be many hours. For continuous pollutant release at a constant rate, the ITF would be evaluated as the steady-state limit of equation (1): $C\,Q_B/E$. The pollutant concentration caused by a localized emission source will generally vary with position. Typically, the ITF would be computed for a hypothetical individual who remains at a fixed location and so the ITF would vary with position.

For some purposes, it is of interest to consider not only the dose to individuals, but also the dose to an entire population. The population inhalation transfer factor is obtained by summing individual ITF values over a population of interest.

Case (a): ITF for an outdoor point source

Outdoor pollutant emissions have been the focus of traditional air pollution control programs. Sources are typically divided into stationary and mobile categories, with control measures varying for each type. We have investigated several different outdoor release scenarios. Here, we focus on one common case: continuous emissions from an elevated point source in

an urban air basin. This case could apply, for example, to toxic air pollutants emitted from an incinerator or a chemical refinery.

The individual ITF can be expressed as

$$\mathrm{ITF} = \frac{Q_B \overline{C(x,y,0)}}{E} \qquad (2)$$

where the ground-level concentration, C, is a function of coordinate position $(x, y, 0)$ relative to the point of release, $(0, 0, H)$. The overbar indicates that we seek the time-averaged concentration (thereby smoothing any turbulent fluctuations). (The difference bewteen the ground-level concentrations and the breathing height concentrations are negligible for the cases considered here).

A Gaussian plume model can be used to predict pollutant concentrations for point source emissions [3]. The ground-level concentration is given by

$$\overline{C(x,y,0)} = \frac{E}{\pi U \sigma_y \sigma_z} \exp\left[-\frac{1}{2}\left(\frac{y}{\sigma_y}\right)^2\right] \exp\left[-\frac{1}{2}\left(\frac{H}{\sigma_z}\right)^2\right] \qquad (3)$$

where U is the wind speed (assumed to align with the x coordinate direction), and σ_y and σ_z are the dispersion parameters in the horizontal and vertical direction, respectively, which are functions of x [4].

The population ITF is obtained by substituting equation (3) into equation (2) and numerically integrating over a domain $X_{min} \le x \le X_{max}$ and $-Y_{max} \le y \le Y_{max}$ where dimensions X_{max} and Y_{max} are selected to be representative of the domain of an urban air basin. The parameter X_{min} is taken to be 0.1 km, because of an absence of dispersion data for smaller downwind distances. In these evaluations, population density is assumed to be constant at values appropriate for an urban air basin, typically in the range 1000-6000 persons km^{-2}.

Case (b): ITF for emissions into a well-mixed building

A useful model for relating concentrations to emissions for the indoor environment is derived by applying a material balance for a completely mixed flow reactor [5]. Because of large surface-to-volume ratios encountered indoors, reaction and deposition of pollutants on indoor surfaces should be considered for reactive gases and particles. When transport and mixing within a building is poor, a more complex simulation model that accounts for interzonal flow may be required. We have calculated ITF values for nonreactive and reactive/depositing species in a single well-mixed indoor environment and in a six room, single-story residence. In this paper, we focus on the case of a single well-mixed environment.

For a pollutant that is emitted from some indoor source and removed from indoor air by ventilation and first-order reaction/deposition on indoor surfaces, the individual ITF can be written as

$$\mathrm{ITF} = \frac{Q_B}{Q + \beta V} \qquad (4)$$

where V is the indoor volume, Q is the ventilation rate (volume times air-exchange rate), and β is the loss rate coefficient for reaction/deposition on indoor surfaces (h^{-1}). The loss rate for particles depends on particle size and for gases depends on their reactivity on surfaces. The loss coefficient also depends on the nature and intensity of air flow near indoor surfaces [6].

RESULTS AND DISCUSSION

With the equations developed in the previous section, we can now evaluate ITF for both outdoor and indoor pollutant releases. For Case (a), we considered wind speeds (U) ranging from 1 to 10 m s^{-1} and an individual breathing rate (Q_B) of 1 m^3 h^{-1}. In addition, we considered source heights between 0 and 100 m and three Pasquill stability classes: B (unstable), D (neutral) and E (slightly stable) [3,4]. The highest ITF values occur for stability class E with low wind speed. The maximum ITF always occurs along the central line downwind of the source, i.e. $y = 0$. Figure 1 shows a representative ITF contour plot. The maximum ITF in this case is 3×10^{-8} and occurs at $(x,y) = (0.95\text{ km}, 0)$. For a densely populated area (6000 persons per km^2), the population ITF in this case varies in the range 2×10^{-4} for $(X_{max}, Y_{max}) = (10\text{ km}, 10\text{ km})$ to 10×10^{-4} for $(X_{max}, Y_{max}) = (100\text{ km}, 10\text{ km})$. The population ITF is directly proportional to population density. Lower values of population ITF occur if stability class B or D is assumed to prevail, if the wind speed increases, or if the stack height increases.

Figure 2 shows the simulation results for the indoor emission scenario with Q_B of 0.7 m^3 h^{-1}, Case (b). We determined the individual ITF for particles of different sizes, using a recently developed deposition model for β [6] and assuming a typical value of the friction velocity near room surfaces. The aerodynamic properties of the particle are evaluated based on unit density spherical particles. The ITF was calculated for a small residence ($V = 60$ m^3, as, for example, in a studio apartment) with air-exchange rates of 0.2 h^{-1} and 2 h^{-1}. As shown in Figure 2, the ITF for this case ranges from 0.002 for large particles at a high air-exchange rate to 0.057 for 0.03-1.0 µm particles at a low air-exchange rate. Figure 2 shows that increasing the air-exchange rate while holding the volume fixed tends to decrease the ITF. Likewise, increasing the indoor volume while holding the air-exchange rate fixed will decrease the ITF. As 60 m^3 is a reasonable estimate of building volume *per occupant* in many cases, and 0.2-2 air changes per hour is representative of typical ventilation conditions, Figure 2 is a fair approximation of the population ITF for a typical indoor air release of particles. It is noteworthy that the smallest ITF in this case, 0.002, exceeds by a factor of 2 the maximum population ITF reported in the previous paragraph for Case (a). Typically, the population ITF for an indoor air pollutant release is of order 10^{-2}, about 2-4 orders of magnitude larger than the population ITF for outdoor air releases under typical circumstances (stability class D, wind speeds of 1-10 m s^{-1}, release from ground level up to 100 m above the surface, and population density of 1000 persons km^{-2}).

CONCLUSION

Risk assessments are frequently used to make environmental policy decisions. In this paper, we have introduced the concept of an inhalation transfer factor (ITF), a parameter designed to facilitate the conduct of preliminary or routine health risk assessments. The concept was illustrated by computing the ITF for two pollutant release scenarios. We found that the population ITF for release of pollutants into indoor air can exceed by several orders of magnitude the population ITF for pollutant release from an elevated outdoor stack. This finding echoes a statement by Wallace that the "hundreds of thousands of tons of benzene emitted annually by all outdoor sources provide only about 20% of the total population exposure, whereas the mere 30 tons per year delivered in mainstream cigarette smoke accounts for 50% of the total population exposure" [7]. In their development of a quantitative

scheme for determining health risk, Zartarian *et al.* [8] recognized that one of the key exposure assessment issues is determining the effectiveness of delivery "from the source to the target." To this end, we have proposed the use of an inhalation transfer factor and computed values for a few exposure scenarios. Further development of this concept can lead to more efficient and transparent health risk assessments associated with air pollution emissions.

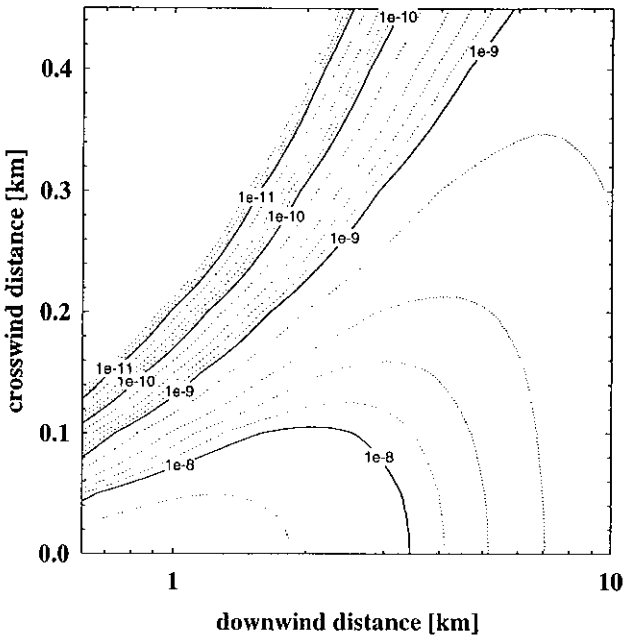

Figure 1. Case (a) results: Contour plot of the individual inhalation transfer factor (ITF) as a function of downwind position for stability class E (slightly stable), wind speed $U = 1$ m s^{-1}, and stack height $H = 30$ m.

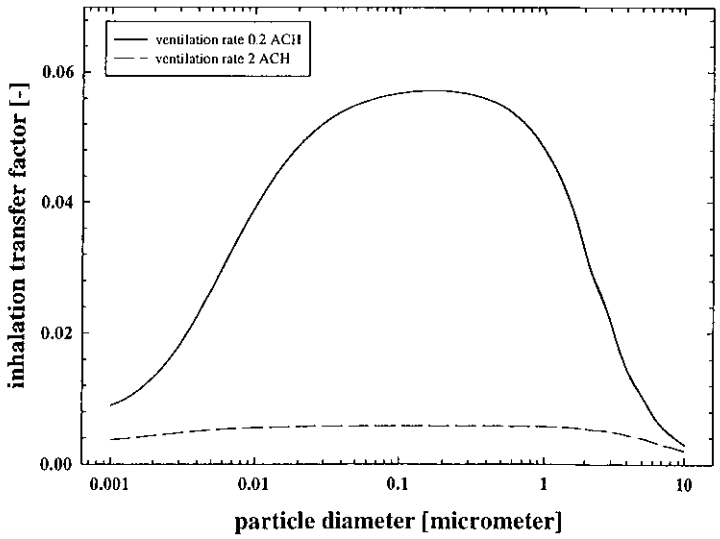

Figure 2. Case (b) results: Individual inhalation transfer factor (ITF) as a function of particle diameter for a small apartment ($V = 60$ m^3) at two ventilation rates.

ACKNOWLEDGEMENT

This work was supported by the Office of Research and Development, Office of Nonproliferation and National Security, U.S. Department of Energy under Contract No. DE-AC03-76SF00098.

REFERENCES

1. Paustenbach, D J, Jernigan, J D, Finley, B L., et al. 1990. The current practice of health risk assessment: Potential impact on standards for toxic air contaminants. *Journal of the Air & Waste Management Association.* Vol. 40, pp 1620-1630.

2. Dockery, D W, and Trichopoulos, D. 1997. Risk of lung cancer from environmental exposures to tobacco smoke. *Cancer Causes & Control.* Vol. 8, pp 333-345.

3. de Nevers, N. 1995. *Air Pollution Control Engineering.* McGraw Hill. Chapter 6.

4. Davidson, G A. 1990. A modified power-law representation of the Pasquill-Gifford dispersion coefficients. *Journal of the Air & Waste Management Association.* Vol. 40, pp 1146-1147.

5. Wadden, R A, and Scheff, P A. 1983. *Indoor Air Pollution: Characterization, Prediction, and Control.* Wiley. Chapter 6.

6. Lai, A C K, and Nazaroff W W. 1999. Modeling indoor particle deposition from turbulent flows onto smooth surfaces. Submitted to *Journal of Aerosol Science.*

7. Wallace, L A. 1989. The exposure of the general population to benzene. *Cell Biology and Toxicology.* Vol. 5, pp 297-314.

8. Zartarian, V G, Ott, W R, and Duan, N. 1997. A quantitative definition of exposure and related concepts. *Journal of Exposure Analysis and Environmental Epidemiology.* Vol. 7, pp 411-437.

REDUCING UNCERTAINTIES IN QUANTIFYING SOURCE/EXPOSURE RELATIONSHIPS FOR PARTICULATE MATTER: AN ITERATIVE APPROACH BASED ON MEASUREMENTS AND MODELS

T. E. McKone
University of California, Lawrence Berkeley National Laboratory, USA

ABSTRACT

The specific aims of this research are (i) to develop an exposure model framework that addresses features unique to particulate matter (PM); (ii) to define the level of confidence required from this model to meet environmental performance objectives, and (iii) to calibrate and validate human exposure and source/exposure assessments using current and emerging data sets. To meet these aims, we have constructed an indoor/outdoor total human exposure (activity-pattern/micro-environmental) model for PM. In contrast to previous activity-pattern-exposure models, this model uses calibrated stochastic process sub-models instead of simple empirical concentration distributions to construct exposure distributions. Explicit treatment of uncertainty and variability within the modeling framework improves the way that decision-making needs are factored into the model. We use this model to define the value of measurements of particles at fixed monitoring sites to measured human exposures for particles of 2.5 μm diameter or less.

KEYWORDS: Dust, exposure assessment, mass-balance model, particles, air infiltration

INTRODUCTION

Environmental health scientists frequently must assess exposures of human populations to a wide range of pollutants in indoor/residential environments, over a wide range of space and time scales. The models and measurements used for this purpose must often address multiple sources and multiple media. Controlling the exposure of human populations to environmental contaminants requires that we find and understand the links between cumulative intake and the multiple exposure pathways and multiple pollutant sources that most significantly contribute to cumulative intake. To advance the science of exposure analysis in a way that will be useful to health agencies, two essential scientific research tools, models and measurements, must be integrated. Models provide the means to integrate and interpret measurements, design hypothesis-driven experiments, and predict the effectiveness of risk management strategies. Measurements, in turn, provide tests of the models and "ground truth."

In this paper I describe the development and early application at Lawrence Berkeley National Laboratory of a model designed to assess and rank the cumulative contributions of indoor and outdoor sources of PM to total human intake. The methods and criteria used to develop the model framework are presented first. Next I provide the resulting form of the model and examples of its capabilities and the types of insight provided. This is followed by discussion of results to date and consideration of future activities.

METHODS

The specific aims of this research are (i) to develop an exposure model framework that addresses features unique to PM; (ii) define the level of confidence required from this model to meet environmental performance objectives, and (iii) to calibrate and validate human exposure and source/exposure assessments using current and emerging data sets. To meet these aims, we have constructed an indoor/outdoor total human exposure (activity-pattern/micro-environmental) model for PM. This model includes a mass-balance model for each micro-environment considered; the use of inter-media (outdoor/indoor, soil/air, dust/air, etc.) transfer factors; and the explicit treatment of uncertainty and variability. Many existing models of total exposure to PM are based primary on sampling from empirical distributions of particle concentrations in various microenvironments [1, 2]. In contrast our model uses a mass-balance approach similar to what has been used for persistent multimedia pollutants. Sources of PM are balanced with dilution and transport in each microenvironment needed to characterize cumulative exposure.

Model framework

The model used in this project is built around the concept of simulating a series of "exposure events." Exposure events are human activities that bring people in contact with PM concentrations in any microenvironment. To construct exposure events, one must link an individual or a population cohort with both a series of time-specific activities and with the microenvironments associated with those activities as illustrated in Figure 1. In addition, it is necessary through a combination of databases and stochastic/process models to define PM concentrations in each microenvironment. Each microenvironment is represented by a stochastic process sub-model, in which random and uncertain events are modeled with parameters whose value range is defined by a probability density function.

The first purpose of this model is to relate measurements of PM at fixed monitoring sites to actual human exposures. The principal focus of this model is currently on particles of 2.5 μm diameter or less. However, larger particle sizes have not been excluded from the model development. Model development has relied on validated sub-models of indoor microenvironments. Both ambient air and indoor air sources can be handled in our current prototype framework.

Two novel features for the PM inhalation route have been added to the model. First is the use of breathing-rate adjusted exposure concentrations. Second is use of penetration factors that apply at different time scales. The inhalation exposure model follows a standard approach that divides a long-term exposure into a subset of exposure events that take place over discreet time periods (i.e. 1 hour). However, to make an appropriate link with ambient air concentration measurements, there is a need to have a penetration/infiltration model that can attribute indoor environment concentrations to the appropriately time-average ambient environment concentrations, and this has been added.

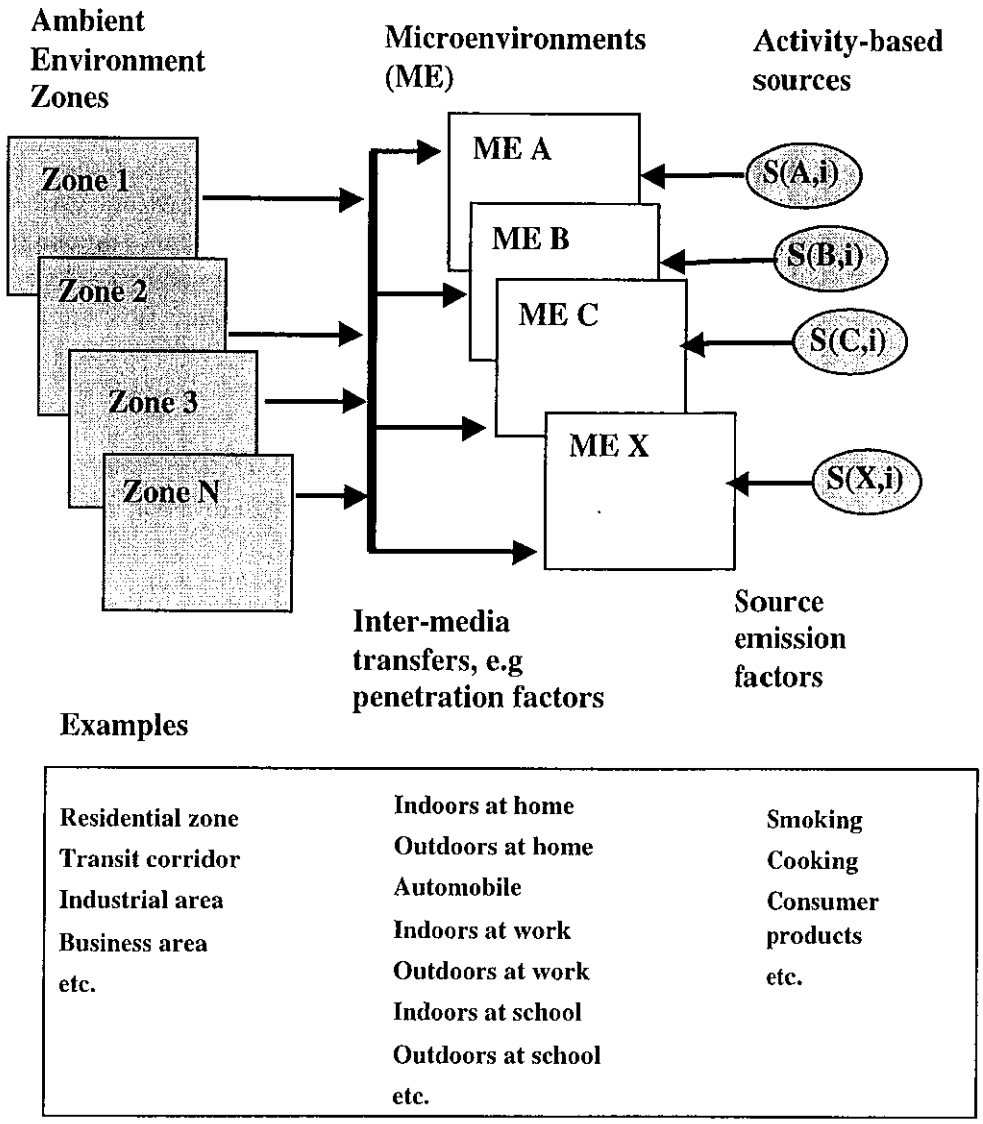

Figure 1. Approach for developing a time-activity-pattern exposure model for PM.

Explicit treatment of uncertainty and variability

The model has been set up so that each model input is a probability distribution. This facilitates uncertainty/sensitivity analyses. Sensitivity analysis methods for ranking the relative importance of parameters in complex models are well-established [3]. However, little information is available for actually identifying the minimum set of variables that are essential for a particular modeling scenario. We use classification and regression trees (CART) methods and the regional sensitivity analysis (RSA) method [4] to rank the source data, parameters, and model components in terms of their impact on model reliability

RESULTS

Our efforts to construct an indoor/outdoor model for aggregate human exposure to PM have provided important insight on the model development process, the relative importance of different PM sources, and the process for using data to calibrate model components.

Model development

Each model component as well as the overall model framework have been developed as a prototype using either a spreadsheet system with imbedded programming or a simulation language. Advantages of this a approach are (a) the rapid building and editing of prototypes, (b) easy links to many of the available data bases (c) and the use of add-ins for Monte Carlo simulation, graphical analyses, and sensitivity analyses (such as elasticity tests and classification and regression trees). Spreadsheets also facilitate the early development and evaluation of the framework architecture. However, the disadvantage of the spreadsheet approach is that it can be computationally inefficient and slow.

Modeling Procedures

The basic exposure-event function defines the exposure as the product of a concentration and exposure duration during an exposure event:

$$E_{z,m}(t) = C_{pm}(i,k,l,t)\, ET_z(i,k,l,t) \qquad (1)$$

where

$E_{z,pm}$ is the PM exposure experienced by person z during time step t, given that person z is at location i in micro-environment k conducting activity l during that time step.

C_{pm} is the PM concentration at location i in microenvironment k, associated with activity l, during time step t, mg/m^3.

$ET_{z,pm}$ is the exposure duration of person z at location i in microenvironment k conducting activity l during time step t.

i refers to geographical location in which the exposure takes place, i.e., exposure district.

k refers to the microenvironment in which the exposure occurs.

l is an activity code that describes what the individual is doing at the time of exposure, e.g. resting, working, preparing food, cleaning, eating.

During a relatively long time period, such as a day, week, or year, individuals have different time/activity budgets and occupy different microenvironments with different PM concentrations. To address exposure in such situations the standard approach is to use the model equations

$$EC_{z,pm} = \sum_t C_{pm}(i,k,l,t)\, ET_z(i,k,l,t) \Big/ \left[\sum_t \text{time steps}\right] \qquad (2)$$

In this model, $EC_{z,pm}$ is the average PM exposure concentration of person z over averaging time T where T is given by $T = \sum$ time steps.

Case Studies

The model framework is being calibrated and validated through a series of case studies. The purpose of the first case study is to build on experience with activity pattern data sets (e.g., NHAPS, CHAD), Monte-Carlo-based population exposure modeling, and indoor fate and transport models. Currently we are working with environmental tobacco smoke source models and outdoor-indoor infiltration models for sources such as wood smoke to determine the reliability with which one can model the variability in human exposures to PM.

Preliminary model results for PM, reveal that cumulative PM exposure cannot be assessed without explicit consideration of the indoor environment and residential source factors, such as tobacco smoke and cooking. We are also exploring the relative importance of tracked-in soil particles as a source of cumulative PM exposure.

Bayesian updating and the inverse problem

When both variability and uncertainty are explicitly modeled, iterative updating of the model can be carried out using a Bayesian approach [5] as illustrated in Figure 2. In a model where there is a lack of relevant and complete information, initial simulations have very wide confidence intervals. This is illustrated in the upper plot of Figure 2. Both parameter variability and uncertainty are

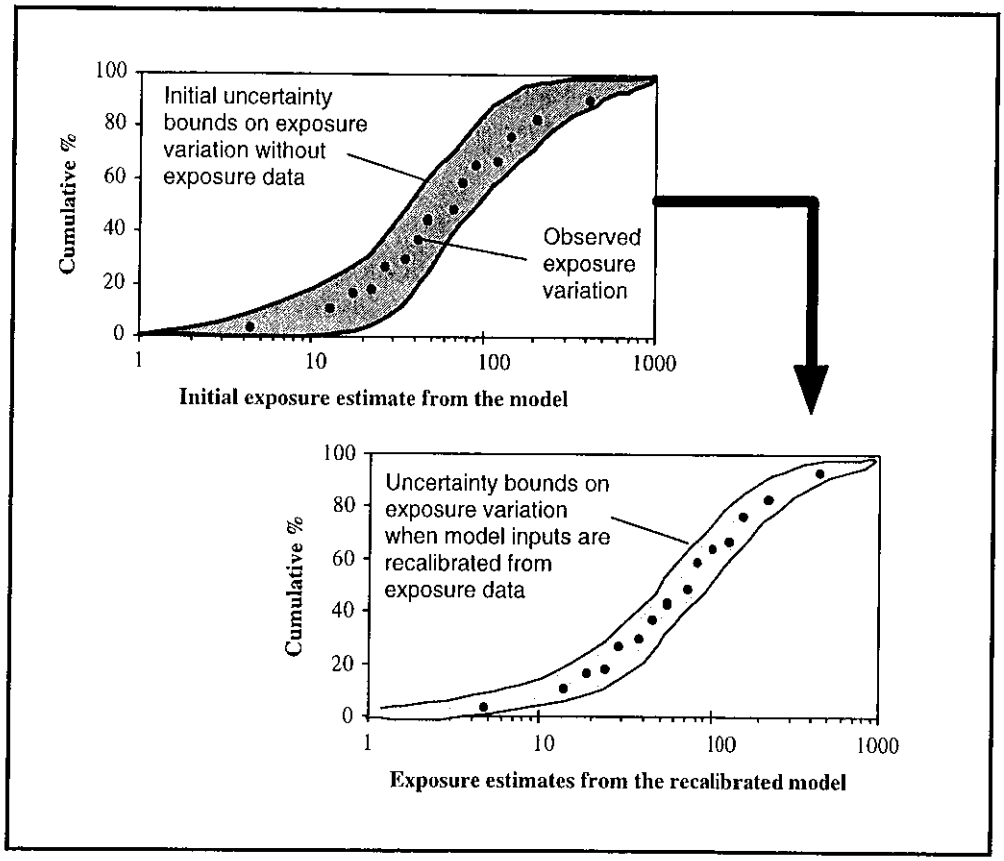

Figure 2. An illustration of how pathway-specific population exposure data can be used to reduce uncertainty in the variability of modeled exposure.

included in the exposure simulations. Each simulation is carried out as a two-dimensional Monte Carlo simulation consisting of two calculation phases [6]. In the first phase, a single realization is obtained from the distribution of each uncertain parameter, followed by repeated sampling from the variable parameters. This process is repeated until a large number (~ 500) of uncertain parameter value sets are taken in the outer phase and a larger number (~1000) of variable parameter values are selected in the inner loop. Large uncertainties in the selection of parameter values results in wide uncertainty bands as shown in the upper diagram of Figure 2. As more

data is collected and used to calibrate the models, the uncertainty bands are reduced and the ability to resolve variability of exposure increases as shown in the lower diagram.

DISCUSSION

There are two important issues that should be considered with regard to the uncertainty and variability of source-to-dose models for PM. First, there are large variations in the precision and accuracy of the information needed to characterized source-to-dose relationships. Second, this type of model is an open system. Therefore the influence from one stage to the next is not solely connected to the previous stage. For example, the concentration of PM indoors is not solely linked to the emissions from within the building, but could be attributable to several sources in the region. As has been pointed out by Oreskes et al.[7] such open-ended systems models, which are common in engineering and health sciences, cannot be fully verified or validated because the operative processes are always incomplete. Nevertheless, such models can be confirmed and can be used to put bounds on the likely range of outcomes. In this sense the models can offer something of value to the policy-making process.

ACKNOWLEDGEMENTS

This work was carried out at the Lawrence Berkeley National Laboratory under the U.S. Department of Energy contract No. DE-AC03-76SF00098. Funding was provided by the United States Environmental Protection Agency National Exposure Research Laboratory through Interagency Agreement # DW89938190-01-0.

REFERENECES

1. Sexton, K and Ryan, P B. 1988. Assessment of human exposure to air pollution: methods, measurements, and models. In *Air Pollution, the Automobile, and Public Health*, National Research Council. Washington, D.C: National Academy Press.

2. Ott, W. 1995. Human exposure assessment: the birth of a new science. *Journal of Exposure Analysis and Environmental Epidemiology* **5**(4):449-472.

3. Morgan, G M and Henrion, M. 1990. *Uncertainty: A Guide to Dealing with Uncertainty on Quantitative Risk and Policy Analysis*. Cambridge, Cambridge University Press.

4. Spear, R C, Grieb, T M and Shang, N. 1994. Parameter uncertainty and interaction in complex environmental models. *Water Resources Research* **30**(11):3159-3169.

5. Box, G E P and Tiao, G C. 1973. *Bayesian Inference in Statistical Analysis*. Wiley Classics.

6. Bogen, K T and Spear, R C.1987. Integrating uncertainty and interindividual variability in environmental risk assessment. *Risk Analysis* **7**(4):427-436.

7. Oreskes, N, Shrader-Frechette, K and K Belitz. 1994. Verification, validation, and confirmation of numerical models in the earth sciences. *Science* **263**(5147):641-646.

ENHANCED PARTICLE FILTRATION IN A NON-PROBLEM OFFICE ENVIRONMENT: SUMMARY FINDINGS FROM A DOUBLE-BLIND CROSSOVER INTERVENTION STUDY

MJ Mendell[1], WJ Fisk[2], M Petersen[1], MX Dong[2], CJ Hines[1], D Faulkner[2], JA Deddens[1], AM Ruder[1], D Sullivan[2], and MF Boeniger[1]

[1] National Institute for Occupational Safety and Health, USA
[2] Lawrence Berkeley National Laboratory, USA

ABSTRACT

In a double-blind crossover study in an office building without known complaints, enhanced particle filtration greatly reduced concentrations of submicron airborne particles and was associated with slight improvements in most questionnaire outcomes. However, chance effects could be excluded only for confusion, too stuffy, and too humid. Higher temperatures even within conventional comfort limits were related to significant worsening of many questionnaire outcomes.

INTRODUCTION

Previous evidence suggests unidentified indoor particulate contaminants may increase nonspecific symptoms and thermal dissatisfaction in office workers [1, 2]. The authors conducted a controlled, double-blind crossover study of enhanced particle filtration in an office building without known complaint history. Summary information on this study has been previously published [3, 4].

METHODS

Standard filters (estimated 3% efficiency at 0.3 microns) in ventilation systems of two floors were replaced, on alternate floors weekly over four weeks, with highly efficient particle filters (estimated ≥95% efficiency at 0.3 microns). Weekly questionnaires assessed worker symptom severity, performance indicators, and environmental dissatisfaction. Temperature, humidity, ventilation rate, particle concentrations, and microbiological parameters (endotoxin, ergosterol, and beta-1,3-glucans) were measured. Repeated-measures ANOVA analysis models were used.

RESULTS

Eighty percent (392) of eligible participants returned the initial questionnaire. Weekly response rates averaged 63% over the four crossover weeks; usable questionnaires averaged 58%. Baseline symptom prevalences were average and ventilation rates were typical for US office buildings. Microbiological parameters measured were very low. Temperature and relative humidity were mostly within accepted comfort limits. Enhanced filtration greatly reduced concentrations of submicron size particles, but not particles larger than 2 microns. Enhanced filtration was associated with slight improvements in 13 of 16 worker outcomes (see examples in Table), but chance effects could be excluded only for the confusion scale, "too stuffy," and "too humid" (p-values=0.005, 0.01, 0.03). Higher temperatures even within the accepted comfort range (observed range 22.2-25.6°C) were strongly related to worsening of many outcomes (examples in Table). Temperature adjustment changed some filtration effect estimates substantially.

Table. Estimated changes in selected outcomes with enhanced filtration and increased temperature

Outcome	With enhanced filtration		Per 1°C temperature increase	
	change in outcome*	p-value	change in outcome*	p-value
headache	-3.6%	0.51	20.2%	0.02
confusion scale	-3.7%	0.005	8.9%	0.0001
too stuffy	-6.1%	0.01	20.0%	0.0001

* estimated in models including terms for filtration and temperature; change expressed as percent of outcome mean

DISCUSSION

Enhanced filtration in this blinded study was associated with slight improvements in 13 of 16 questionnaire outcomes, with three of these improvements unlikely to be due to chance. We can only speculate on mechanisms through which removal of submicron airborne indoor particles in a building without known contamination or occupant complaints could improve mental clarity and thermal comfort. Replication of this intervention will be necessary to confirm the findings in similar buildings and to assess potentially greater benefits in buildings with higher particulate contaminant levels or lower ventilation rates. Study findings also suggest that keeping summer office temperatures at the lower end of the current comfort range may substantially improve occupant symptoms and performance. Our analyses indicate that careful measurement of and adjustment for indoor temperatures is critical in studying subtle effects of indoor environments.

ACKNOWLEDGMENTS

This work was supported by NIOSH/CDC, by the U.S. Department of Energy under contract no. DE-AC03-76SF00098, and by the Office of Research and Development, U.S. EPA. Any opinions expressed in this paper are those of the authors and do not imply official endorsement by the sponsors.

REFERENCES

1. Mendell, MJ. 1993. Non-specific symptoms in office workers: a review and summary of the epidemiologic literature. *Indoor Air*. Vol 3, pp 227-36.

2. Leinster, P, Raw, G, Thomson, N, et al. 1990. A modular longitudinal approach to the investigation of Sick Building Syndrome. *Proceedings of the 5th International Conference on Indoor Air Quality and Climate — Indoor Air '90*, Toronto, Vol 1, pp 287-92.

3. Fisk WJ, Faulkner D, Sullivan D, et al. 1998. The Healthy Building Intervention Study: objectives, methods, and results of selected environmental measurements. Berkeley, CA: Lawrence Berkeley National Laboratory (LBNL-41546).

4. Mendell MJ, Fisk WJ, Petersen M, et al. 1999. Effects on occupants of enhanced particle filtration in a non-problem office environment: preliminary findings from a double-blind crossover intervention study. *American Journal of Industrial Medicine* (in press).

PREDICTING AND MAPPING INDOOR RADON CONCENTRATIONS IN THE U.S., USING MONITORING DATA AND PREDICTIVE VARIABLES

P N Price[1], A V Nero[1], K L Revzan[1], A Gelman[2]

[1]Indoor Environment Program, E. O. Lawrence Berkeley National Laboratory, USA
[2]Department of Statistics, Columbia University, USA

ABSTRACT

We describe results of the High-Radon Project at Lawrence Berkeley National Laboratory, a federally funded effort to develop methods of mapping radon distributions, using measured indoor radon concentrations along with various explanatory variables. The role of geologic explanatory variables is briefly discussed.

INTRODUCTION

Radon is a naturally occurring radioactive gas that is known to cause lung cancer when high concentrations are inhaled for a long period. The U.S. government, along with many individual states, has programs to promote radon monitoring and remediation. An important aspect of many of these programs is radon risk mapping: locating areas in which a large fraction of homes are likely to have dangerously elevated radon levels.

Many radon mapping efforts in the U.S. and elsewhere attempt to map "radon potential", a usually ill-defined parameter that is putatively related the expected indoor radon level in a conventional home built on a given site (but that does not actually provide a prediction for what that level will be).

METHODS

An alternative approach is to attempt to predict or summarize quantitatively the distribution of indoor radon concentrations within homes, as a function of location (e.g. census tract, county, etc.) Perhaps the ultimate realization of this latter approach is the radon maps of England [1 that are based on so many measurements that little processing required in order to make a map at a fairly detailed spatial resolution. Unfortunately, in the U.S. there is no suitable data base that allows duplication of the UK's program.

We instead used a statistical method for radon mapping that combines use of predictive variables with direct use of measured radon concentrations to predict radon distributions by area. Random-sample radon data were used, and results were calibrated [2] to predict annual-average living-area concentrations. Variables used for predicting geometric mean concentrations by U.S. county included measured surficial radium content, a climate variable, geology indicator variables, some building type information, and variables specifying which counties contain the measured homes. A Bayesian mixed effects regression model [3] was fit to determine the coefficients associated with these variables [4-5] while avoiding a statistical problem known as "overfitting".

RESULTS

We have applied the statistical methods mentioned above to several sets of radon data, including data from most counties in the U.S. (along the same lines as [5]) and individual townships in New Hampshire [6]. The state of New York is currently using our methods (and computer programs) to map radon concentrations by township. In each of these cases, results of the research include estimates for the various model parameters (including geologic effects) as well as predicted indoor concentration distributions.

Some of the radon maps and other results of our analyses can be seen at http://eande.lbl.gov/IEP/high-radon; some application of the maps to cost-benefit analysis of radon remediation strategies can be found at http://www.stat.columbia.edu/radon.

DISCUSSION

The analyses suggest that although a few high-radon areas are clearly associated with specific geologic features, most of the available geologic information in the U.S. has only modest predictive value in radon mapping at all spatial scales thus far investigated. Although geologic factors are obviously profoundly important in controlling indoor radon concentrations, available geologic data sets apparently do not provide substantial information on those particular parameters. At least, they do not adequately capture the spatial variation of the important geologic parameters, nor their variability. This is not to say that the geologic information is not useful, only that it does not have the overriding importance that has sometimes been assumed. Use of radon measurements in conjunction with other variables, as in our work [4-6], is thus essential if accurate radon maps are to be produced.

REFERENCES

1. Kendall, G M, Miles, J C H, Green, K D, et al. 1994. Exposure to radon in UK dwellings. Chilton, NRPB-R272.

2. Price, P N and Nero, A V. 1996. Joint analysis of long- and short-term radon monitoring data from the Northern U.S. *Environment International*, Vol 22. Suppl.1, pp. S699-S714.

3. Gelman, A, Carlin, J B, Stern, H S, Rubin, D B. 1995. *Bayesian Data Analysis*. Chapman and Hall: New York.

4. Price, P N, Nero, A V, and Gelman, A. 1996. Bayesian prediction of mean indoor radon concentrations for Minnesota counties. *Health Physics*, Vol. 71, pp. 922-036.

5. Price, P N. 1997. Predictions and maps of county mean radon concentrations in the mid-Atlantic states. *Health Physics*, Vol 72, pp. 893-906.

6. Apte, M G, Price, P N, Nero, A V, and Revzan, K L. 1999. Predicting New Hampshire indoor radon concentrations from geologic information and other covariates. *Environmental Geology*, to appear.

IV. VENTILATION AND FILTRATION

VENTILATION EFFICIENCIES OF TASK/AMBIENT CONDITIONING SYSTEMS WITH DESK-MOUNTED AIR SUPPLIES

D Faulkner[1], W J Fisk[1], D P Sullivan[1], and D P Wyon[2]

[1]Indoor Environment Department, Lawrence Berkeley National Laboratory, USA
[2]Controls Group, Johnson Controls, Inc., USA

ABSTRACT

In laboratory experiments, we investigated the ability of two task/ambient conditioning systems with air supplied from desk-mounted air outlets to efficiently ventilate the breathing zone of heated manikins seated at desks. In most experiments, the task conditioning systems provided 100% outside air while a conventional ventilation system provided additional space cooling but no outside air. Air change effectiveness (i.e., exhaust air age divided by age of air at the manikin's face) was measured. Tracer gases simulated the release of pollutants from nearby occupants and from the floor covering, and the associated pollutant removal efficiencies (i.e., exhaust air concentrations divided by concentrations at manikin's face) were also measured. High values of air change effectiveness (~ 1.3 to 1.9) and high values of pollutant removal efficiency (~ 1.2 to 1.6) were measured when these task conditioning systems supplied 100% outdoor air at a flow rate of 7 to 10 L s^{-1} per occupant.

INTRODUCTION

Task/ambient conditioning (TAC) is a method for providing occupants with control of a local supply of air so that they can adjust their individual thermal environment. Controlled variables can be the supply-air temperature, flow rate, direction and the ratio of room air to main air handling system supply air. TAC systems may provide all or part of the conditioned air to the occupied space. TAC systems have the potential to improve ventilation at the occupant's breathing zone because they can provide supply air (which is generally less polluted than room air) preferentially toward the breathing zone [1, 2, 3]. In addition, prior research has shown increased thermal comfort while using TAC systems [4, 5].

The objectives of this research were to determine ventilation efficiencies obtained through the use of two desk-mounted TAC systems operating in conjunction with a conventional (ceiling supply and return) heating ventilation and air conditioning (HVAC) system. In this paper, to characterize the improvement in ventilation at the breathing zone we use two "ventilation efficiency" parameters (see [6] for more details). The first is the air change effectiveness (ACE), defined as the age of air that would occur throughout the room if the air was perfectly mixed, divided by the average age of air where occupants breathe. Because the average age of air exiting the room is identical to the age of air that would occur throughout the room if the indoor air were perfectly mixed, the ACE is also the exhaust-air age divided by the average age of air where occupants breathe. A short-circuiting flow pattern decreases the exhaust-air age and causes ACE to be less than unity. Perfect mixing results in an ACE of unity.

Preferentially ventilating the breathing zone with outside air will cause the ACE to be greater than unity.

The second ventilation efficiency parameter is the pollutant removal efficiency (PRE). We define the PRE as the time-average concentration of pollutants in the exhaust air divided by the time-average concentration where occupants breathe. The PRE is a function of the locations of pollutant sources, the indoor airflow pattern and the nature of the pollutant emission process, e.g., emitted with or without momentum. In many configurations, values of PRE may be correlated to the values of ACE.

TASK/AMBIENT CONDITIONING SYSTEMS

The first TAC system evaluated is the Personal Environmental Module (PEM). A mixing box with a fan, located underneath the desk, draws air from a dedicated air-handling unit (AHU) via a flexible duct connected directly to AHU supply ducts or to an under-floor supply air plenum. Normally (but not in our experiments) another stream of air enters the mixing box from beneath the desk. After passing through the mixing box, the mixture of AHU supply air and room air exits two air supply outlets located at the back corners of the desk. The air supply outlets on top of the desk can be rotated 360° in the horizontal direction and contain movable vanes which can be rotated ± 30° in the vertical direction. The PEM has a control panel from which the air flow rate, percent of room air that is mixed in the mixing box with air from the main AHU, and other parameters can be changed.

The second TAC system is the Climadesk. A panel attached to the underside of a conventional desk is connected by a flexible duct to a portable fan-filter unit placed next to the desk. The fan-filter unit is supplied with air from the AHU or draws air from outdoors. Supply air exits two adjustable outlets underneath and close to the underside of the worksurface. These outlets are located close to a seated worker's knees and direct air horizontally above the seated worker's thighs and towards the torso. In the horizontal plane, the angle of air supply from these outlets is manually adjustable. There is an additional, non-adjustable outlet at the front edge of the desk, which directs air almost vertically upwards, but slightly away from a seated occupant. A proportion of the total airflow (0-100%) can be directed to this third outlet, as desired by the occupant.

RESEARCH METHODS

All experiments were performed in a controlled environment chamber (CEC) with a 5.5 m by 5.5 m floor and 2.5 m high ceiling. The CEC resembles a modern office space. Figure 1 shows the floor plan of the workstations in the chamber. During experiments, two identical TAC systems were operated with heated manikins seated in workstations 2 (WS2) and WS3, while a conventional HVAC system supplied air through a perforated diffuser located in the ceiling. All measurements were performed at steady state conditions. Air was exhausted from the chamber through a ducted ceiling-level return grill.

EXPERIMENTAL CONDITIONS

Each workstation with the TAC system and manikin were configured identically for each test. PEM air supply outlets were either pointed toward the occupant or parallel to the side walls of the workstation. The Climadesk supplied air either horizontally under the desk, vertically upward from the front edge of the desk or approximately equally from both the horizontal and vertical directions. Except as noted in Table 1, all of the outside air was supplied through either the PEM or Climadesk nominally at 10 L/s-occupant and 19 °C. The room temperature was controlled at ~25 °C. The manikins were seated upright with their faces located about 15 cm back from the edges of the desks, except during four tests with the manikins leaning slightly forward with their faces in the vertical air supply jets exiting the Climadesks.

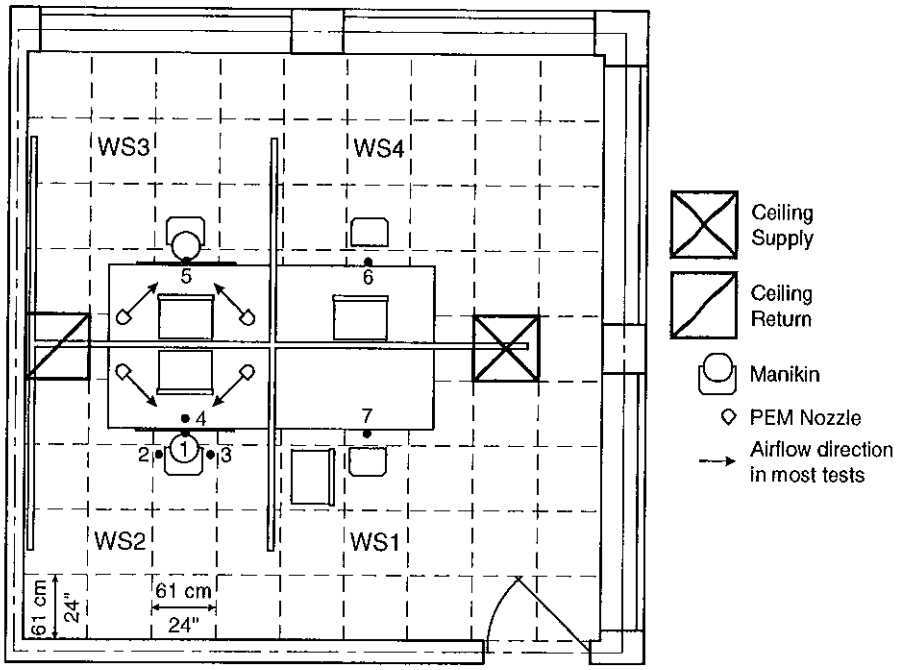

Figure 1. Plan view of CEC with workstations denoted WS1, WS2, WS3 and WS4. All sample points were 1.1 m above the floor. Points 1 and 5 are 3 cm below the tip of the nose; points 2 and 3 are immediately above each shoulder; point 4 is 15 cm in front of the nose; points 6 and 7 are at the edge of the desk.

MEASUREMENT METHODS

ACE was measured using a tracer-gas stepup procedure. After steady state test conditions were established, sulfur hexafluoride (SF_6) tracer gas was injected at a steady rate into the supply or outside air duct. Concentrations were measured every four minutes at locations shown in Figure 1. Ages of air (τ) were determined from the SF_6 tracer data via the equation

$$\tau = \frac{1}{C(t_{end})} \int_0^{t_{end}} [C(t_{end}) - C(t)]dt \qquad (1)$$

where C(t) is the tracer-gas concentration at the point in question, $C(t_{end})$ is the steady-state concentration at the end of the stepup, and t is the time elapsed since the start of tracer-gas injection. The ACE is defined as the ratio, $\tau_{return} / \tau_{bl}$, where τ_{return} is the age of the return/exhaust air and τ_{bl} is the average age of air at the breathing level in WS2 and WS3.

Table 1. Experimental conditions and results.

				From each TAC			Ceiling Air Supply per (TAC unit)		ACE	PRE	
TEST	TAC[1]	Air Supply Direction	Manikin Position[2]	%OA[3]	Flow (L/s)	Temp (C)	%OA[3]	Flow (L/s)		Floor Source	Body Source
130	C	Vertical	Upright	100	7	19.1	0	36	1.03	0.88	1.04
132	C	Vert/Horiz	Upright	100	7	19.6	0	35	1.06	1.00	1.28
145	C	Vert/Horiz	Upright	100	7	18.4	0	31	1.15	1.14	1.47
131	C	Horizontal	Upright	100	7	20.2	0	35	1.37	1.15	1.35
140	C	Horizontal	Upright	100	7	25.8	0	33	1.33	1.17	1.31
141	C	Vertical	Lean	100	7	19.4	0	31	1.73	1.55	1.44
142	C	Vertical	Lean	100	7	19.1	0	31	1.83	1.49	1.52
143	C	Vertical	Lean	100	3	24.4	12	31	1.75	1.38	1.52
144	C	Vertical	Lean	100	3	26.1	12	31	1.94	1.35	1.58
135	P	Parallel	Upright	21	37	19.2	0	17	NA	0.92	1.11
136	P	Parallel	Upright	19	38	19.1	0	30	NA	0.93	1.08
137	P	Parallel	Upright	20	38	19.3	0	31	1.04	0.98	1.09
133	P	Toward	Upright	100	10	19.7	0	33	1.63	1.25	1.54
139	P	Toward	Upright	100	9	19.6	0	34	1.42	1.20	1.46
134	P	Toward	Upright	100	10	19.5	0	34	NA	1.20	1.43
138	P	Toward	Upright	15	15	19.0	20	34	1.17	1.00	1.07

1. C: Climadesk; P: PEM
2. Upright: Manikin seated upright about 15 cm from edge of desk.
   Lean: Nose of manikin in vertical jet from Climadesk.
3. %OA: Percent Outside Air

For the measurements of PRE, three different perfluorocarbon tracer-gases were used to simulate sources of indoor-generated pollutants. Passive emitters of the first tracer was placed on the floor in each of the four workstations simulating emissions from the floor covering. Passive emitters of the second and third tracer gases were placed on the manikins in WS2 and WS3, respectively. The PRE for the "Floor" and "Body" pollutants were calculated from the equations:

$$PRE_{Floor} = \frac{C_{Floor}^{Return}}{\frac{1}{2}\left(C_{Floor}^{BL2} + C_{Floor}^{BL3}\right)} \qquad PRE_{Body} = \frac{1}{2}\left(\frac{C_{Body2}^{Return}}{C_{Body2}^{BL3}} + \frac{C_{Body3}^{Return}}{C_{Body3}^{BL2}}\right) \qquad (2)$$

where the superscript denotes the measurement location (Return duct, Breathing Level in either WS2 or WS3) and the subscript denotes the location of the pollutant source (floor, manikin in WS2 or WS3). The values of PRE_{Body} indicate the efficiency of the ventilation process in controlling exposures to pollutants from the occupants in the adjoining workstation.

RESULTS

The highest values of ACE and PRE were measured, with either of the TAC systems supplying 100% OA at approximately 7 - 10 L/s per occupant, with the air supply directed toward the manikin's face. With the PEM, the nozzles were pointed toward the manikin's face and with the Climadesk, the manikin leaned into the vertical air jet exiting the front edge of the desk. In experiments with the Climadesk (Tests 141 - 144), the high values of ACE and PRE were very localized at the mouth and nose, as measurements of ACE and PRE 15 cm in front of the nose and mouth were close to unity. High values of ACE and PRE were not measured with the manikin seated upright (i.e., with the face not located directly in the vertical supply air jet) and air supplied through the vertical outlet of the Climadesk (Test 130).

The Climadesk also produced high ACE and PRE values when the air supply was entirely horizontal (Tests 131 and 140), directed toward the manikin's torso from beneath the desk. Tests with a smoke tube suggest that some of the outside air supplied horizontally by the Climadesk was entrained in the thermal plume flowing upward along the body and carried into the region of the nose and mouth. Under these operating conditions, high values of ACE and PRE were also measured 15 cm in front of the nose and mouth.

With approximately equal amounts of air supplied vertically and horizontally from the Climadesk, the ACE and PRE values were not consistent. Results from Test 132 indicated little or no improvement in ACE or PRE, whereas results from Test 145 indicate enhanced ACE and PRE as expected. As discussed above, the improved ACE and PRE values with this configuration may be highly dependent upon the manikin position relative to the location of the vertical jet of air exiting the Climadesk.

In two tests with the Climadesk, high values of ACE and PRE were maintained when approximately half of the total outside air supply was provided by the conventional overhead ventilation system. We anticipated a decrease in performance under these operating conditions. However, these results were obtained in tests with the manikin's head located directly in the vertical air supply jet. As discussed above, under these conditions the ACE and PRE will vary considerably with small changes in the position of the head and an optimal location of the manikin's head may have counteracted the expected performance decrease.

DISCUSSION AND CONCLUSIONS

In our previous research [1] with air supplied from the PEM at much higher flow rates (19 to 94 L/s), PREs and ACEs were significantly above unity only if 100% outside air was directed toward the occupants face – a condition that is not likely to be comfortable [7]. Directing the air away from the face made conditions more comfortable but resulted in ACEs and PREs close to unity. These prior results suggest that high rates of air supply from TAC systems may vigorously mix the air within the workstation, making it difficult to preferentially ventilate the breathing zone. With the lower supply flow rates employed in this current set of experiments, ventilation efficiencies were high and thermal comfort conditions were acceptable [8].

For the Climadesk unit operating with a vertical air supply jet, a superior ventilation performance was achieved with the occupant's head located precisely within the vertical jet of air. However, our data and understanding of system performance suggest that supplying air

horizontally toward the body's thermal plume is the more robust method of assuring high ventilation efficiencies.

Our findings indicate that energy savings could be realized while maintaining a typical level of IAQ at the breathing zone by allowing rates of outside air supply to be reduced. Values of ACE from 1.3 to 1.9 translate to a 23% to 47% decrease in the design ventilation rate, assuming the airflow pattern is not significantly changed. Alternatively, IAQ at the breathing zone could be improved while maintaining typical rates of outside air supply.

ACKNOWLEDGMENTS

This work was supported by Johnson Controls, Inc. and the Assistant Secretary for Energy Efficiency and Renewable Energy, Office of Building Technology, State, and Community Programs, Office of Building Systems of the U.S. Department of Energy (DOE) under contract No. DE-AC03-76SF00098.

REFERENCES

1. Faulkner, D, Fisk, W J, and Sullivan, D P.1993. Indoor Airflow and Pollutant Removal in a Room With Desktop Ventilation. *ASHRAE Transactions* Vol. 99(2) pp 750-758.

2. Fisk, W J, Faulkner, D, Pih D, et al. 1991. Indoor Air Flow and Pollutant Removal in a Room with Task Ventilation. *Indoor Air* 3, pp 247-262.

3. Faulkner, D, Fisk, W J, and Sullivan, D P.1995. Indoor Airflow and Pollutant Removal in a Room With Floor-based Task Ventilation: Results of Additional Experiments. *Building and Environment*. Vol. 30(3) pp 323-332.

4. Bauman, F S and Arens, E A. 1996. Task/Ambient Conditioning Systems: Engineering and Application Guidelines. Center for Environmental Design Research, University of California, Berkeley, CA. Publication number CEDR-13-96.

5. Bauman, F S, Carter, T G, Baughman, A V, and Arens, E A. 1998. Field Study of the Impact of a Desktop Task/Ambient Conditioning System in Office Buildings. *ASHRAE Transactions*, Vol. 104 (1) pp 125-142.

6. Faulkner, D, Fisk, W J, Sullivan, D P, Wyon, D P. 1999. Ventilation Efficiencies of Desk-Mounted Task/Ambient Conditioning Systems. E.O. Lawrence Berkeley National Laboratory Report LBNL-42700. *Indoor Air,* in press.

7. Bauman, F S, Arens, E A., Benton, C C, and Zhang, H. 1993. Localized Comfort Control with a Desk-top Task Conditioning System: Laboratory and Field Measurements. *ASHRAE Transactions* Vol. 99(2), pp 733-749.

8. Tsuzuki, K, Arens, E A, Bauman F S, and Wyon, D P. 1999. Individual Thermal Comfort Control With Desk-Mounted and Floor-Mounted Task/Ambient Conditioning Systems. Center for Environmental Design Research, University of California, Berkeley, CA. *To be presented at Indoor Air 99.*

PARTICLE CONCENTRATIONS IN AN AIR-CONDITIONED OFFICE BUILDING WITH NORMAL AND HIGH EFFICIENCY FILTRATION

William J. Fisk*, David Faulkner*, Doug Sullivan*, and Mark J. Mendell[+]

*Indoor Environment Department, Lawrence Berkeley National Laboratory, USA
[+]National Institute for Occupational Safety and Health, USA

ABSTRACT

Indoor and outdoor particle concentrations and ventilation rates were measured versus time in a large office building without tobacco smoking. Periodically, high efficiency filters replaced the normal filters in air handling systems. For all particle sizes, indoor concentrations varied considerably with time. Even with the normal air filters, which have a low efficiency for submicron particles, number concentrations of submicron particles were a factor of three to six smaller indoors compared to outdoors. The high efficiency filters reduced the indoor-outdoor particle concentration ratio for submicron particles by 70% to 95%. For larger particles, the decreases in indoor concentrations were substantially smaller. Comparisons of model predictions with measured data indicate a large rate of removal of submicron indoor particles by some process other than ventilation or air filtration, and also provide evidence of significant indoor generation or resuspension of particles larger than 1 μm.

INTRODUCTION

There is evidence from epidemiological studies that increased morbidity and mortality are associated with increased exposures to small particles [1]. Although these studies have relied on outdoor particle data, most people's exposures to particles occur primarily indoors. Indoor air contains indoor-generated particles and particles that enter the building with outside air. The published literature provides very limited information on the time variation of particle concentrations and size distributions in large commercial buildings. Additionally, the effectiveness of high efficiency filters in reducing indoor particle concentrations has not been well documented. This paper presents and discusses such data, obtained during a study of the influence of high efficiency filtration on office workers' acute health symptoms.

RESEARCH METHODS

The study was performed on two floors of a large, urban, air-conditioned office building with sealed windows. The floor area and occupancy were 4130 m^2 and 165 persons on Floor 2 and 4840 m^2 and 280 persons on Floor 4. The floors were almost entirely open plan, with extensive carpeting and fabric-covered partitions. Smoking was prohibited. Each floor had four identical air handling units (AHUs). For each AHU, outside air mixed with recirculated indoor air drawn from the mechanical room and the mixture passed through a bank of eight filters, each with nominal cross-sectional dimensions of 0.6 m by 0.6 m. The filtered air passed through the supply fan, cooling coils, and supply air ducts and entered the occupied space through diffusers in the suspended ceiling. Return air was drawn through grilles in the suspended ceiling and flowed through the ceiling plenum to the mechanical rooms. The rated maximum supply air flow from each set of four AHUs was 18.4 $m^3\ s^{-1}$. Outside air dampers were in the minimum open position during occupancy, except during one 0.5 h period.

Particle concentrations as a function of time were measured outdoors and at two indoor locations per floor at a height of 1.8 m. Laser optical particle counters measured number concentration in five size bins (0.3-0.5 μm, 0.5-0.7μm, 0.7-1.0μm, 1.0-2.0μm, >2.0 μm). Monitoring occurred during the workday periods of Thursdays and Fridays, for seven consecutive weeks during summer, 1996. There are a few periods of missing data. The particle counters were factory calibrated before and after the study. Additionally, all particle counters were intercompared twice and measured data have been "corrected" using one of the instruments as a reference. Many additional environmental parameters were measured, but only the ventilation rate measurements are pertinent to this paper. The tracer gas procedure used to measure equivalent steady outside air ventilation rates (ESVRs) is described elsewhere [2]. The ESVRs are averages for the workday periods of Thursday and Friday.

During weeks three and five, high efficiency air filters were installed in the AHUs on Floor 4. During weeks four and six, these filters were installed on Floor 2. At other times, the building's normal air filters were utilized. At the start of the study, all air filters were new. Using data for filters with the same ASHRAE efficiency rating [3], the estimated efficiency of the normal filters is 3%, 15%, 40%, and 80% for particles with diameters of 0.3 μm, 0.85 μm, 1.5 μm, and 3 μm, respectively. The high efficiency filters have an efficiency rating of 95% for 0.3 μm particles. From filter theory, their efficiency should be higher than 95% for particles either smaller or larger than 0.3 μm. Switching between the normal and high efficiency filters caused no discernible change in the supply air flow rate. Based on filter performance data, the loading of less than 10 g of dust on these filters during the study should not significantly change their air flow resistance or efficiency.

To aid in interpretation of the experimental data, a steady state mass balance equation for a well-mixed space was employed for particles in each size range:

$$S + (Q_o - Q_{\text{inf}})(1-E)\,C_o + Q_{\text{inf}}\,PC_o = Q_o\,C + \lambda_{dep}\,VC + Q_r\,EC \qquad (1)$$

where: S = indoor particle generation rate; Q_0 = rate of outside air entry based on the tracer gas measurements; Q_{inf} = rate of air infiltration flow through the building envelope (not filtered); E = the filter efficiency; C_o = outdoor particle concentration; P = penetration factor for infiltrating particles; C = indoor particle concentration; λ_{dep} = a particle deposition coefficient that accounts for particle deposition on indoor surfaces; V = indoor air volume; and Q_r is the rate at which recirculated indoor air flows through the filters; $[Q_r = Q_s - (Q_o - Q_{\text{inf}})]$, where Q_s is the total supply air flow rate. Three of the model parameters can be only roughly estimated. A reasonable value of the product of Q_{inf} and V is ~ 0.1 h^{-1}; however, if the AHUs pressurizes the building (the design intent), Q_{inf} may be negligible during AHU operation. For particles smaller than ~0.7 μm, P may be very close to unity [4,5,6]. Table 1 provides reported values of λ_{dep} as a function of particle size. The base case values are based on a compilation of data from three papers [6, 7, 8]. Relative to the base-case values, Lewis [5] reported a factor of three to four higher deposition coefficients for submicron particles under quiescent conditions and even higher deposition coefficients under turbulent conditions. Values for the particle generation rate S in large office buildings are not known; however, valuable information can be gained from modeling with S set equal to zero.

RESULTS

Within each floor, the measured values of ESVR were relatively constant, ranging from 1.8 to 2.1 $m^3 s^{-1}$ on Floor 2 and from 3.2 to 3.5 $m^3 s^{-1}$ on Floor 4. There were no significant correlations between particle concentrations and ventilation rates, presumably because of the small range in ventilation rates. However, the higher particle concentrations on Floor 4 during normal filtration may be a consequence of the higher ventilation rates on Floor 4.

Figure 1 provides an example of the time-averaged particle number concentrations in each size range. Three observations follow. First, the particle number concentration is dominated by the smallest particles. Second, even with normal filters, indoor concentrations of submicron particles are lower than outdoor concentrations by a factor of three to six. Third, number concentrations of submicron particles are much lower with high efficiency filtration.

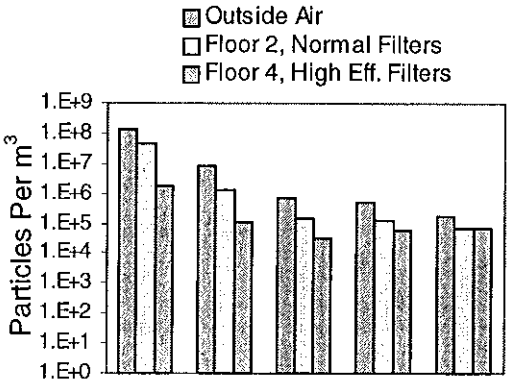

Figure 1. Particle size distribution on week 5.

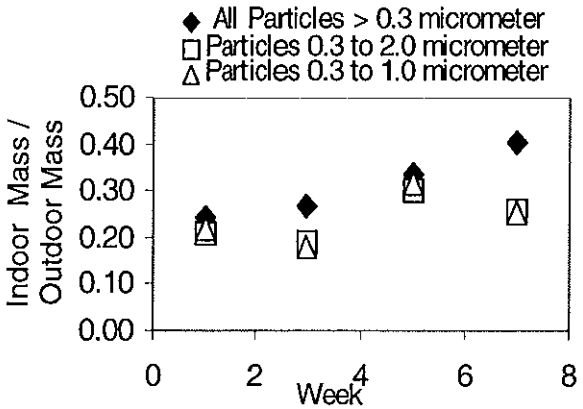

Figure 2. Indoor-outdoor ratios of particle mass concentrations with normal filtration, Floor 2.

The particle mass in each size bin was calculated using a particle density of 2.5 g cm^{-3} and particle sizes of 0.4, 0.6, 0.85, 1.5, and 3.0 μm for the five bins. During normal filtration, the smallest and largest bins contained 70% to 86% of the particle mass. During high efficiency filtration, particles larger than 1.0 μm accounted for 87% to 96% of the particle mass.

There were large week-to-week and within-day variations in particle number concentrations. Indoor concentrations roughly tracked outdoor concentrations, at least with normal filtration. There were numerous spikes in indoor particle concentrations at specific locations. Episodic localized releases or resuspensions of particles are one potential explanation for the spikes. Figure 2 plots the estimated indoor-to-outdoor (I/O) particle mass ratios versus week for Floor 2. Indoor mass concentrations track outdoor concentrations, although quite imperfectly. Considering particles smaller than 2 μm, the I/O mass ratios ranged by approximately a factor of two. The corresponding outdoor particle mass concentrations varied over a range of six.

Table 1 provides measured ratios of indoor particle number concentrations to outdoor concentrations (I/O ratios) from periods with normal filtration. The I/O ratios are only 0.15 to 0.55, thus, outdoor particle data are a poor direct measure of indoor particle exposures. The highest measured I/O ratios occur for the largest particles. Table 1 includes predictions of the I/O ratios for the three sets of particle deposition coefficients. For these predictions, we used the measured ESVRs and the previous estimates of filter efficiency. We assumed that supply

air flow rates were 66% of the maximum, that the product- Q_{inf} V - (i.e., infiltration rate) was 0.1 h^{-1}, and that the P was unity. Finally, the predictions assume negligible indoor particle generation, which is most likely to be a reasonable assumption for the smallest particles.

For the submicron particles and the base-case or Lewis quiescent deposition coefficients, the predicted I/O ratios exceed the measured ratios by a factor of two to three. Accounting for indoor particle generation would increase the discrepancy. Doubling the air infiltration rate or decreasing P to 0.5 reduces this discrepancy insignificantly. Doubling the filter efficiency, which is probably unrealistic, leaves discrepancies near a factor of two. Therefore, the comparison of measured and predicted ratios suggests that particle deposition coefficients are underestimated or that there is some large unexplained removal process for submicron particles. For example, the discrepancy between the predicted and measured I/O ratios diminished substantially with the higher Lewis turbulent deposition coefficients in the model.

Table 1. Measured and predicted ratios of indoor-to-outdoor particle number concentration.

Floor	Part. Size (μm)	Filter Eff.	Base Case λ_d (h^{-1})	Lewis Quies-cent λ_d (h^{-1})	Lewis Turbu -lent λ_d (h^{-1})	Measured (C_{in}/C_{out})	Predicted C_{in}/C_{out} With Base Case λ_d	Predicted C_{in}/C_{out} With Lewis Quiescent λ_d	Predicted C_{in}/C_{out} With Lewis Turbulent λ_d
2	0.3-0.5	0.03	0.06	0.26	2.2	0.27	0.75	0.57	0.17
2	0.5-0.7	0.1	0.09	0.26	1.4	0.15	0.52	0.43	0.20
2	0.7-1.0	0.15	0.15	0.31	1.7	0.18	0.41	0.35	0.16
2	1.0-2.0	0.4	0.35	0.43	2.0	0.23	0.17	0.16	0.09
2	>2.0	0.8	0.80	0.72	3.1	0.52	0.05	0.05	0.03
4	0.3-0.5	0.03	0.06	0.26	2.2	0.44	0.83	0.67	0.23
4	0.5-0.7	0.1	0.09	0.26	1.4	0.26	0.65	0.56	0.28
4	0.7-1.0	0.15	0.15	0.31	1.7	0.28	0.53	0.47	0.23
4	1.0-2.0	0.4	0.35	0.43	2.0	0.38	0.25	0.24	0.13
4	>2.0	0.8	0.80	0.72	3.1	0.55	0.07	0.07	0.04

For particles larger than 1 μm in size, the measured I/O ratios exceed the predicted ratios, regardless of the choice of particle deposition coefficients. For the largest particles, the discrepancy is about a factor of ten. Reasonable changes in the model inputs will not resolve these discrepancies. Substantial indoor particle generation or resuspension, for particles larger than 1 μm, seems to be the most likely explanation for this discrepancy. Occasional periods with indoor concentrations of particles larger than 1 μm exceeding outdoor concentrations provided additional evidence of indoor generation of these larger particles.

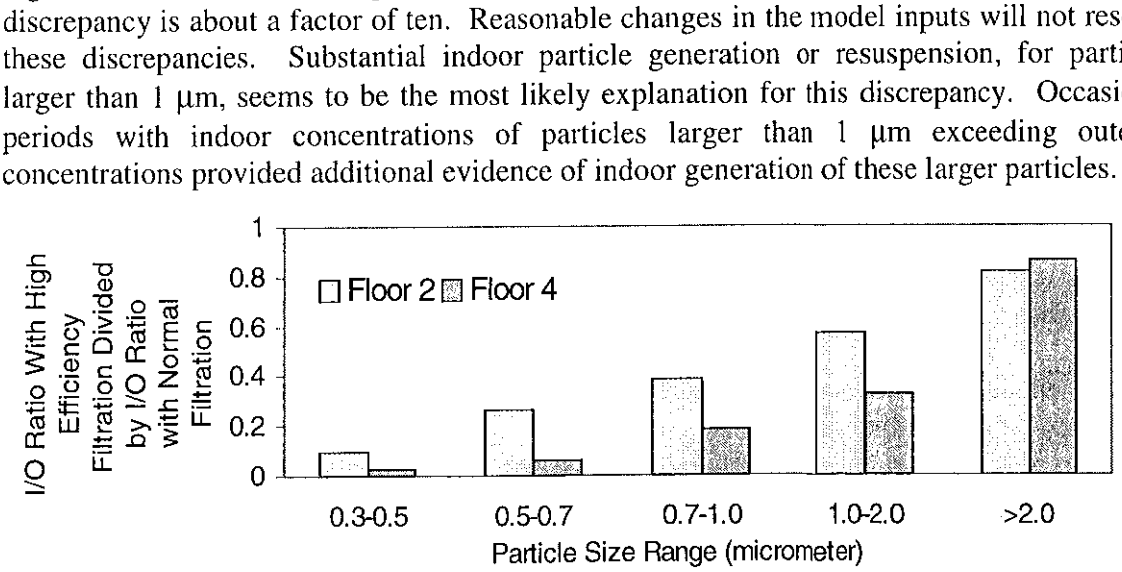

Figure 3. Influence of high efficiency filtration on I/O particle concentration ratios.

To characterize the benefits of high efficiency filtration, the I/O ratios from periods of high efficiency filtration were divided by the I/O ratios from periods of normal filtration. The results in Figure 3 illustrate that high efficiency filtration was associated with a very large reductions in the indoor concentrations for the smallest particles. As particle size increased, the benefits of the high efficiency filtration decreased, presumably because the efficiency of the normal filters increases with particle size. Averaging the results from both floors yields the following reductions in particle number concentrations: 94% for 0.3-0.5 μm; 84% for 0.5-0.7 μm; 72% for 0.7-1.0 μm, 55% for 1.0-2.0 μm ; and 16 % for >2.0 μm particles.

DISCUSSION

Published comparisons of indoor and outdoor particle concentrations in large commercial buildings without smoking are limited. Field studies [9, 10] found that particle mass concentrations were generally smaller indoors. Another study [11] found number concentration of 17 to 700 nm particles in an office building to be 40% less than outdoor concentrations. Thus, our findings that indoor particle concentrations were smaller than outdoor concentrations are typical of findings from commercial buildings without smoking. Several prior studies have also reported large temporal variations in particle concentrations within commercial buildings [e.g., 11, 12]. These findings suggest that short-term particle concentration measurements, which are very common, have a limited utility for assessment of time average indoor particle exposures.

We identified few papers quantifying the effects of high efficiency filtration in commercial buildings. In a telecommunications building [13], high efficiency filtration was associated with 50% reduction in the I/O number concentration ratios for particles larger than 0.5 μm. In model predictions of the benefits of high efficiency filtration, substantial reductions in indoor concentrations are generally predicted.

Respirable size particles are thought to be the most likely cause of adverse health effects associated with particles [1]; thus, our findings suggest that using high efficiency filters in building AHUs may be beneficial for health. However, high efficiency filters would not be expected to decrease health effects associated with indoor particles larger than approximately two micrometers in size because normal filters are relatively efficient for these large particles. Many of the intact bioaerosols may be larger than two micrometers.

CONCLUSIONS

The most important conclusions from this study follow: (1) Indoor concentrations of respirable size particles in large sealed mechanically ventilated buildings without tobacco smoking can be substantially lower than outdoor concentrations. (2) Indoor particle concentrations vary considerably with time. (3) High efficiency filters can dramatically reduce indoor number concentrations of submicron-size particles. (4) Comparisons of model predictions with measured data indicate a large rate of removal of submicron indoor particles by some process other than ventilation or air filtration, and also provide evidence of significant indoor generation or resuspension of particles larger than 1 μm.

ACKNOWLEDGMENTS

This work was supported by the Assistant Secretary of Energy Efficiency and Renewable Energy, Office of Building Technology, State, and Community Programs, Office of Building

Systems of the U.S. Department of Energy (DOE) under contract No. DE-AC03-76SF00098, by the National Institute for Occupational Safety and Health, Centers for Disease Control and Prevention, and by the Office of Research and Development, U.S. Environmental Protection Agency. Any opinions expressed in this paper are those of the authors and do not necessarily reflect those of the sponsors nor is any official endorsement to be implied.

REFERENCES

1. EPA 1996. Air quality criteria for particulate matter, volume III of III, U.S Environmental Protection Agency, EPA/600/AP-95/001c.

2. Faulkner, D.; Fisk, W.J.; Sullivan, D.P. Thomas, JM Jr. 1997. Characterizing building ventilation with the pollutant concentration index: results from field studies. Proceedings of IAQ and Energy'98. ASHRAE, in press.

3. ASHRAE 1992. *1992 ASHRAE Handbook: HVAC systems and equipment*, American Society of Hearing, Refrigerating, and Air Conditioning Engineers Inc., Atlanta.

4. Ozkaynak, H, Xue, J Spengler, J et al. 1996. Personal exposure to airborne particles and metals: results from the particle team study. *Journal of Exposure Analysis and Environmental Epidemiology* 6(1): 57-78.

5. Lewis, S 1995. Solid particle penetration into enclosures. *Journal of Hazardous Materials* 43: 195-216.

6. Thatcher, TL and Layton DW 1995. Deposition, resuspension, and penetration of particles within a residence. *Atmospheric Environment* 29: 1487-1497.

7. Offermann, FJ, Sextro, RG, Fisk, WJ et al. 1985. Control of respirable particles in indoor air with portable air cleaners. *Atmospheric Environment* 19: 1761-1771.

8. Xu, M, Nematollahi, M, Sextro, RG et al. 1994. Deposition of tobacco smoke particles in a low ventilation room. *Aerosol Science and Technology* 20: 194-206

9. Turk, BH, Grimsrud, DT, Brown, JT et al. 1989. Commercial building ventilation rates and particle concentrations. *ASHRAE Transactions* 95(1): 422-433.

10. Brightman, HS, SE Womble, EL Ronca et al. 1996. Baseline information on indoor air quality in large buildings (BASE'95). *Proceedings of Indoor Air'96,* vol. 3: 1033-1042

11. Jamriska, M and Morawska L 1996. The effect of ventilation and filtration on reduction of indoor air exposure to submicrom pollutant particles – case study. *Proceedings of Indoor Air'96,* vol. 2: 753-758.

12. Weschler, CJ and Shields HC 1988. The influence of HVAC operation on the concentrations of indoor airborne particles. *Proceedings of IAQ'88*: 166-181. ASHRAE..

13. Krzyzanowski, ME and Reagor BT 1990. The effect of ventilation parameters and compartmentalization on airborne particle counts in electronic equipment offices. *Proceedings of Indoor Air'90,* vol. 2: 409-414.

V. POLLUTANT BEHAVIOR IN BUILDINGS

INDOOR TRANSPORT OF ETS PARTICLES AND TRACERS

M G. Apte, L A. Gundel, B C. Singer, D P. Sullivan and R G. Sextro

Indoor Environment Department, Lawrence Berkeley National Laboratory, University of California, Berkeley, CA USA

ABSTRACT

A multi-room environmental chamber has been constructed for examining multi-zone transport and the behavior of environmental tobacco smoke (ETS) and its tracers. The chamber simulates a small home, and it has been constructed of common building materials. One room has been conditioned extensively with ETS, while two adjoining rooms remained smoke-free. When the doors between the rooms were slightly ajar the particles dispersed from the smoking room into the other rooms, eventually reaching the same concentration. On the other hand, nicotine quickly adsorbed on unconditioned chamber surfaces so that nicotine concentrations in these rooms remained very low, even during smoking episodes. The results suggest that when nicotine is used as a tracer of ETS particle concentrations, interpretation of exposure data can be complicated and possibly misleading. Ultraviolet-absorbing particulate matter (UVPM) traced the transport of ETS particles into the non-smoking areas much better than did nicotine. Ongoing research includes investigation of the effectiveness of other chemical ETS tracers such as solanesol and fluorescent particulate matter (FPM).

INTRODUCTION

Environmental tobacco smoke - the smoke released from the burning end of the cigarette, along with exhaled mainstream smoke - is a common source of environmental exposure to carcinogens and other toxic air pollutants by the general public [1]. However, little is known about the extent of exposures to ETS. The objective of this research is to improve the basis for estimating ETS exposures in a variety of indoor environments. The research utilizes experiments conducted in both laboratory and 'real-world' buildings to (1) study the transport of gas- and particle-phase ETS components from room to room, (2) examine the suitability of various chemical tracers for ETS, and (3) evaluate whether re-emission of ETS components from indoor surfaces increases ETS exposure.

Our initial work has focused on pre-conditioning our room-sized chamber spaces so one room is similar to an area in which smoking occurs regularly, while other areas remain 'smoke-free'. Recent work at Berkeley Lab [2] has shown that the indoor behavior of nicotine - often used as an ETS tracer - is so complex that it may not always be a good mimic of ETS particles. Nicotine adsorbs to the walls and other surfaces during smoking until the surfaces are saturated. After smoking nicotine continues to desorb. Particles do not stick to the walls nearly as effectively as does nicotine. Therefore, the prior exposure history of indoor surfaces to nicotine influences its behavior (and hence its effectiveness as a tracer).

An indoor nicotine model [3] was used as a tool for planning the experimental protocols. During chamber conditioning, extensive particle mass and tracer data were collected for improving and extending the nicotine model. The focus of these experiments is the transport of ETS particles and nicotine from the conditioned smoking chamber into the rooms that were initially smoke-free. These data will be used to investigate whether measurements of various

chemical tracers, such as nicotine, solanesol, and ultraviolet-absorbing particulate matter (UVPM), can be used to predict ETS concentrations and potential exposures, as has been suggested by several investigators [2]. One goal is to provide data on which to base improved estimates of ETS exposures to the public. We also hope to show whether tracers can be used to examine how limiting smoking to certain areas of buildings influences ETS exposures in other parts of the building. An improved understanding of these phenomena is important for identifying and mitigating the environmental factors contributing to ETS exposures.

METHODS

Experiments in a 50 m^3 multi-room chamber; a schematic is shown in Figure 1. The chamber contains a "smoking room" (SR), a "corridor" (COR), and a "non-smoking room" (NSR). The walls and ceilings of the multi-room chamber were constructed of painted gypsum wallboard, and the interior walls of the NSR were lined with plastic sheeting prior to installation of the wallboard to reduce the diffusion of nicotine (or other gas-phase species) into the wallboard from the neighboring rooms. The floors were covered with a nylon carpet, typical of that used in residences. The chamber air exchange rate was about 0.02 h^{-1}.

The experimental work was conducted in two phases: the SR was first conditioned with cigarette smoke while the other two rooms remained unexposed. Experiments were then conducted to observe the movement of simulated ETS constituents from the SR, through the COR, and into the NSR. All cigarette smoking was done using an Arthur D. Little smoking machine, drawing one 35 cm^3 puff per minute. The machine was attached to a multiple port 'head' that permitted sequential smoking of up to 12 cigarettes, with programmed ignition and extinguishing. The sidestream smoke was emitted directly into the chamber, while the mainstream smoke -- the smoke drawn through the smoking machine -- was vented outside. The smoking machine was placed on a self-sealing drawer assembly mounted through one wall of the SR so that the smoking machine could be re-loaded without entering the room.

The SR was not ventilated during the conditioning or experimental phase. Small fans located within each chamber ensured adequate mixing before measurements began. Particle samples were collected for periods of 30 to 60 min from each room on filters for gravimetric and tracer chemical analysis. These samples contained only respirable suspended particles (RSP) since the dominant source of particles in these experiments is ETS, which is mainly composed of sub-micron particles. Particle number and size distributions were determined in near real-time with an array instrumentation that we have discussed previously [4].

The experimental protocol for this project includes determination of nicotine and the particle-bound tracers solanesol, scopoletin, FPM, and UVPM. Nicotine samples were collected on Tenax sorbent tubes for periods from 3 to 60 min. The sorbent tubes were thermally desorbed into a GC with flame ionization detection. The ultraviolet absorbance of methanol extracts of the filters was determined from 210 to 350 nm. The same extracts are to be analyzed by high performance liquid chromatography for the other chemical tracers.

Sulfur hexafluoride (SF_6) tracer gas was injected into the SR and the subsequent SF_6 concentrations were measured once every 5 minutes in all three chamber rooms, using a continuous GC monitoring system with electrochemical detection. These data were used to monitor the movement of gases throughout the chamber system and calculate ventilation rates, as shown in Figure 3.

Recently Van Loy et al. [3] examined the behavior of nicotine in a stainless steel chamber that contained common indoor surface materials such as painted wallboard and carpet. This work showed that the sorption and desorption processes are non-linear and are also dependent upon the previous nicotine 'exposure history' of the materials. We used the Van Loy nicotine model to devise a chamber conditioning procedure that emulates ETS behavior in a room where smoking occurs regularly. During a six-week period 36 cigarettes were machine-smoked each weekday in this room. The other rooms remained isolated with the connecting doors closed. Particle mass and nicotine concentrations were measured daily in each room during the conditioning phase.

RESULTS AND DISCUSSION

The observed and modeled gas-phase nicotine concentrations during the chamber conditioning period are shown for the SR as the solid line in Figure 2. The model uses a gas-phase nicotine source strength of 5 mg per cigarette [1]. Nicotine was measured either just after smoking (data points corresponding to the "spikes" in Figure 2), or at least 12 hours after the most recent cigarette (the lower set of data points). The spikes shown in the predicted nicotine concentrations are caused by the daily smoking pattern.

These data provide an evaluation of the model which was developed using parameters that describe the sorption and desorption of pure nicotine in the presence of wallboard and carpet. As shown in Figure 2, the model and measurements are in reasonable agreement. The results also illustrate the gradual increase in background gas-phase nicotine concentrations in the SR as a result of the re-emission of the sorbed nicotine from the wallboard and carpet. Based upon the Van Loy model predictions, it would take several years for the nicotine to reach steady state concentrations in the SR, at a smoking rate of 36 cigarettes per day.

In one experiment a single cigarette was smoked in the SR, while its door to the COR was open 2.5 cm (the COR/NSR door was wide open). Figure 3 shows particle and tracer gas (SF_6) movement in the three chambers. It can be seen that ETS particles reached the same concentration in all three rooms in about 18 hours, while the SF_6 concentrations equilibrated after only six hours. The difference is due to the deposition losses of the particles.

Table 1 shows RSP, nicotine, and UVPM concentrations in the three chamber rooms before, immediately after, and 4 hours after the cigarette was smoked. The RSP/nicotine ratio is an indicator of the effectiveness of nicotine as an ETS tracer. This ratio changed greatly as the ETS particles migrated out of the SR into the other two rooms. In fact, no measurable change in nicotine concentrations was observed outside of the SR, even though RSP concentrations had risen by about a factor of five. Nicotine did not reach the COR or the non-SR, even when ETS particles were easily detected. UVPM traced the movement of ETS accurately over the four-hour time period of this experiment. However, alternate sources of ultraviolet absorbing particles, such as diesel exhaust, were not present.

Particle size distribution data can be seen in Figure 3 and Table 1. The ETS particles were observed to coagulate as they aged. The geometric mean (GM) of the size distribution of the SR particle size distribution rose from 0.14 (GSD=1.8) just after smoking to 0.16 (GSD=2.0) after aging for 22 hours (see "t = 10:00" in Figure 3).

In general, the results indicate the following points: (1) the dynamic behavior of nicotine in chamber studies of ETS can be predicted using the Van Loy model; (2) nicotine sorbs quickly and strongly to the surfaces of rooms where smoking does not occur regularly, so while ETS

particles build up in concentration, nicotine moves from the air into materials; (3) the strong interactions of nicotine with indoor surface materials mean that nicotine will only track concentrations of less reactive tracers such as RSP and UVPM in rooms with well conditioned surfaces and regular smoking; and (4) interpretation of exposure data that were derived from nicotine concentrations can be complicated and misleading.

Planned future work on this project includes conducting additional transport experiments under static flow conditions, and under forced-flow conditions. The investigations will include analysis of a full array of ETS tracers (ultraviolet particulate matter including real-time UVPM, fluorescent particulate matter, solanesol, scopoletin). In addition, analyses of the collected data will include application of simple ventilation air-flow models to the data.

ACKNOWLEDGEMENTS

This work was supported by funds from the California Tobacco-Related Disease Research Program, Grant Number 6RT-0307, and by the Assistant Secretary of Conservation and Renewable Energy, Office of Building Technologies, Building Systems and Materials Division, of the U.S. Department of Energy (DOE) under Contract DE-AC03-76SF00098.

REFERENCES

1. J M Daisey, K R R Mahanama, and A T Hodgson. 1998 Toxic volatile organic compounds in simulated environmental tobacco smoke: Emission factors for exposure assessment, J. Exposure Analy. and Environ. Epidem. **8**, 313-334.

2. J M Daisey. (Accepted for publication). Tracers for Assessing Exposure to Environmental Tobacco Smoke: What are They Tracing? *Environmental Health Perspectives Supplements.*

3. M D Van Loy, V C Lee, L A Gundel, R G Sextro, J M Daisey and W W Nazaroff. 1997. Dynamic behavior of semivolatile organic compounds in Indoor Air. 1. Nicotine in a stainless steel chamber, Environ. Sci. Technol. **31**, 2554-2561.

4. M Xu, A Nematollahi, RG Sextro, AJ Gadgil, and W Nazaroff. 1994. Deposition of tobacco smoke particles in a low ventilation room, Aerosol Sci. Technol. **20**, 194-206.

Table 1. RSP, Nicotine, and UVPM concentrations, and particle size distributions (GM and GSD) in the SR, COR, and NSR at three times after one cigarette was smoked by machine. The SR/COR door was open 2.5 cm and the COR/NSR was wide open. Estimates of measurement uncertainty for RSP, nicotine, and UVPM are 3%, 5%, and 6%, respectively.

Location/Time	Before Smoking			Just After Smoking			4-hrs After Smoking		
ETS Paramter[1]	SR	COR	NSR	SR	COR	NSR	SR	COR	NSR
Nicotine ($\mu g/m^3$)	110	8.0	10	140	12	-	83	13	11
UVPM ($\mu g/m^3$)	480	-	24	900	28	-	230	100	200
RSP ($\mu g/m^3$)	500	17	36	930	30	-	230	87	190
Part. Size GM (μm)	0.14	-	0.16	0.14	0.14	0.11	0.14	0.14	0.13
Part. Size GSD	1.8	-	1.8	1.8	1.7	1.7	1.9	1.7	1.8
RSP/Nicotine	4.4	2.1	3.5	6.7	2.5	-	2.8	7.0	18
RSP/UVPM	1.0	-	1.5	1.0	1.1	-	1.0	0.9	1.0

[1]Note that the initial ETS concentrations in the SR were elevated due to previous smoking during chamber conditioning.

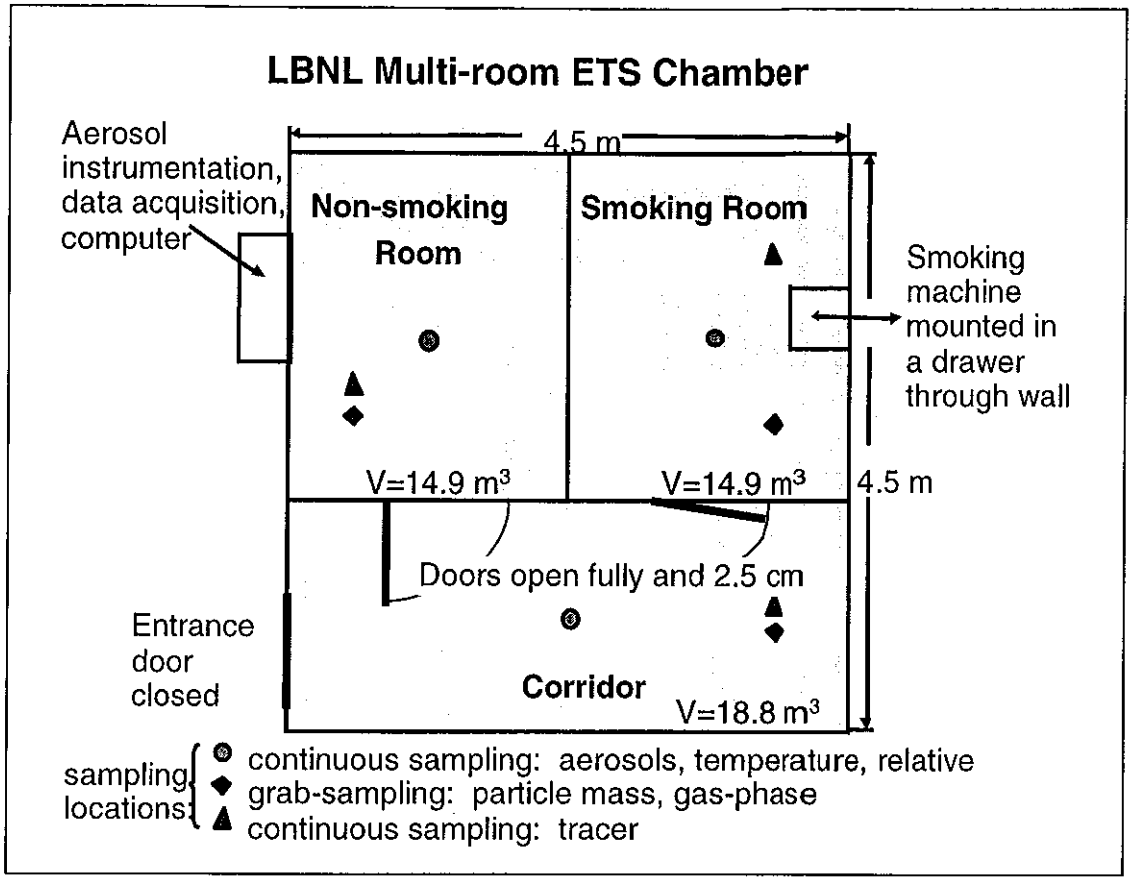

Figure 1. Schematic of the LBNL multi-room environmental chamber.

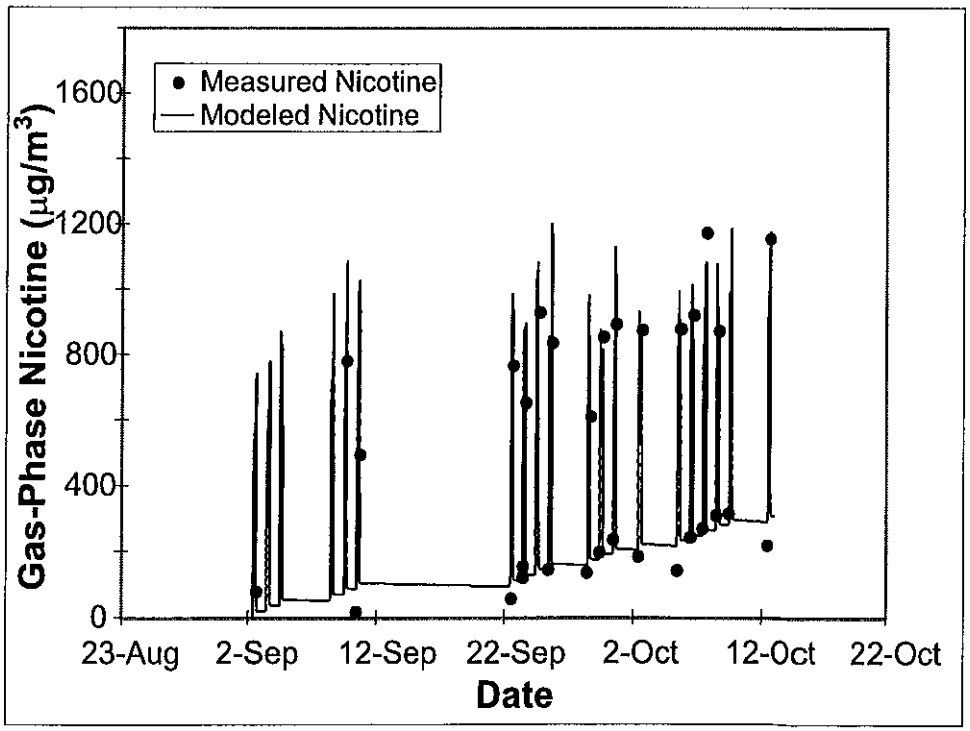

Figure 2. Measured and modeled nicotine concentrations during the LBNL multi-room environmental chamber "smoking room" conditioning phase.

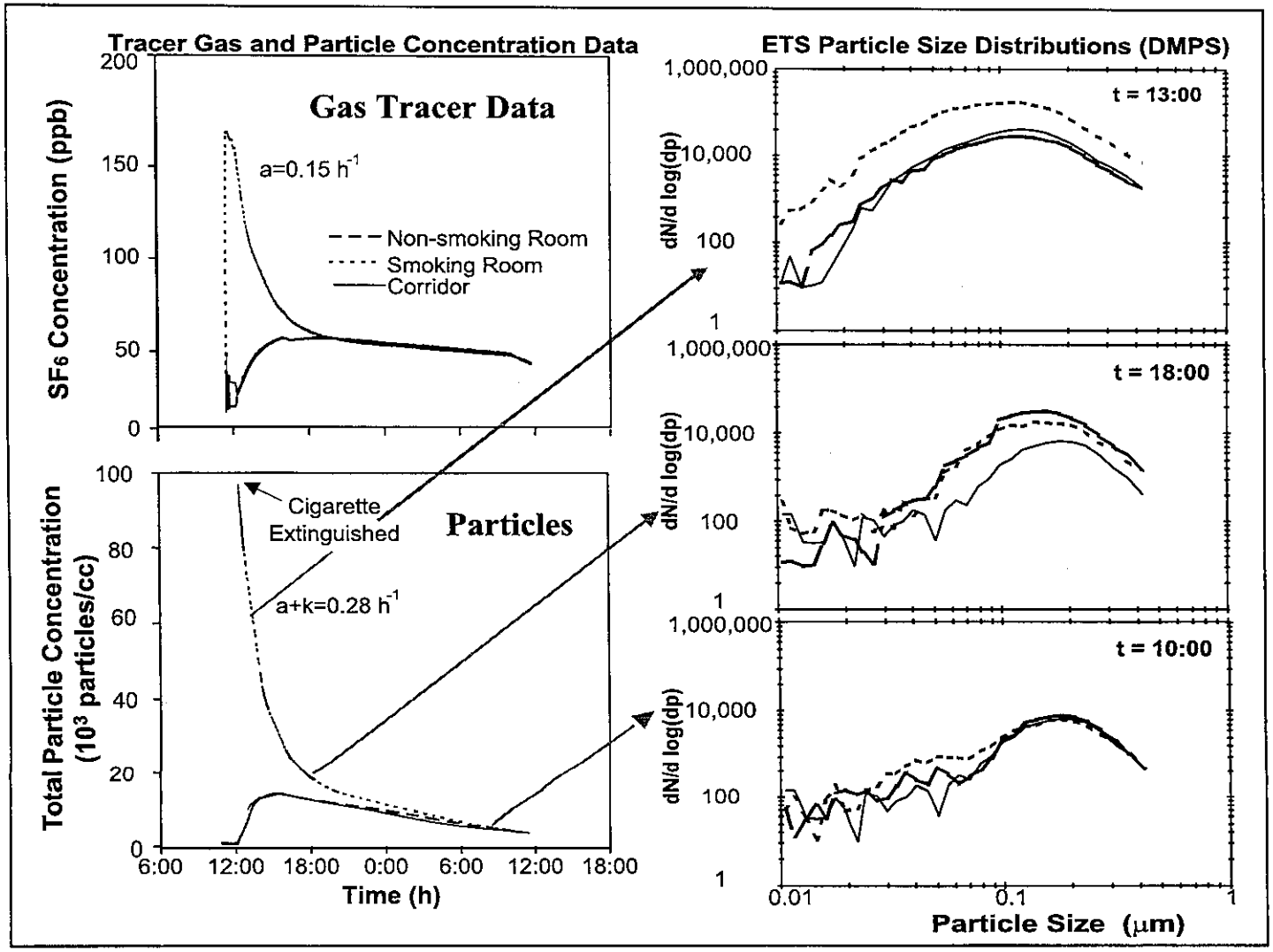

Figure 3. Tracer gas, ETS particle-counts and size distributions as a function of time, for each room, in the LBNL multi-room environmental chamber after smoking one cigarette. The SR/COR door was open 2.5 cm and the COR/NSR door was fully open. The SR inter-room mixing rate and particle deposition rates are denoted by the symbols *a* and *k*, respectively. The right side shows particle size distributions at the times indicated, measured using a Differential Mobility Particle Size Analyzer (DMPS).

COMPARISON OF MODELED AND MEASURED TRACER GAS CONCENTRATIONS IN A MULTIZONE BUILDING

R.G. Sextro, J.M. Daisey, H.E. Feustel, D.J. Dickerhoff, C.Jump

Indoor Environment Dept., Lawrence Berkeley National Laboratory, Berkeley, CA, USA

ABSTRACT

Few detailed comparisons of modeled and measured pollutant concentrations in multizone buildings have been published. The COMIS air flow and contaminant transport model permits simulation of the effects of building and HVAC operation, as well as the influence of the local meteorology, on air flows within the building. We have recently used this model to simulate the release of a gas-phase tracer in a three-story, multi-room building located at Dugway Proving Ground, Utah, USA. Following detailed leakage and flow-path characterization measurements of the building, experiments were conducted in which tracer gas concentrations were measured as a function of time in each room of the building. Comparison of the simulations with these detailed measurements showed reasonable -- and in some cases, quite good -- agreement. The paper describes some details of the experiments and modeling and discusses the differences between the observed and the predicted concentrations.

INTRODUCTION

In conjunction with a series of field tests to investigate the consequences of a domestic chemical/biological incident, transport of airborne pollutants within buildings has been examined both experimentally and theoretically. Measurements of tracer gas concentrations as a function of time were conducted in a multizone building to provide experimental data against which several interior air flow models could be evaluated. In our case, we have used the COMIS air flow and contaminant transport model to simulate the transport and fate of inert gas-phase species in this multizone building. As there have been very few detailed experiments on the behavior of pollutant or tracer gas species in multizone buildings reported in the literature -- particularly in cases where the buildings have been well characterized [1,2, 3] -- this was an important opportunity for model-measurement comparisons.

COMIS is a modular model for simulating air flows among multiple zones in response to the complex, often interacting effects of building and HVAC operations and the influence of the local meteorology [4]. Among the effects simulated by COMIS are flows through cracks, large vertical openings (e.g. doors and windows), fans and duct systems [5]. Based on the assumption that the pollutant concentration within each zone is instantaneously well-mixed, COMIS also calculates, in response to the interzonal air flow, contaminant transport as a function of time via a series of mass-balance equations.

PHYSICAL CHARACTERISTICS OF THE TEST BUILDING

The tests were conducted in one unit of a multi-unit building located at Dugway Proving Grounds, UT. Each three-story unit contains a set of three-rooms on the first and second floors, topped by a single-room, unfinished attic (see Figure 1). The staircase connecting the floors has landings on each floor through which the open staircase passes. The unit contains an air-handling

unit (AHU) that supplies air only to the first and second floor rooms. The AHU has a single air return - a wall-mounted grille located on the first floor in room 1.2a (Fig. 1). Unducted air return registers mounted in the walls connect the rooms on the first floor only; there is no explicit air return to the AHU from the second floor. The AHU does not provide fresh air; it is only for internal air circulation.

Prior to the tracer gas experiments, LBNL researchers conducted extensive blower door tests on the building to determine interzonal flow parameters, leakage rates, AHU flows and operating conditions. The building characterization measurements suggest that the first floor rooms have relatively low leakage rates to the exterior and to the staircase while the second floor rooms and attic are very leaky. The large leakage rates between the rooms on the first floor are due to the presence of the air return registers, while the large leakage rates between the rooms on the second floor are due to large cracks in the floor and within the walls. The AHU air supply rates were measured with all doors open, including the entrance door into the unit. The pressure drops over the supply and return grilles are on the order of 20 Pa.

TRACER GAS RELEASE EXPERIMENTS

The twelve experiments explored different positions of the internal and stairway doors (open or closed), different release locations on the first floor, and different states of AHU operation (on or off). In nine experiments, tracer gas releases were made at the return plenum of the AHU (which was always on for these tests) in room 1.2a, and in three experiments, the tracer gas was released in the center of room 1.3. The nine experiments were grouped into three sets, each set corresponding to a different position of the interior doors (all doors open, staircase doors closed, all doors closed). For the three releases in room 1.3 -- all of which were done with the staircase doors closed and the remaining interior doors open -- two were done with the AHU in operation and one with the AHU switched off. To capture the influence of the weather conditions on tracer gas transport, the three releases in each set were done at different times of the day (morning, mid-day, or afternoon).. There were no mixing fans to provide tracer gas mixing within each zone, apart from the mixing induced by the air flow from the AHU.

During the experiments, measurements of indoor air temperatures and propylene tracer gas concentrations were performed at 30-second intervals at the center of each room and on each of the three stairwell landings. Two measurement stations were located in room 2.2 - in the center of each half (i.e., at 2.2a and 2.2b in Fig. 1). Weather data were recorded at 15-minute intervals at two fixed sites within 2 - 3 km of the test building. The modeling groups used the weather and interior temperature data, along with the building characterization information, as input to their simulations, and reported the calculated indoor propylene concentrations before gaining knowledge of the measured concentrations.

The tracer gas was released by bursting a propylene-filled balloon containing approximately 20 g of material. However, the exact the mass of tracer gas released in each experiment was not measured, so it was necessary to adjust the predicted concentrations to facilitate model-measurement comparisons. We used the total amount of measured tracer gas within the building between five and ten minutes after tracer release as our normalization period.

Because of space limitations we only discuss in this paper the results of experimental trials 1 and 13 (one experiment had to be repeated), as they yield the best and worst results of the model-measurement comparison.

DISCUSSION OF RESULTS

Trial 1 (all doors open; release at AHU return; AHU on):

Figure 2 shows the measured and predicted tracer gas concentrations as a function of time for room 1.2a (the tracer release room). In this room, both mixing and transport times are fairly rapid with the AHU running and the measured and calculated concentrations differ very little. Comparing the measured and calculated tracer gas concentrations for the attic (room 3.1) provides a somewhat different picture (see Figure 3). COMIS overestimates the time-dependent tracer gas concentration. We believe this may be due to lack of mixing in the attic so that the large air leakage of the attic will exhaust the tracer gas entering through the staircase door before the gas can reach the sensor.

Trial 13 (staircase doors closed; release in room 1.3; AHU off):

In this trial the mixing of tracer gas in the unit and the transport into the upper floors is reduced because the staircase doors are closed and the AHU is off. The predicted and measured concentrations in room 1.2a are shown in Figure 4. The predicted and measured peak concentrations occur at about the same time, though the modeled concentration is lower than the measured for the first thirty minutes. The differences between measured and calculated concentrations for room 3.1 are shown in Figure 5, where the predicted and measured peak concentrations occur at about the same time. However, for almost three hours after tracer gas release there is more total transport of tracer gas into the attic than the model predicts. After that time COMIS over-predicts the concentration. As before, the lack of good mixing within the attic and the possibility that some of the tracer may be exhausted from the attic before reaching the sensor could explain the difference between the observed and predicted concentration decay.

Comparison of 'exposures':

Figure 6 shows the differences in exposure (i.e. the product of concentration and time between the modeled and measured values (as a fraction of the measured value) at various times after the tracer gas release for trial 1. The largest differences are seen for rooms 1.3 and 3.1 within the first five minutes after tracer release. After twenty minutes differences stay below +50 and –15% for all rooms of the unit. After an hour, exposure differences are reduced to less than 20% for all rooms but the attic. The large differences at the beginning of the decay period are again due to the modeling assumption of perfect mixing. In the case of the attic, the tracer gas needs some time to travel within the staircase from the first floor to the third floor landing. COMIS assumes that the tracer gas concentrations equalize immediately within the staircase.

The relative differences in exposure for trial 13 are shown in Figure 7. Because the AHU was off for this experiment, comparisons in exposure for 5, 10 and 20 minutes after tracer release are not very useful due to the lack of mixing. After 40 minutes, the largest differences are between the observed and predicted exposures in the second floor rooms. In contrast, the first floor rooms show differences of less than 25%. The are several possible explanations for the overpredicted exposure values on the second floor, including more rapid actual removal of tracer via ventilation to the outside than the model predicts.

CONCLUSIONS

The COMIS model performed well in the Dugway experiments when the model assumption of rapid mixing within a zone was met. Differences between measured and modeled values were largest in the 10 to 20 minutes immediately after the release, illustrating the lack of adequate mixing time. Leakage characterization and pressure distribution of the attic and roof may not have been adequate due to the unusual shape of the roof. The assumption of perfect mixing is more difficult to meet when the AHU is not operating. particularly for zones which either have a large vertical dimension (staircase) or have high leakage values to the outside (attic).

ACKNOWLEDGEMENTS

The authors like to thank R. Liebert and J. Rafferty from Dugway Proving Ground for their logistics and measurement support. This work was supported by the Office of Research and Development, Office of Nonproliferation and National Security, U.S. Department of Energy under Contract No. DE-AC03-76SF00098. The Dugway field tests and overall model-measurement comparison - conducted as part of the 911Bio Advanced Concepts Technology Demonstration - was sponsored by of Counterproliferation Office of the Office of the U.S. Secretary of Defense.

REFERENCES

1. Haghighat, F. and Megri, A.C. 1996. A Comprehensive Validation of two Airflow Models - COMIS and CONTAM, *Indoor Air*, Vol. 6, pp. 278-288.
2. Liddament, M.W. 1996. Two Air Flow Studies Completed, *Air Infiltration Review*, Vol. 17, No. 4.
3. Fürbringer, J.M., Roulet, C.-A., and Borchiellini, R. 1996. Annex 23 Subtask II&III Report - Evaluation of COMIS, Vol. 1 and Vol. 2, EPFL, Lausanne, Switzerland.
4. Feustel, H. E. 1996. Annex 23 - An International Effort in Multizone Air Flow Modeling, In Proceedings, ROOMVENT '96, Yokohama.
5. Feustel, H.E., and Raynor-Hooson, A. (Editors). 1990. COMIS Fundamentals, Air Infiltration and Ventilation Centre, Technical Note 29, Lawrence Berkeley Laboratory Report, LBL-28560.

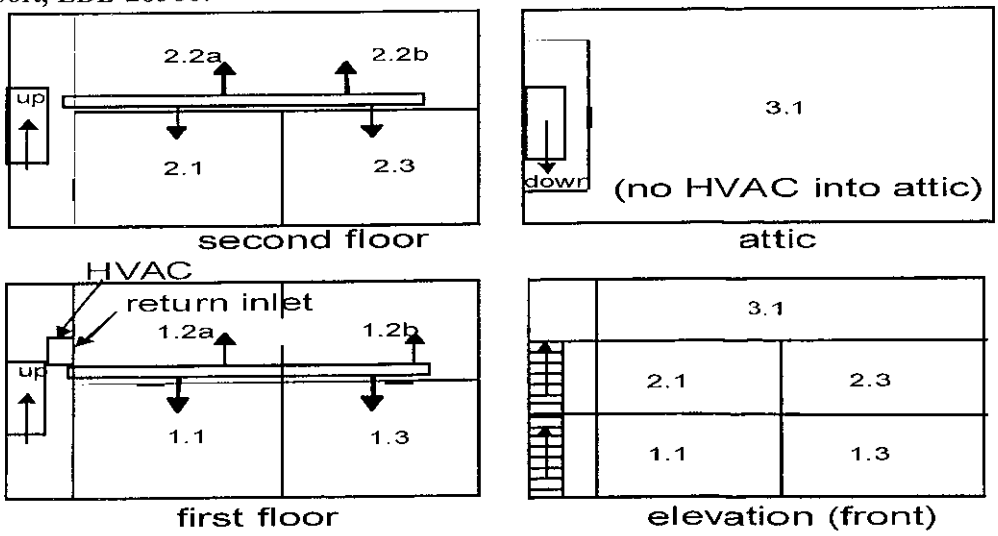

Figure 1: Plan and elevation views of the multizone unit.
AHU supply flows are indicated by arrows.

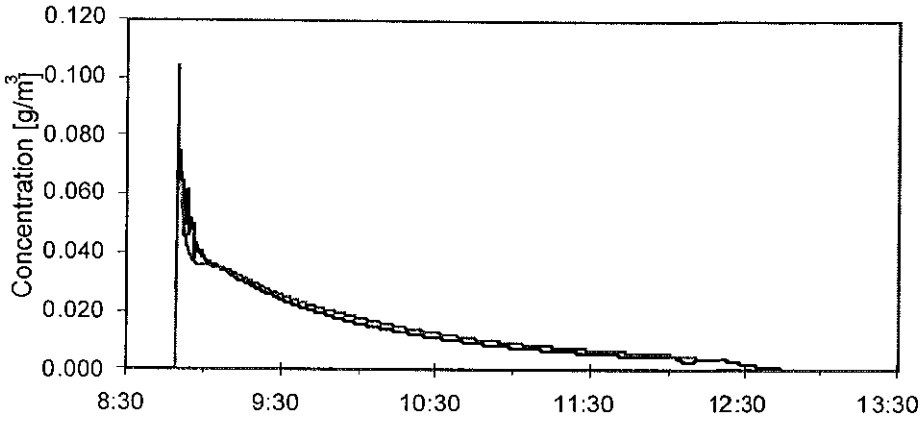

Figure 2: Trial 1 measured (black) and modeled (grey) gas concentrations for room 1.2a.

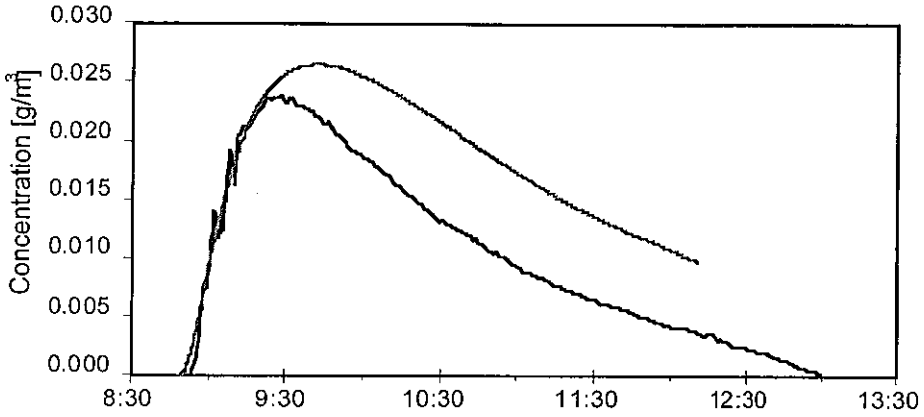

Figure 3: Trial 1 measured (black) and modeled (grey) gas concentrations for room 3.1.

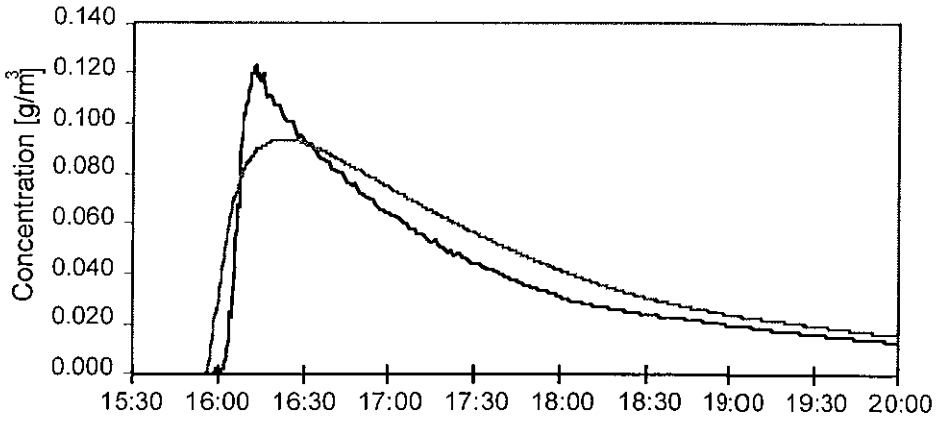

Figure 4: Trial 13 measured (black) and modeled (grey) gas concentrations for room 1.2a.

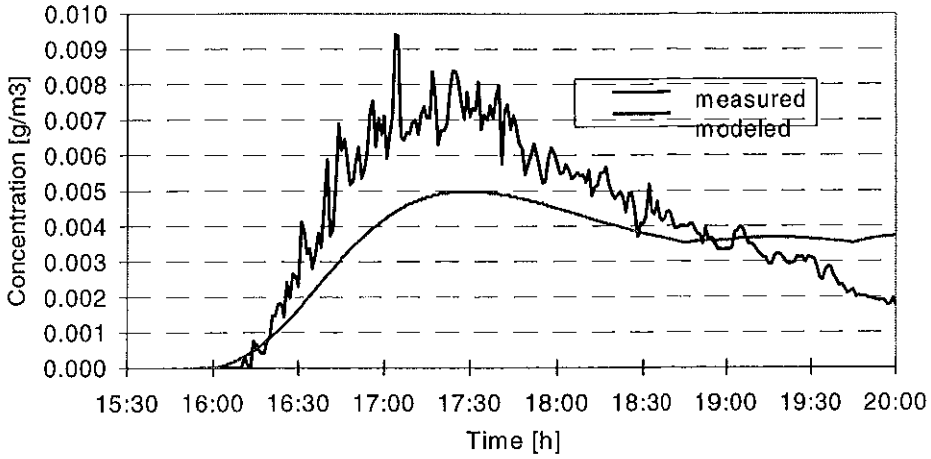

Figure 5: Trial 13 measured and modeled gas concentrations for room 3.1.

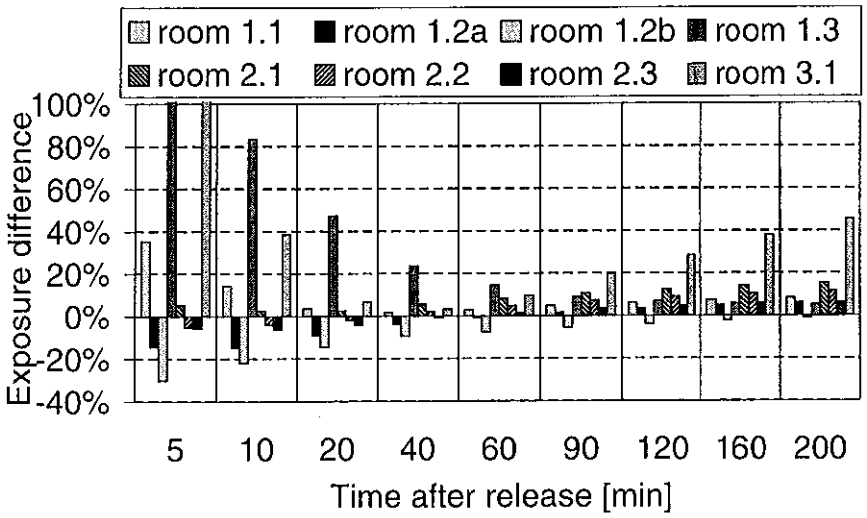

Figure 6: Difference between modeled and measured gas exposures over time for Trial 1.

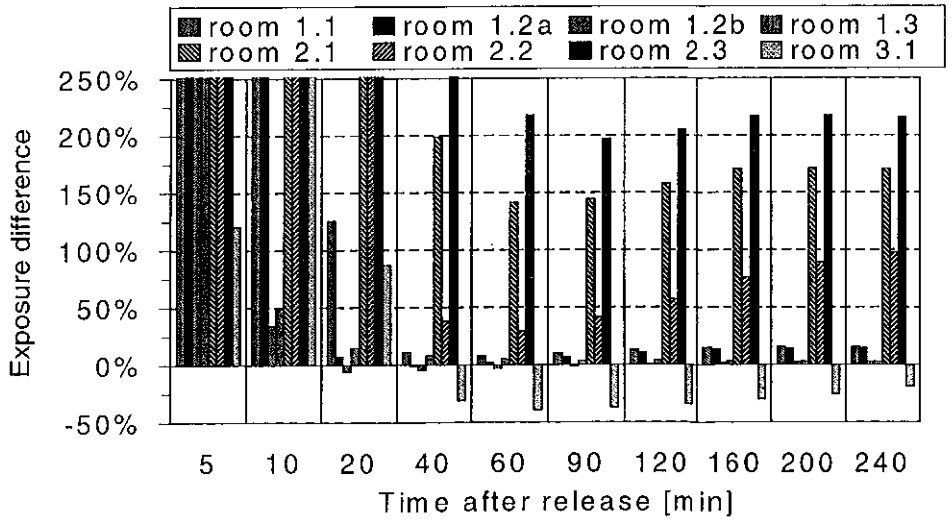

Figure 7: Difference between modeled and measured gas exposures over time for Trial 13.

DETERMINING TRANSFER FACTORS FOR OUTDOOR AEROSOL PLUMES ENTERING BUILDINGS

T L Thatcher[1], W W Nazaroff [2] and R G Sextro[1]

[1] Indoor Environment Dept., Lawrence Berkeley National Laboratory, Berkeley, CA USA
[2] Dept. of Civil and Environmental Engineering, University of California, Berkeley, CA USA

ABSTRACT

An important component for predicting the effects of outdoor air pollutant releases is to determine the relative protection offered by buildings. A set of experiments has been designed to evaluate the rate at which particles enter a building under different release conditions. Experimental results are parameterized in terms of an inhalation transfer factor: the fraction of the released pollutant that would be inhaled by a typical occupant of the building. The experiment involves generating an aerosol plume upwind of a test building. Indoor and outdoor particle concentrations are measured continuously during and after plume generation. The air-exchange rate and plume entry rate are measured using two tracer gases. Mass balances are used to determine particle deposition and penetration rates as functions of particle size. Data from initial experiments will be presented at Indoor Air '99.

INTRODUCTION

The amount of protection offered by sheltering within a building during incidents of industrial accident and other sudden pollutant releases is a critical factor in predicting health effects and in developing response plans. In the event of a release, information may be available on the maximum amount of material discharged and the chemical or physical nature of that material. No experiments have been reported that investigate the relationship between the amount and condition of pollutant release outdoors and the resulting indoor concentrations. We have designed experiments to investigate the entry of airborne particles into a building after upwind release. Initial experiments will be performed without mechanical ventilation, mimicking a "sheltering in place" response. An inhalation transfer factor (ITF) will be calculated for each experimental run based on measurement data. The ITF represents the fraction of the generated pollutant which would be inhaled by a building occupant. The experimental data will also be used to estimate indoor deposition velocities and penetration factors for the building shell as functions of particle size.

METHODS

Test aerosols will be generated using an atomizing spray nozzle (Spraying Systems, Inc., Model SU13) directly upwind of a small conference facility located in Richmond, California. The facility is a single-story, flat-roofed building with plan dimensions of approximately 15×15 m. The spray atomizer will use a solution consisting of three components: (1) a highly volatile liquid (isopropyl alcohol) which will evaporate quickly to reduce the droplet size, (2) a low volatility liquid (oleic acid) which will remain to form droplets whose size (a broad distribution centered at about 5 μm) is constant over time, and (3) a fluorescent tracer (fluorescein) which will facilitate sensitive filter-based measurements of total particle. Particles will be measured continuously both indoors and outdoors using two cross-calibrated real-time multi-channel particle counters (TSI, model APS 3320). The air-exchange rate and plume entry rate will be measured simultaneously at a central location indoors. Integrated filter samples of airborne particles will be taken at several locations inside and outside the building and analyzed

fluorometrically to determine the concentration of generated particles at each sampling location. After 2 hours, particle generation will be halted. The decay in indoor particle and tracer gas concentrations will continue to be monitored for one additional hour. Meteorological conditions will be monitored throughout the experiments.

Experimental results will be analyzed to determine the inhalation transfer factor (ITF), defined as the fraction of the generated pollutant which would be inhaled by a typical occupant (presented dose). The inhalation transfer factor (ITF) can be expressed mathematically as:

$$ITF = \frac{\text{mass inhaled}}{\text{mass emitted}} = \frac{\int C_i(t)\, Q_B(t)\, dt}{\int G(t)\, dt} \qquad (1)$$

where C_i is the concentration of generated particles in indoor air (g m^{-3}), Q_B is the occupant's breathing rate (m^3 h^{-1}), and G is the particle generation rate, g h^{-1}. By measuring the time integrated indoor air concentration and particle generation rate, the ITF can be experimentally evaluated for any given constant breathing rate and particle size. The effective dose could be calculated based on expected uptake as a function of particle size. In addition, transfer rates for size ranges (PM_{10} or $PM_{2.5}$) can be calculated by consolidating data for all particles within the range. However, these values may depend on the specific size distribution of the particles.

To predict inhalation transfer factors for different situations, we need to improve our understanding of particle transport into buildings. A well-mixed, single box model can be used to describe the indoor environment. Since the building studied in these experiments will be unoccupied, no resuspension or generation will occur inside. Under these conditions, the particle concentration within the building is governed by the following equation:

$$\frac{dC_{in}}{dt} = \lambda_v P C_o - \left(\frac{A_d v_d}{V} + \lambda_v\right) C_{in} \qquad (2)$$

where C_{in} is the concentration of a specific size particle in indoor air (# m^{-3}), λ_v is the air exchange rate (h^{-1}), P is the size-dependent fraction of infiltrating particles which penetrate the building shell (unitless), C_o is the size-dependent particle concentration in the infiltration air (# m^{-3}), A_d is the indoor surface area for deposition (m^2), and v_d is the area-averaged indoor deposition velocity (m h^{-1}). This equation can be used to interpret the time-dependent experimental measurements of indoor and outdoor particle concentration and air-exchange rate to infer the size dependent deposition velocity (v_d) and penetration factor (P).

CONCLUSIONS

Developing appropriate emergency response plans for industrial accidents and other unexpected releases requires an understanding of the effect of such a release on building occupants. The proposed experiments aim to improve our knowledge of the intake dose that would occur for specific release characteristics and meteorological conditions. The results will increase our general understanding of indoor particle exposure resulting from outdoor sources and will serve as a basis to improve the effectiveness of emergency response plans.

ACKNOWLEDGEMENT

This work was supported by the Office of Research and Development, Office of Nonproliferation and National Security, U.S. Department of Energy under Contract No. DE-AC03-76SF00098.

MODELING PARTICLE PENETRATION THROUGH CRACKS IN BUILDING ENVELOPES

D-L Liu[1] and W W Nazaroff[1,2]

[1]Department of Civil and Environmental Engineering, University of California, Berkeley, USA
[2]Indoor Environment Dept., Lawrence Berkeley National Laboratory, Berkeley, CA, USA

ABSTRACT

Particle penetration through rectangular, smooth-walled cracks is modeled. Steady-state airflow is determined from crack geometry and the pressure difference across the building envelope. Three particle deposition mechanisms are considered: gravitational settling, Brownian diffusion, and impaction. Predictions are made for particle diameters over the range 0.001 to 100 μm, pressure differences of 4-10 Pa, crack heights of 0.05-1.0 mm, and a crack length of 3 cm. Particle size and crack height strongly affect particle penetration. Particles with diameter in the range 0.1- 1.0 μm are predicted to have the highest penetration factors, ≥ 0.85 for a crack height of 0.25 mm or larger. Gravitational settling controls the deposition of large (supermicron) particles and Brownian diffusion controls deposition of small (submicron) particles. The contribution of impaction to particle deposition is insignificant under the conditions analyzed.

INTRODUCTION

Particle inhalation is an important pathway for human exposure to toxic substances. People spend most of their time indoors, so a sound understanding of particle penetration through building envelopes would improve our knowledge of the contribution of ambient particles to total human exposure.

In some studies, the penetration factor (F, also known as fractional penetration) has been evaluated simply as the ratio of indoor to outdoor particle concentrations [1]. In this case, the resulting penetration factors were found to be significantly less than one. However, even in the absence of indoor emissions, the indoor-outdoor concentration ratio depends on penetration through the building envelope and on particle deposition rates to indoor surfaces. Accurate field assessments of particle penetration require that other mechanisms of particle loss from indoor air and indoor generation be either negligible or properly taken into account [2]. The penetration factor is defined to be the fraction of particles in infiltrating air that remain airborne as air passes through cracks in a building's shell. The penetration factor is expected to be a function of particle diameter, crack geometry, and pressure drop across the crack.

In this paper, we evaluate the particle penetration factor for an idealized single rectangular crack, based on the published information on airflow characteristics in cracks and available knowledge on particle deposition mechanisms.

METHODS

The study of particle penetration through building cracks starts by postulating three idealized slot configurations — straight-through, L-shaped, and double-bend — which represent the cracks commonly found in buildings (Figure 1). Such cracks can occur where dissimilar materials are joined, and around windows and doors. The crack height and flow length are denoted as d and z, respectively. Airflow through the cracks is driven by the pressure

difference (ΔP) across the building envelope, induced by imbalanced fan-induced flows, wind, and indoor/outdoor temperature differences. Under ordinary conditions, ΔP is less than about 10 Pa. For the present analysis, it is assumed that the crack geometry is regular, the surface is perfectly smooth, and the airflow within a crack is steady. It is also assumed that the extent of the crack (w) in the third dimension (into the page in Figure 1) is much larger than either d or z and so the system can be treated as two-dimensional.

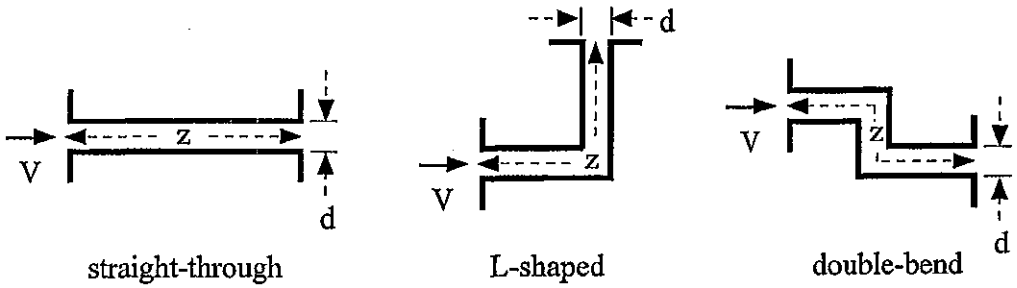

Figure 1. Three types of idealized crack configurations.

In a study of leakage through windows, it has been reported that the pressure drop (ΔP) and volumetric flow rate (Q) are related by a quadratic expression of this form [3]:

$$\Delta P = m\,Q + n\,Q^2 \tag{1}$$

where m and n are related to crack dimensions and fluid characteristics. In another study, m and n were determined from theoretical derivation [4]:

$$m = \frac{12\,\mu\,z}{w\,d^3} \tag{2}$$

$$n = \frac{K\rho}{2\,d^2\,w^2} \tag{3}$$

where μ is the dynamic viscosity of air, ρ is the air density, and K is the loss coefficient of the crack. The loss coefficient (K) for straight-through, L-shaped, and double-bend cracks was experimentally determined to be 1.4, 2.3 and 3.3, respectively [4].

The average flow velocity through the crack (V) equals airflow rate (Q) divided by cross-sectional crack area (wd). For a given pressure drop (ΔP) and crack geometry (d and z), the average flow velocity (V) can be evaluated by substitution and rearrangement after solving for the positive root of (Q) from equation (1):

$$V = \frac{-12\,\mu\,z + \sqrt{(12\mu z)^2 + 2\,K\,\rho\,\Delta P\,d^4}}{K\,\rho\,d^2} \tag{4}$$

Particle penetration was determined by separately analyzing deposition according to three mechanims: Brownian diffusion, gravitational settling, and impaction. Impaction was only considered for the acceleration around bends in the L-shaped and double-bend cracks. In the analysis, particles were assumed to be spherical with a density of 1 g cm^{-3}. Particle diameters from 0.001 to 100 μm were considered because of growing interest in the health effects of ultrafine particles [5], as well as the possibility of exposure by ingestion caused by nonrespirable large particles.

Assuming homogeneous particle concentration at crack inlet, the penetration factor as a result of gravitational settling alone (F_g) is obtained by [6]:

$$F_g = 1 - \gamma \qquad \gamma \leq 1 \qquad (5)$$

where $\gamma = (V_s z)/(d V)$ and V_s is particle settling velocity. For $\gamma \geq 1$, there is complete deposition and no particle penetration at all ($F_g = 0$).

For particle loss due to Brownian diffusion, the penetration factor (F_d) is determined by [7]:

$$F_d = 0.915 \exp(-1.885\ \phi) + 0.0592 \exp(-223\ \phi) + 0.026 \exp(-152\ \phi) + \ldots \qquad (6)$$

where ϕ is given by:

$$\phi = \frac{4 D z}{d^2 V} \qquad (7)$$

Here D is particle diffusion coefficient.

Particle deposition due to impaction is expected to be a function of particle Stokes number (St) which is a ratio of particle stopping distance to the characteristic length associated with the accelerating flow ($d/2$). The penetration factor F_i (1-collection efficiency) was estimated from a collection efficiency curve for rectangular impactor nozzles [8].

By assuming that the three particle deposition mechanisms occur independently, the overall penetration factor was estimated by multiplying the penetration factors from each individual mechanism:

$$F = F_g F_d F_i \qquad (8)$$

In addition to information about air flow through cracks and particle deposition mechanisms, realistic crack dimensions have to be considered in evaluating penetration factors. One investigation of air infiltration through gaps around windows suggested that the range of crack thickness of air paths is normally less than 2.5 mm (0.1 in.) [3]. The dimensions tested in that study were in the range 0.13-2.54 mm. In the present analysis, the airflow length (z) was fixed at 3 cm and various crack heights (d = 0.05, 0.10, 0.25, and 1.0 mm) were considered.

RESULTS AND DISCUSSION

The average airflow velocities are identical for the three crack configurations given the same dimensions of crack height (d), airflow length (z), and pressure difference (ΔP). Some parameters associated with crack flow characteristics are presented in Table 1. For the crack dimensions in our study, it is reasonable to state that the airflow is laminar and fully-developed due to the small flow Reynolds number (Re) and the small ratio of entrance length to crack airflow length (x_e/z).

Figure 2 presents the particle penetration factor as a function of particle diameter, crack height, and pressure difference for straight-through cracks. The result show that accumulation mode particles (0.1-1 μm) have the highest penetration efficiency. This is expected, because particles in this size range diffuse and settle slowly compared with smaller particles (for which diffusion dominates transport) and larger particles (for which settling dominates). The

penetration factors for L-shaped and double-bend cracks are very similar to the curves in Figure 2. As indicated in Figure 2, the penetration factors approach one for accumulation mode particles for crack heights exceeding 0.25 mm. For a crack height of 1 mm, particle penetration is essentially complete (≥ 90%) for particle diameters between 0.01 and ~ 7 μm. Similar calculations were also carried out for a 3.0 mm crack height, and it was found that the penetration factors are just only slightly higher than those for a 1.0 mm crack. It appears that there is a threshold crack height; and the penetration scenarios would be very similar above this threshold.

Table 1. Characteristics of air flow through a crack, given an airflow length of $z = 3$ cm and a pressure difference of $\Delta P = 10$ Pa.

crack height d (mm)	air speed V (cm/s)	Reynolds no. Re	entrance length x_e/z
0.05	0.4	1.3×10^{-2}	8.6×10^{-7}
0.10	1.5	1.0×10^{-1}	1.4×10^{-5}
0.25	9.6	1.6	5.4×10^{-4}
1.0	132	88	1.2×10^{-1}

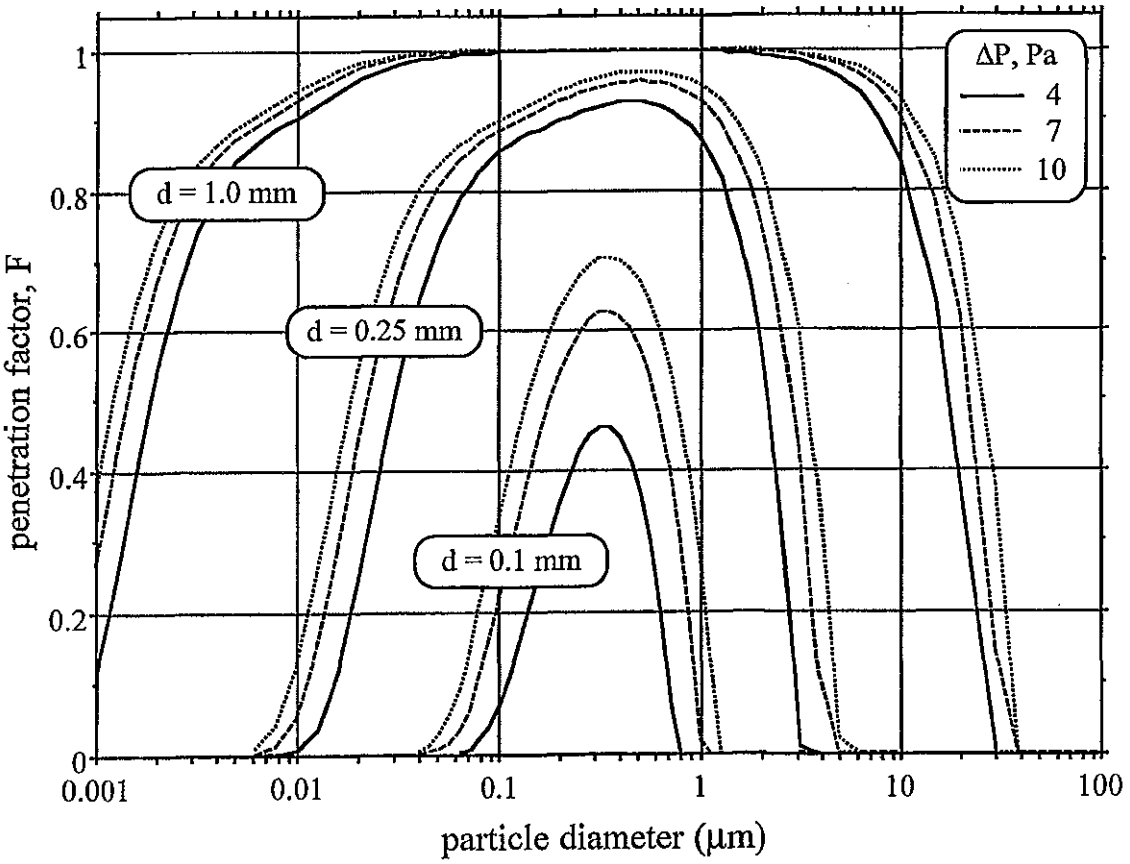

Figure 2. Calculated particle penetration factors with respect to particle size, crack height and pressure difference for an idealized straight-through crack.

For cracks smaller than 1 mm, penetration varies significantly with crack height. For crack height of 0.25 mm, particles of 0.1-1.0 μm have penetration factors greater than 0.85. For a crack height of 0.1 mm, only about half of the 0.3 μm particles penetrate and the penetration is essentially zero for diameters smaller than 0.04 μm or greater than about 1.2 μm. Particle penetration is essentially zero (< 2%) for crack heights of 0.05 mm, independent of particle size.

With regard to particle loss in L-shaped and double-bend cracks due to impaction alone, the collection efficiency is essentially zero for particles with *St* smaller than 0.36 [8]. Particles with *St* greater than 0.36 are large enough to deposit because of gravitational settling. As a result, impaction does not enhance deposition in bent cracks in these model calculations.

In real building cracks, however, the roughness of the crack surface as well as irregularities in crack geometry would alter the detailed influence of particle deposition mechanisms and thus could change the penetration results. Further studies are needed to address these complexities.

ACKNOWLEDGEMENT

This work was supported by the Office of Research and Development, Office of Nonproliferation and National Security, U.S. Department of Energy under Contract No. DE-AC03-76SF00098. Additional support was provided by the UC Toxic Substances Research and Training Program.

REFERENCES

1. Spengler, J D, Dockery, D W, Turner, W A, et al. 1981. Long-term measurements of respirable sulfates and particles inside and outside homes. *Atmospheric Environment.* Vol. 15, pp 23-30.

2. Thatcher, T L, and Layton, D W. 1995. Deposition, resuspension, and penetration of particles within a residence. *Atmospheric Environment.* Vol. 29, pp 1487-1497.

3. Thomas, D A, and Dick, B A. 1953. Air infiltration through gaps around windows. *JIHVE.* Vol. 21, pp 85-97.

4. Baker, P H., Sharples, S and Ward, I C. 1987. Airflow through cracks. *Building and Environment.* Vol. 22, pp 293-304.

5. Oberdörster, G, Gelein, R M, Ferin, J, and Weiss, B. 1995. Association of particulate air pollution and acute mortality: Involvement of ultrafine particles? *Inhalation Toxicology.* Vol. 7, pp 111-124.

6. Fuchs, C N. 1964. *The Mechanics of Aerosols.* Pergamon.

7. Taulbee, D B and Yu, C P. 1975. Simultaneous diffusion and sedimentation of aerosols in channel flows. *Journal of Aerosol Science.* Vol. 6, pp 443-441.

8. Marple, V A and Willeke, K. 1976. Impactor design. *Atmospheric Environment.* Vol. 10, pp 891-896.

MODELING AEROSOL BEHAVIOR IN MULTIZONE INDOOR ENVIRONMENTS

M.D. Sohn[1], A. Lai[1], B.V. Smith[1], R.G. Sextro[1], H.E. Feustel[1], W.W. Nazaroff[1,2]

[1]Indoor Environment Department
Lawrence Berkeley National Laboratory
Berkeley, CA 94720-0001, U.S.A.

[2]Department of Civil and Environmental Engineering
University of California
Berkeley, CA 94720-1710, U.S.A.

ABSTRACT

A publicly available aerosol dynamics model, MIAQ4, is coupled to a widely used multizone air flow and transport model, COMIS, to better understand and quantify the behavior of particles in indoor environments. MIAQ4 simulates the evolution of a size and chemically resolved particle distribution, including the effects of direct indoor emission, ventilation, filtration, deposition, and coagulation. COMIS predicts interzonal air-exchange rates based on pressure gradients (due to wind, buoyancy, and HVAC operation) and leaks between the zones and with the outside. The capabilities of the coupled system are demonstrated by predicting the transport of particles from two sources in a residence: environmental tobacco smoke (ETS) and particles generated from cooking. For ETS, MIAQ4 predicts particle size distributions that are similar to the emission source profile because ETS particles, concentrated in the size range 0.1 - 1 μm, are transformed by coagulation and deposition slowly compared with the rates of transport. For cooking, MIAQ4 predicts that the larger-sized particles will settle rapidly, causing a shift in size distribution as emissions are transported to other rooms.

INTRODUCTION

Understanding the dynamic behavior of indoor aerosols is essential for accurately predicting the concentrations and fates of these species within a building. Processes such as coagulation, deposition, and removal by filtration are strongly dependent on particle size, which can alter the particle size distribution in building air and ultimately affect lung deposition in exposed individuals. In addition, predicting indoor particle concentrations also requires a sound understanding of the building's airflow characteristics and its effects on particle transport.

State-of the-art particle dynamics models can simulate particle interaction processes in great detail, but do not incorporate a predictive capability for simulating building airflow characteristics. Conversely, existing multizone indoor air flow and transport models are capable of simulating interzonal air flow in great detail, but have limited ability to address complex pollutant dynamic behavior, usually relying, for example, on average settling rates without honoring the influences of particle size. In this work, we report the coupling of an aerosol dynamics model, MIAQ4, to a widely used multizone indoor air flow and transport

model, COMIS. The coupled models are capable of predicting in detail the relationship between particle emissions and indoor air concentrations, and will permit detailed study of the factors governing inhalation exposures and dose.

MIAQ4 [1, 2] simulates a size and chemically-resolved particle distribution, tracking the particle as it is affected by inter-room transport, ventilation, filtration, emission, coagulation, and deposition onto indoor surfaces. Evaporation, condensation and homogeneous nucleation are not included in the model. The model has been successfully used to study the concentration and fate of particles from cigarette smoke in a single chamber [1] and the concentration of particulate matter in museums [2]. In addition, it has been experimentally validated in a two-room study of environmental tobacco smoke [3]. In simulating these interzonal transport, MIAQ4 requires that the air flows be provided as inputs.

COMIS [4] predicts interzonal air flows based on pressure gradients (due to wind, buoyancy, and HVAC operation) and leaks between the zones and with the outside. It is a multizone infiltration model that assumes that air acts as an ideal gas (transport is affected only by temperature and pressure gradients) with transport based on interzonal conservation of mass. Transport components include flow through cracks, large openings, and duct-work. It has been used to predict the airflow in single-family houses, test cells, flats, and small office buildings [5, 6, 7].

For the present purposes, the two models have been coupled using text transferring script files. We are in the process of more completely integrating MIAQ4 into the COMIS modeling framework to improve processing time and reducing the number of input and output files that must be handled.

ILLUSTRATIVE APPLICATION

The attributes of an integrated model are demonstrated using a hypothetical single-floor residential building with an attic space that spans the entire floor area (Figure 1). Interior and exterior temperature distributions are set to represent typical conditions found in a poorly insulated single-family home during a Pacific-coast winter. Wind is assumed to blow from the west at a steady rate of 3 m/s. The exterior doors and windows are closed, the interior doors are open and no HVAC system is operating. Representative air leakage characteristics were estimated from data compiled by Lidament [8] to represent a moderately tight building. Figure 1 summarizes the predicted inter-room flow rates.

Two aerosol pollutant releases are considered: (1) environmental tobacco smoke particles (ETS) and (2) particles emitted during cooking. Both are released in the kitchen for ten minutes with approximate release rates of 1.32 mg/min and 100 mg/min for ETS and cooking, respectively. Figure 2 shows the particle size distribution for the two sources. The normalized emission rate profile is used to illustrate the distributed emission rate as a function of particle size and will be used to compare the predicted concentrations to the emissions. Development of the source profiles are based on literature estimates (see [9] for ETS and [10, 11] for cooking) and engineering judgment.

Figure 3 illustrates the predicted transport for all rooms. Predicted peak concentrations are approximately 4-6 times greater in the kitchen than the other rooms. The bedrooms and bathroom exhibit similar time-series profiles as the living room. Figure 4 illustrates the

predicted eight-hour average concentration in the living room, normalized by dividing by the largest average concentration in a particle size bin. Similar trends are observed in the other rooms so are not presented. For ETS, the eight-hour average predicted concentration (Figure 4a) has a particle size distribution similar to the source distribution (Figure 2a). Unlike ETS particles, large amounts of cooking particles are generated in the supermicrometer size range. Because of rapid deposition, the eight-hour average concentration shows fewer particles greater than 1μm than are present in the source profile (compare Figures 2b and 4b).

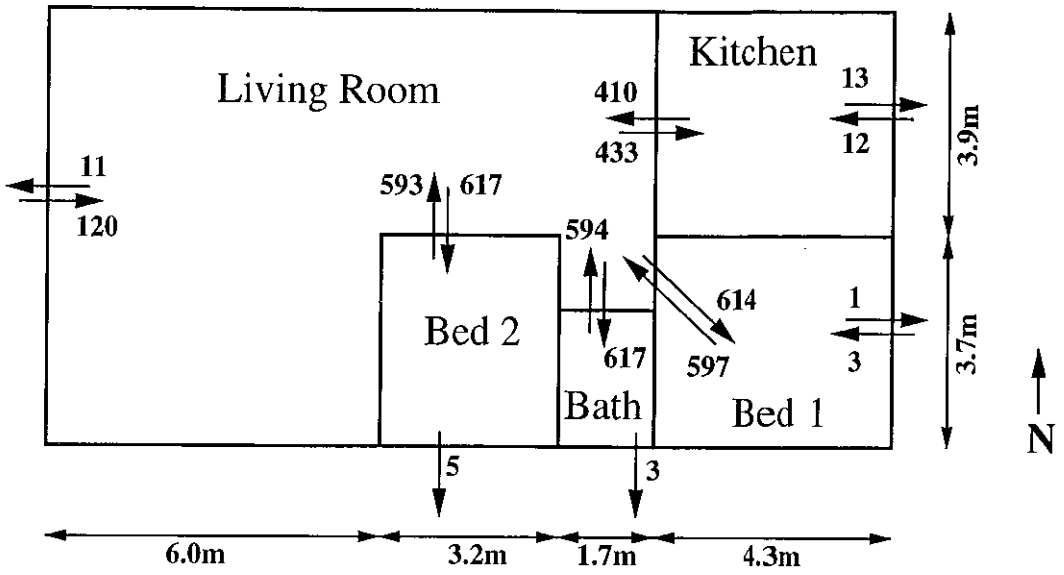

Figure 1: Floor plan for the residential building studied in this paper. A single-zone attic is located above the floor plan and is topped by a gable-end pitched roof. The height of the rooms is 2.7 meters. Wind blows from the west at a steady 3 m/s at 10°C. The flow rates are in units of m^3/hr. Flows into the attic from each of the rooms are approximately 20 m^3/hr.

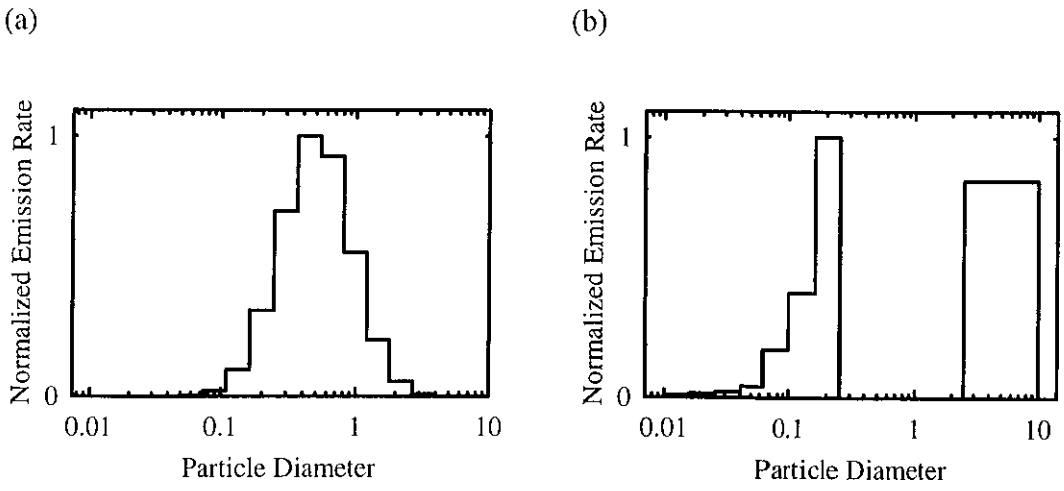

Figure 2: Particle size distribution for (a) ETS and (b) particles generated during cooking emissions. The emission rate profiles are normalized by dividing the emission rate by the largest rate in a given particle size bin. Smoking corresponds to a single standard commercial cigarette. Cooking is based on pan-flying meat.

(a)

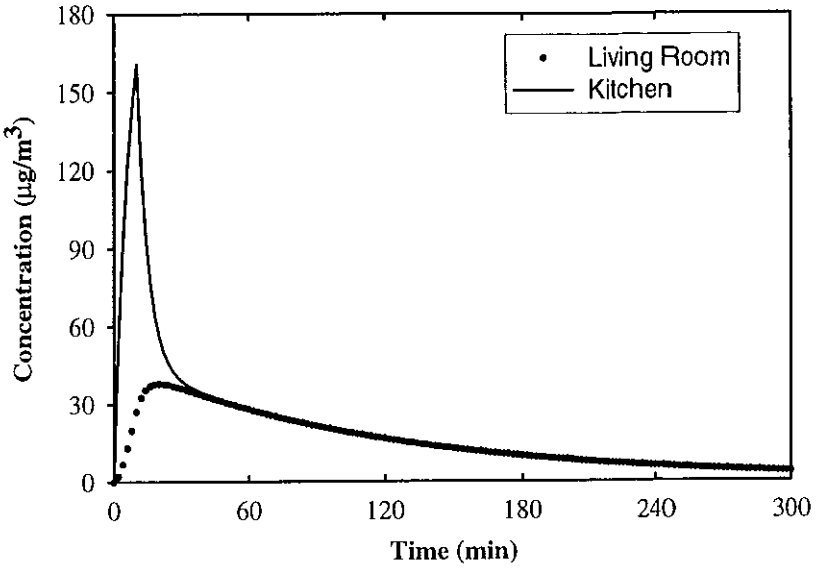

(b)

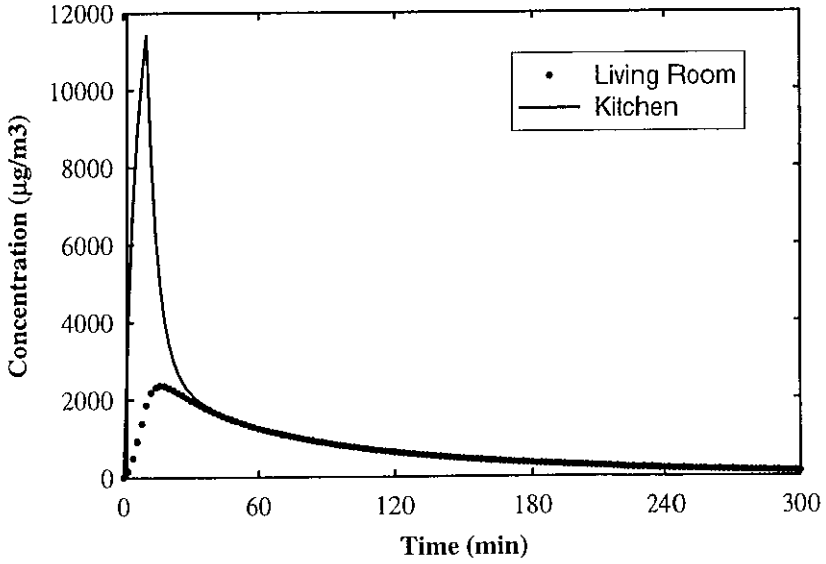

Figure 3: Time series plots of (a) ETS and (b) particles generated from cooking. The releases were in the kitchen and persisted for ten minutes, beginning at time t = 0. The bedrooms and bathroom exhibit profiles similar to the living room.

CONCLUDING REMARKS

These results demonstrate the benefits of integrating a particle dynamics model with a multizone transport model to better understand the indoor air quality impacts of particle emissions. For particles that are in the size range 0.1 – 1 μm, like ETS, predicted particle concentrations do not indicate significant size-dependent effects. In this case, a qualitative first-order settling value used in a transport model may yield reasonable predictions (although

COMIS does not have this capability, such first-order decay models are readily available). However, when larger or smaller particles are considered, size-dependent particle dynamics necessitates an advanced dynamics model to accurately predict particle concentrations.

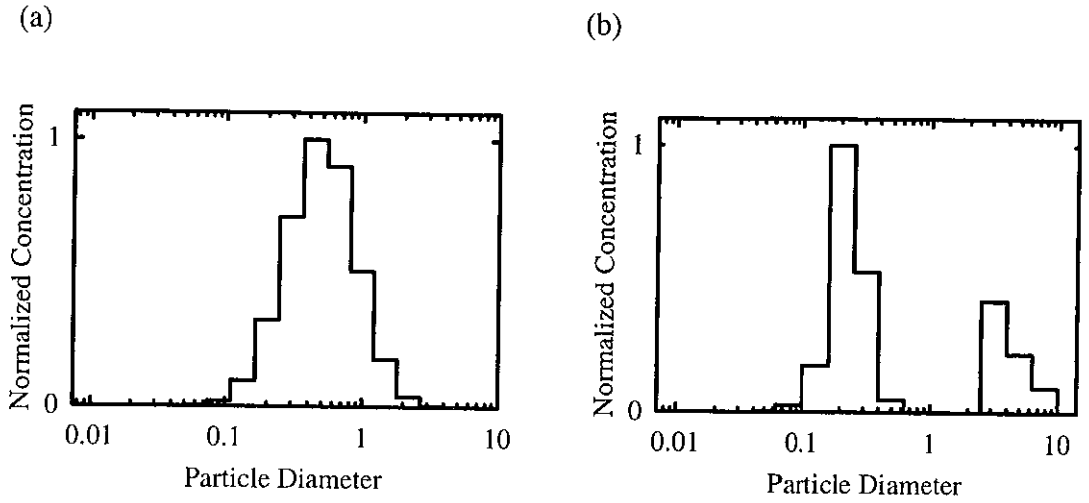

Figure 4: Eight-hour averaged concentration of (a) ETS and (b) particles generated from cooking for the living room. The concentrations are normalized by dividing by the largest concentration in a given particle size bin. The 8-hour averaged particle concentration is 10 $\mu g/m^3$ and 450 $\mu g/m^3$ for (a) ETS and (b) cooking, respectively.

Acknowledgements: This work was supported by the Office of Research and Development, Office of Nonproliferation and National Security, U.S. Department of Energy under Contract No. DE-AC03-76SF00098.

REFERENCES

1. Nazaroff, W. W., and Cass, G. R. 1989. Mathematical modeling of indoor aerosol dynamics. *Environ. Sci. Technol.* Vol. 23, pp 157-166.

2. Nazaroff, W. W., Salmon, L. G., and Cass, G. R. 1990. Concentration and fate of airborne particles in museums. *Environ. Sci. Technol.* Vol. 24, pp 66-77.

3. Miller, S. L. 1996. Characterization and control of exposure to indoor air pollutants generated by occupants. Ph.D. Dissertation, University of California, Berkeley.

4. Feustel, H.E. and Rayner-Hooson, A. 1990. COMIS fundamentals. Lawrence Berkeley National Laboratory Report LBL-28560.

5. Fürbringer, J.M., C.-A. Roulet, and R. Borchiellini 1996. Annex 23 Subtask II/III Report-Evaluation of COMIS, Vol. 1 and 2. EPFL Lausanne, Switzerland.

6. Haghighat, F. and Megri, A. C. 1996. A comprehensive validation of two airflow models – COMIS and CONTAM. *Indoor Air.* Vol. 6, pp 278-288.

7. Zhao, Y., Yoshino, H., and Okuyama, H. 1998. Evaluation of the COMIS model by comparing simulation and measurement of airflow and pollutant concentration. Indoor Air. Vol. 8, pp 123-130.

8. Lidament, M. W. 1986. Air infiltration calculation techniques – An applications guide. AIVC Document: AIC-AG-1-86.

9. Nazaroff, W. W., Hung, W. Y., Sasse, A. G. B. M., and Gadgil, A. J. 1993. Predicting regional lung deposition of environmental tobacco smoke particles. *Aerosol Sci. Technol.* Vol. 19, pp 243-254.

10. Hildemann, L. M., Markowski, G. R., Jones, M. C., and Cass, G. R. 1991. Submicrometer aerosol mass distribution of emissions from boilers, fireplaces, automobiles, diesel trucks, and meat-cooking operations. *Aerosol Sci. Technol.* Vol. 14, pp 138-152.

11. Rogge, W. F. (1997) Private communication.

PARTICLE DEPOSITION FROM TURBULENT DUCT FLOW

MR Sippola[1], WW Nazaroff[1] and TL Thatcher[2]

[1] Dept. of Civil and Environmental Engineering, University of California, Berkeley, CA USA
[2] Indoor Environment Dept., Lawrence Berkeley National Laboratory, Berkeley, CA USA

ABSTRACT

Particle deposition from turbulent duct flow is modeled and related to particle penetration of a ventilation system for a commercial office building. Three published turbulent deposition models capable of accommodating surface roughness are compared to experimental data and used to determine the penetration of 0.1–10 μm spherical particles through a sample duct run. Depending on the model employed, penetration fractions varied from 0.40-0.94 for 0.1 μm particles and 0.28-0.73 for 10 μm particles. Penetration is predicted to be independent of particle size for particle diameters less than 2 μm. Almost all the deposition is predicted to occur in short sections of the duct runs where the wall roughness is larger than in other duct sections because of the duct construction material.

INTRODUCTION

Exposure to airborne particles may contribute to human health effects including impairment of the respiratory system, lung tissue damage, and mortality. Particulate matter less than 10 μm in diameter (PM_{10}) is a criteria pollutant in the United States with an ambient air quality standard of 50 $\mu g/m^3$ on a yearly average basis and 150 $\mu g/m^3$ on a 24-hour average basis. No analogous U.S. standard exists for particles in indoor air. Epidemiological evidence suggests a positive correlation between outdoor PM_{10} concentrations and mortality in urban areas. This finding is surprising because most exposure to airborne particles occurs indoors and exposure does not correlate well with ambient concentrations [1]. In buildings with ducted air handling systems, particle deposition in ducts is a potentially important factor in influencing human exposure to particles.

A typical air supply system in a commercial building consists of an air handling unit which draws outside air through a filter and into a very large diameter duct, followed by a series of successively smaller, branched ducts which transport the air to different locations in the building. Generally, ducts are made of galvanized steel or aluminum and may be lined with fiberglass on the interior to reduce noise. Airflow in ventilation ducts is turbulent. Table 1 shows the range of duct dimensions and air velocities encountered in most commercial ventilation systems. Filter efficiencies at the air intake for particles less than 10 μm in diameter are low, commonly less than 10% for particle diameters ranging from 0.1 to 3.0 μm [2]. Thus, particle deposition from turbulent flow in the ventilation system is important for evaluating penetration into buildings and exposure of building occupants to outdoor particles.

Table 1. Approximate range of duct dimensions and flow conditions

	Duct Diameter	Wall Roughness	Air Velocity	Reynolds No.
Minimum value	0.15 m	0.001 mm	1 m/s	10^4
Maximum value	1.5 m	5 mm	10 m/s	10^6

Particle deposition to walls from turbulent airflow in a tube has significance in many engineering applications and has been widely studied. Experimentally, particle deposition has been observed to depend most strongly on particle size [3], surface roughness [4], and flow Reynolds number [5]. Mechanisms by which a particle may move in turbulent flow and can be captured at a solid surface include Brownian diffusion, turbulent diffusion, gravitational settling, inertial impaction, electrophoresis, thermophoresis, shear-induced (Saffman) lift, and interception. Several empirical and mechanistic models of deposition from turbulent duct flow have been proposed.

In this paper, three published models of particle deposition from turbulent pipe flow are evaluated and used to predict the fraction of particles which penetrate a single duct run of a ventilation system from a representative five-story commercial office building.

METHODS

The modeled duct run is from the ventilation system of a five-story commercial office building. The duct run begins at the air intake located on the roof of the building and terminates at a third floor office. Air traveling this path is carried in eight distinct duct sections, the characteristics of which are summarized in Table 2. Airflow rates are assumed to be constant at the designed rates. The flow path also includes two T-junctions, five 90° bends, and flow past numerous T-junctions and is selected to be representative of a typical duct run for a commercial office building. Analysis suggests that inertial impaction at the flow bends contributes a negligible amount to the overall deposition, thus, impaction at bends has been ignored in all simulations.

Table 2. Characteristics of modeled duct run

Section #	Orientation (-)	Material (-)	Roughness (mm)	Hydraulic Diameter (m)	Length (m)	Air Velocity (m/s)
1	Horizontal	Steel	0.15	1.50	1.1	10.6
2	Vertical	Steel	0.15	1.06	4.9	9.1
3	Horizontal	Fiberglass Liner	0.5	0.78	6.1	5.3
4	Horizontal	Steel	0.15	0.71	6.7	4.4
5	Horizontal	Steel	0.15	0.67	5.5	3.4
6	Horizontal	Steel	0.15	0.54	5.8	3.6
7	Horizontal	Steel	0.15	0.25	22.9	2.0
8	Horizontal	Flexible Aluminum	1.0	0.25	2.0	2.0

Three models have been used to evaluate particle penetration through the duct run: the modified free-flight model of El-Shobokshy and Ismail [6], the empirical free-flight model recommended by Wood [7], and the empirical correlation of the sublayer model presented by Fan and Ahmadi [8]. All three models predict dimensionless deposition velocity as a function of the particle dimensionless relaxation time to both smooth and rough surfaces. Input parameters are the particle diameter and density, duct diameter and roughness, and air velocity. Particle deposition velocity is defined as follows:

$$V_d = N / C \tag{1}$$

where N is the particle flux to the surface and C is the average particle concentration in the air stream. Deposition velocity is nondimensionalized by dividing by the friction velocity, u*:

$$V_d^+ = V_d / u^* \tag{2}$$

Particle dimensionless relaxation time is calculated by:

$$\tau^+ = \frac{C_c \rho_p d_p^2 u^{*2}}{18 \mu \upsilon} \tag{3}$$

where C_c is the slip correction factor, ρ_p is the particle density, d_p is the particle diameter, μ is the dynamic viscosity of air, and υ is the kinematic viscosity of air. For the airflow velocities and duct sizes of interest here, τ^+ is in the range of 5×10^{-5} to 5 for $0.1 < d_p < 10$ μm. If the deposition velocity is known, the fraction of a given sized particle penetrating a duct is:

$$f = \exp\left(-\frac{V_d P L}{U A}\right) \tag{4}$$

where f is the fraction of particles that pass through the duct, P is the duct perimeter, L is the duct length, U is the average air velocity, and A is the duct cross-sectional area.

All three models considered account for Brownian diffusion, turbulent diffusion and interception, and ignore electrophoresis and thermophoresis. The effect of gravity in horizontal ducts has been accounted for by the method outlined in Anand and McFarland [9]. The models of El-Shobokshy and Ismail [6] and Wood [7] are based on the free-flight concept which theorizes that particles attain a radial velocity while entrained in turbulent eddies, then deposit to the tube wall after being ejected from the eddy and coasting across the laminar boundary layer due to inertia. The sublayer model of Fan and Ahmadi [8] involves solving the Lagrangian equations of particle motion in a turbulent flow field, which accounts for turbulent bursts and fluid downsweeps at the tube wall. Fan and Ahmadi's model includes the shear-induced lift force. This phenomenon is theorized to account for the rapid increase in deposition with particle size which has been observed for particles in the range $1 < \tau^+ < 10$. Surface roughness elements shorten the distance for inertial coasting in the free flight models and increase the fraction of particle trajectories that encounter the wall in the sublayer model.

For the simulations, the duct wall is assumed to be a perfect sink for particles, and all roughnesses are assumed to be three-dimensional sand-grain type roughness. Turbulence is assumed to be fully developed. The particles considered are spherical with a density of 1.0 g/cm^3 and a diameter range from 0.1 to 10 μm.

RESULTS AND DISCUSSION

Comparisons of the three models to experimental data on particle deposition from turbulent pipe flow are presented in Figures 1 and 2. Figure 1 shows data collected from flow through small diameter (≈ 1 cm),vertically oriented, smooth and rough tubes at a Reynolds number of 10^4. The data of Liu and Agarwal [3] are considered the best available data for deposition in smooth tubes and the investigation by El-Shobokshy [4] is one of the few to thoroughly investigate and report the effects of surface roughness. The data collected by Shimada and Okuyama [5] are for very small diameter particles (d_p = 0.01-0.04 μm) that are influenced by Brownian motion. All deposition models show a general U-shaped trend. Starting at the left, the initial decrease in deposition velocity is due to the decreasing importance of Brownian

diffusion as particle size, or τ^+, increases. As particle size increases further, deposition is expected to increase as a result of turbulent diffusion and interception. All the models show a decrease in the particle size dependence of deposition velocity as roughness increases, and all models predict roughness has less influence on particle deposition as particle size increases. The models of El-Shobokshy and Ismail [6]and Wood [7] show good agreement with the smooth pipe data over the entire range of τ^+, while that of Fan and Ahmadi [8] underpredicts V_d^+ in the range $0.1 < \tau^+ < 10$. All three models predict a dramatic increase in V_d^+ with surface roughness in the range $5 \times 10^{-3} < \tau^+ < 3$, with the model of Fan and Ahmadi [8] predicting the strongest effect. All model predictions for deposition to rough surfaces lie below the bulk of the equivalent experimental data. The model of El-Shobokshy and Ismail [6] agrees most closely with the experimental data over the range of roughnesses considered.

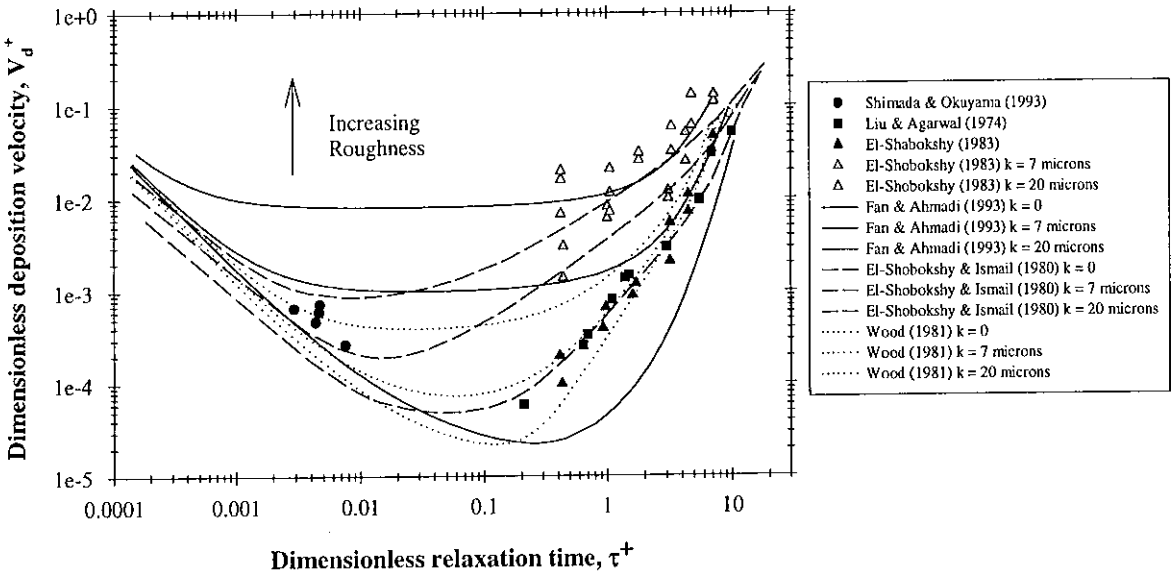

Figure 1. Model comparison to experimental data collected in vertical, small diameter tubes at Re = 10,000 and various wall roughnesses

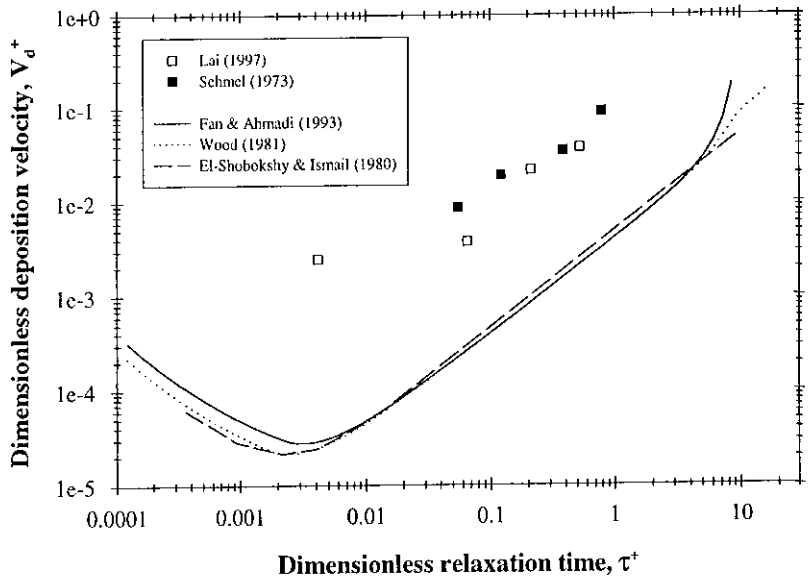

Figure 2. Model comparison to experimental data collected in large, smooth, horizontal ducts at $4.4 \times 10^4 < Re < 10^5$

Figure 2 displays data obtained from smooth, larger diameter (15-60 cm), horizontally oriented ducts at Reynolds numbers ranging from 4.4×10^4 to 10^5 [10, 11], which is more representative of conditions in a real ventilation duct. The models give similar predictions over the range $10^{-4} < \tau^+ < 4$. The agreement between models in the range $0.01 < \tau^+ < 4$ is the result of gravitational settling being the controlling deposition mechanism. The effect of the shear-induced lift force is seen to be important in Fan and Ahmadi's [8] model only for $\tau^+ > 4$. All three models are observed to underpredict the experimental values of V_d^+ by one to two orders of magnitude. In addition to smooth wall deposition data, Lai [11] collected deposition data for different roughness arrangements in a large, horizontal duct. However, because the models are only able to accommodate sand-grain type roughness, a valid comparison between model and experiment is not possible.

The fractional penetration of particles through the modeled duct run as calculated by each model is shown in Figure 3. All three models predict that penetration is essentially independent of particle size for particles less than 2 μm in diameter. A decrease in particle penetration due to the effect of gravitational settling is predicted for particles greater than 2 μm by all three models. The model of Fan and Ahmadi [8] yields the lowest penetration fractions and the model of Wood [7] yields the highest penetration fractions for all particle sizes. All three models predict the majority of particle deposition to occur in sections 3 and 8 of the duct run. These ducts have higher surface roughness than the rest of the system because section 3 is acoustically lined with fiberglass and section 8 is a flexible aluminum duct with repeated ribbed roughness elements. Although these two duct sections comprise only 15% of the total length of the duct run, deposition in these ducts is expected to account for almost 99% of the total deposition in the system for particles smaller than 2 μm. These results indicate that deposition may significantly modify the particle concentrations in air flowing through ventilation ducts. In general, deposition models are observed to agree poorly with one another and with the experimental data, especially when rough surfaces are considered. More experimental data on deposition to large duct walls with quantified roughness are required for more complete model validation.

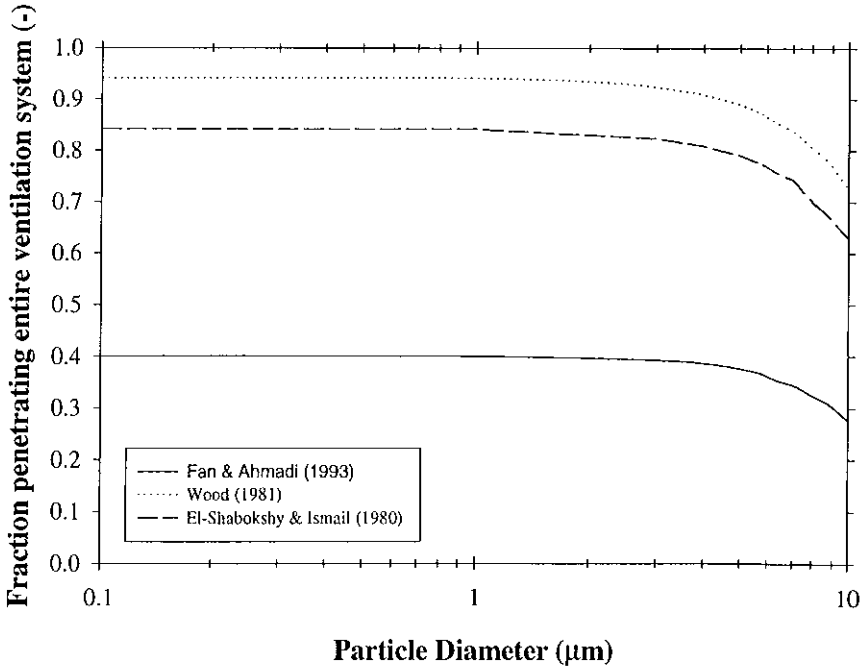

Figure 3. Fraction of particles penetrating the entire ventilation system versus particle diameter.

ACKNOWLEDGMENT

This work was supported by the Office of Research and Development, Office of Nonproliferation and National Security, U.S. Department of Energy under Contract No. DE-AC03-76SF00098

REFERENCES

1. Wallace, L.A. 1996. Indoor Particles: A Review, *Journal of the Air and Waste Management Association.* Vol. 46, pp. 98-126.

2. Hanley, J.T., Ensor, D.S., Smith, D.D., and Sparks, L.E. 1994. Fractional Aerosol Filtration Efficiency of In-Duct Ventilation Air Cleaners. *Indoor Air.* Vol. 4, pp. 169-178.

3. Liu, B.Y.H. and Agarwal, J.K. 1974. Experimental Observation of Aerosol Deposition in Turbulent Flow. *J. Aerosol Sci.* Vol. 5, pp. 145-155.

4. El-Shobokshy, M.S. 1983. Experimental Measurements of Aerosol Deposition to Smooth and Rough Surfaces. *Atm. Env.* Vol. 17(3), pp. 639-644.

5. Shimada, M. and Okuyama, K. 1993. Deposition of Submicron Aerosol Particles in Turbulent and Transitional Flow. *AIChE J.* Vol. 39(1), pp. 17-26.

6. El-Shobokshy, M.S. and Ismail, I.A. 1980. Deposition of Aerosol Particles from Turbulent Flow onto Rough Pipe Wall. *Atm. Env.* Vol. 14, 297-304.

7. Wood, N.B. 1981. A Simple method for Calculation of Turbulent Deposition to Smooth and Rough Surfaces. *J. Aerosol. Sci.* Vol. 12, 275-290.

8. Fan, F.G. and Ahmadi, G. 1993. A Sublayer Model for Turbulent Deposition of Particles in Vertical Ducts with Smooth and Rough Surfaces. *J. Aerosol Sci.* Vol. 24(1), pp. 45-64.

9. Anand, N.K. and McFarland, A.R. 1989. Particle Deposition in Aerosol Sampling Lines Caused by Turbulent Diffusion and Gravitational Settling. *Am. Ind. Hyg. Assoc. J.* Vol. 50(6), pp. 307-312.

10. Sehmel, G.A. 1973. Particle Eddy Diffusivities and Deposition Velocities for Isothermal Flow and Smooth Surfaces. *J. Aerosol Science.* Vol. 4, pp.125-138.

11. Lai, C.K. 1997. An Experimental Study of the Deposition of Aerosol on Rough Surfaces and the Implications for Indoor Air Quality Control. *PhD Thesis.* University of London, Imperial College.

CHARACTERIZING INDOOR AIRFLOW AND POLLUTANT TRANSPORT USING SIMULATION MODELING FOR PROTOTYPICAL BUILDINGS. 1. OFFICE BUILDINGS

M.D. Sohn, J.M Daisey, H.E. Feustel
Indoor Environment Department
Lawrence Berkeley National Laboratory
Berkeley, CA 94720, U.S.A.

ABSTRACT

This paper describes the first efforts at developing a set of prototypical buildings defined to capture the key features affecting airflow and pollutant transport in buildings. These buildings will be used to model airflow and pollutant transport for emergency response scenarios when limited site-specific information is available and immediate decisions must be made, and to better understand key features of buildings controlling occupant exposures to indoor pollutant sources. This paper presents an example of this approach for a prototypical intermediate-sized, open style, commercial building. Interzonal transport due to a short-term source release, e.g., accidental chemical spill, in the bottom and the upper floors is predicted and corresponding HVAC system operation effects and potential responses are considered. Three-hour average exposure estimates are used to compare effects of source location and HVAC operation.

INTRODUCTION AND MOTIVATION

Buildings are constructed and operated in many different ways. Unfortunately, this complexity makes understanding and predicting a building's air flow and pollutant transport patterns a site-by-site evaluation process. However, in the event of a hazardous pollutant release in or near a building, decisions must be made quickly with little or no information on how the pollutant is likely to be distributed within the specific building. For example, a cleaning solvent spill in an office building's printing shop can result in a sudden chemical release that can result in exposures to occupants in other parts of the building. Unfortunately, emergency response personnel must make appropriate decisions despite the limited information about the building and its operating conditions. One approach to providing useful information for these responders and building operators is to model airflow and pollutant transport on a set of prototypical buildings defined to capture key features of the building stock. The prototypical buildings can then be used to evaluate possible pollutant release scenarios and identify possible responses prior to such an event. The simulations can also be used to train the first-responders and building managers to react to similar incidents and to identify information that should be gathered prior to and during an incident. This approach can also be used to more quantitatively understand key building features affecting the transport of indoor pollutants in multizone buildings. The purpose of this paper is to demonstrate this approach and provide examples of effects of source location and HVAC operation and of possible responses. Specifically, the paper describes an intermediate-sized prototypical office building, the results of simulations for two pollutant release locations and

three HVAC system operations, and their implications for emergency response and for pre-planning mitigation measures.

METHODS

In defining prototypical office buildings, we first considered the features of office buildings most important for determining transport and fate of a released toxic agent. These include floor heights, number of floors, floor plan layout (e.g., open plan versus closed individual rooms), HVAC system layout and operation, size and number of shafts (e.g., elevator and utility), and leakage between zones. Many of the parameters defined for prototypical office buildings were selected using the EPA Building Assessment Survey and Evaluation (BASE) study database [1]. The BASE database includes responses to questionnaires and experimental monitoring data to assess current indoor air quality in large commercial office buildings. As of this date, 70 U.S. buildings, from 10 regions across the United States, have been sampled and additional buildings are in the process of being investigated. A summary of the information for the first 40 buildings is provided in Table 1. Additional information about the sampling procedures, questionnaires, and new/updated data are available at http://www.epa.gov/iedweb00/base/base.html.

Table 1 Summary statistics (arithmetic averages) for office buildings in BASE study database.

Classification	No. of Buildings	No. of Floors Above Grade	Gross Floor Area (m^2)	Occupancy (m^2/person)	Ceiling Height (m^2)
High Rise	13	19	49,500	27	2.7
Interm. Rise	23	5	22,000	28	2.7
Low Rise	5	2	8,700	14	2.9

The prototypical building used in the simulation and analysis procedure was an intermediate-sized, open-style, five-floor, commercial building with a total floor area of 22,000 m^2 (see Table 1 and Figure 1). The open style floor plan is characterized by a single central zone that is surrounded by zones along its perimeter. The central well-mixed zone represents office and conference spaces, hallways, and general interior building area which are all believed to exhibit reasonably similar building flow conditions. Connected to this zone are perimeter facade zones that represent office spaces facing the exterior windows. A facade zone encompasses all of the offices on a perimeter wing since they are believed to exhibit similar flow communication with the outside and the interior. A small zone located within the central zone represents the elevators, stairs, and utility shafts and is connected to adjoining floors to represent the stairwell/shaft system.

The COMIS multizone flow and pollutant transport model [2] was applied to the prototypical building to predict and evaluate pollutant transport from possible release scenarios and alternative responses. Flow characteristics for each zone were estimated by summing the number of doors, cracks, and windows likely in each room that is characterized by the well-mixed zone and estimating representative parameters for the flow and transport modeling from data compiled by Lidament [3] to represent a moderately tight building. Since the purpose of this approach is to understand the general trends of the inter-zone and inter-floor flows representative of typical flow patterns in this size and style of building, only general estimates of flow and transport parameters are used and do not represent the actual flow in a specific building. Hence, not all specific parameters for the modeling are presented here.

However as an estimate of the overall building tightness, 7.2 air changes per hour (ACH) are predicted if the building was pressurized to 50 Pa (≈0.36 ACH normalized leakage).

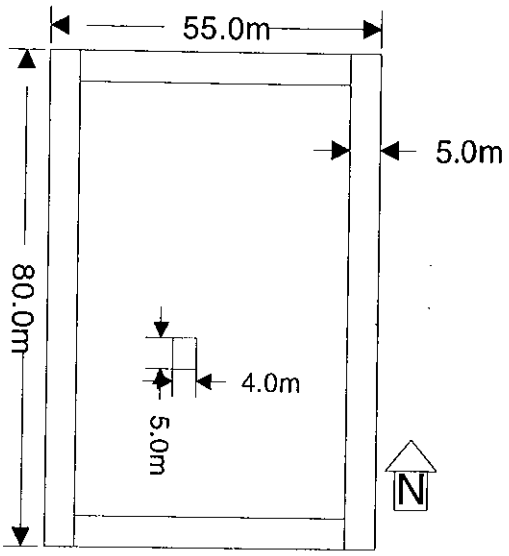

Figure 1: Open-style floor plan for a five-floor prototypical office building. The temperature of each zone is 20°C; the outside temperature is 15°C. Wind blows from the west at 3 m/s. The floor plan is identical for each floor. The HVAC unit is located on the roof of the building with a single air handler supplying each floor and zone.

Two scenarios were considered, release of a pollutant in the central zone of the (1) first and the (2) fifth floor for ten minutes at 1 g/s. The incident could represent a chemical spill, e.g., ammonia from a spill of cleaning solution that volatilizes but is quickly contained or intermittent emissions from a malfunctioning photocopier. The pollutant transport was predicted under three alternative HVAC operating conditions: (1) no HVAC operation, (2) HVAC with 100% air recirculation at 4 building ACH, and (3) HVAC with no air recirculation at 4 ACH (i.e., once-through ventilation). A general HVAC system layout was assumed at this stage of the analysis, i.e., a single air handler located on the roof that serves all of the floors (and zones) with complete mixing of outlet and return air.

RESULTS AND DISCUSSION

Figures 2 and 3 illustrate the pollutant transport in the central zone of the first and fifth floors for a source release in the first floor and the fifth floor, respectively. The zones adjacent to the central zone on a given floor exhibited approximately 30% lower concentrations but with similar time-series profiles.

Table 2 summarizes the three-hour time-averaged exposure (concentration x time) to building occupants in the central zone of the first and fifth floors. The average exposure is used to compare the differences in exposure from the alternative HVAC operating conditions. In both source release scenarios, as expected, the exposure for occupants in both the first and fifth floors is least with the HVAC system operating with no recirculated air. Contaminated air is removed from the building and is replaced by outside air. Hence, under this open-style building configuration, HVAC system operation with no recirculated air reduces the exposure regardless of the location of the source.

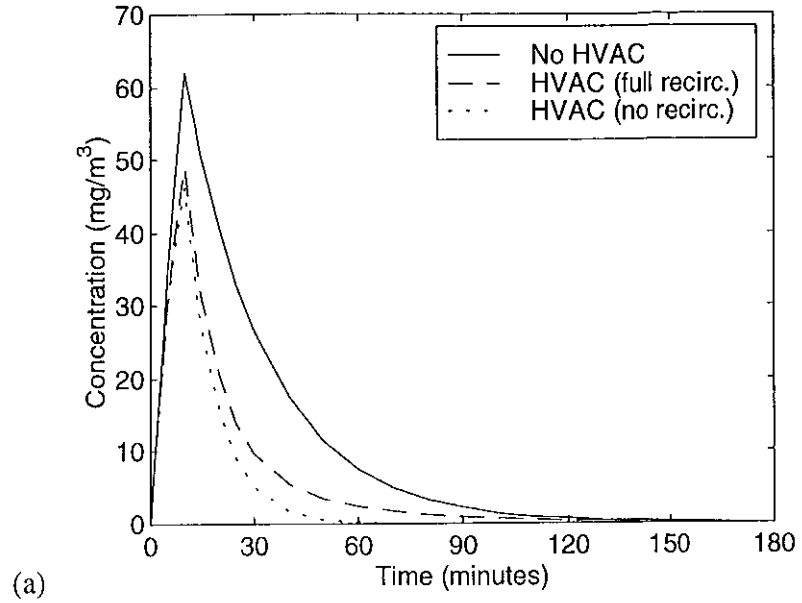

(a)

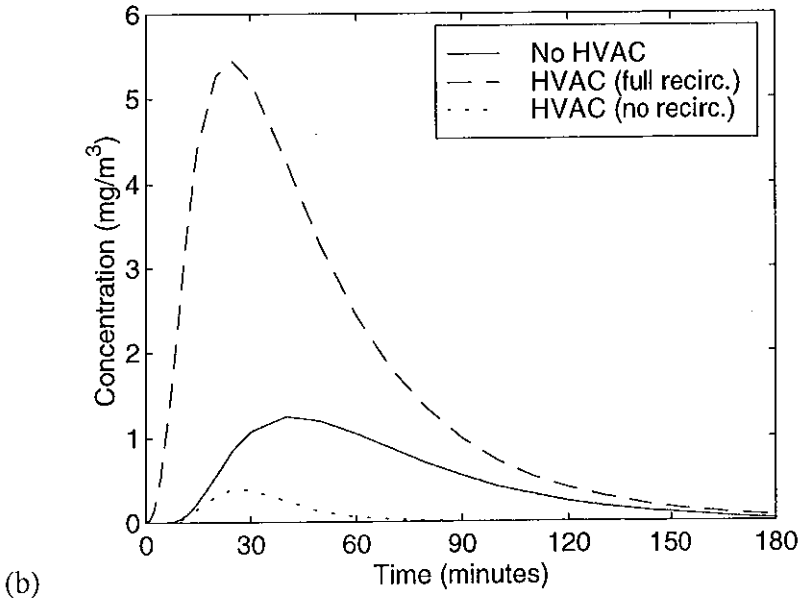

(b)

Figure 2: Predicted concentration profiles in the central zones of the first (a) and fifth (b) floors from a pollutant released in the central zone of the first floor. The pollutant is released for ten minutes at 1 g/s. Note that the scale for concentration differs by a factor of ≈10 between the two figures.

If the HVAC system is recirculating some of the indoor air, and/or a switch-over to all outside air requires a considerable amount of time, then an alternative decision between shutting down the HVAC system or continuing to run with air recirculation must be made. With the HVAC system not operating, the pollutant mass is slowly transported to the other zones and floors such that exposure is high in the source zone and much less elsewhere. However, if the HVAC unit operates with recirculated air, the mass of the pollutant is more quickly dispersed in the building but will dilute the building wide average concentration. Hence lower exposure is observed in the source zone and higher exposure is observed elsewhere than without HVAC operation. These results suggest that the toxicity of the pollutant released may dictate the

appropriate response. For example, if the pollutant is toxic at relatively high concentrations, then possibly diluting the pollutant concentration (e.g., while evacuation was being conducted) may be the most prudent immediate response. However, if the pollutant is toxic at relatively low concentrations, then containment of the pollutant to the source zone by shutting down the HVAC system may better protect the most building occupants (and possibly individuals outside and down-wind of the building). Hence response recommendations may be made according to chemical toxicity in conjunction with building operation.

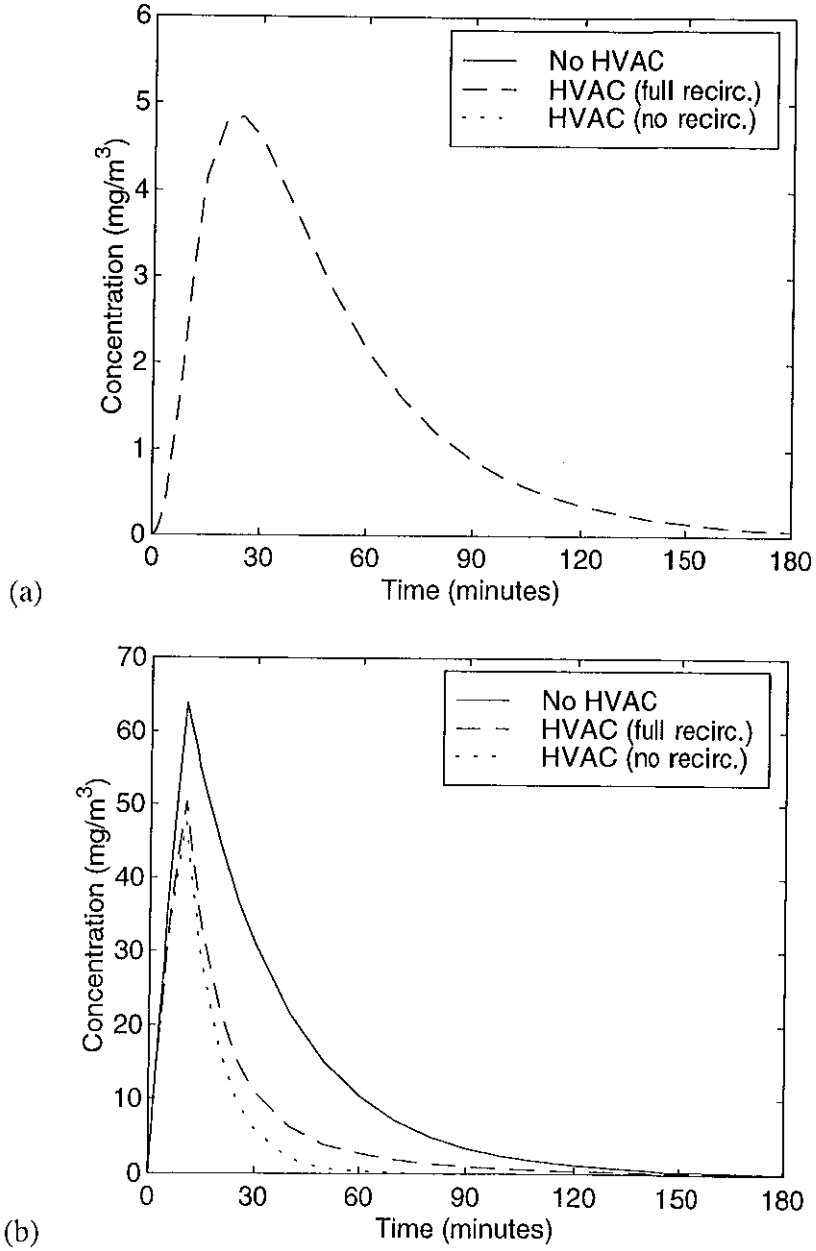

Figure 3: Predicted concentration profiles in the central zones of the first (a) and fifth (b) floors from a pollutant released in the central zone of the fifth floor. The pollutant is released for ten minutes at 1 g/s. The curves for "No HVAC" and "HVAC (no recirculation)" in (a) are effectively at zero concentration so are not apparent on the figure. Note that the scale for concentration differs by a factor of ≈10 between the two figures.

Table 2: Summary of source scenarios, alternative HVAC operating conditions, and corresponding three-hour exposure estimates. The source locations are in the central zone of the indicated floor and HVAC operation is at 4 ACH.

Scenario		Exposure (mg-min/m^3)	
Source Location	Type of HVAC	First Floor	Fifth Floor
First floor	None	1600	80
" "	Full recirculation	890	280
" "	No recirculation	640	10
Fifth floor	None	0	1900
" "	Full recirculation	250	950
" "	No Recirculation	0	670

CONCLUSIONS

The prototypical buildings will be used as a base framework for understanding pollutant transport through buildings and for evaluating possible emergency responses and control options. The example presented here illustrates the approach and indicates the general scope of the work. In subsequent work, efforts will be made to better characterize the link between building operation, environmental conditions, and exposure. In addition, the prototypical building development will also assist in identifying and quantifying other features of a building that are not well known to affect the air flow and pollutant transport by comparing the effects on transport and exposure if various building features are adjusted. Hence a fully characterized prototypical building system will provide a baseline by which other systems or operations can be compared.

Acknowledgements: This work was supported by the Office of Research and Development, Office of Nonproliferation and National Security, U.S. Department of Energy under Contract No. DE-AC03-76SF00098.

REFERENCES

1. EPA 1993. EPA Large Building Studies Integrated Protocol. prepared by L. Sheldon and R. Fortman. RTI/4479/013.

2. Feustel, H.E. and Rayner-Hooson, A. 1990. COMIS fundamentals. Lawrence Berkeley National Laboratory Report LBL-28560.

3. Lidament, M. W. 1986. Air infiltration calculation techniques – An applications guide. AIVC Document: AIC-AG-1-86.

VI. COMPUTATIONAL FLUID DYNAMICS MODELING AND MODEL VALIDATION

MEASURING DISPERSION OF GASES IN A LARGE SCALE INDOOR ENVIRONMENT USING AN OPEN PATH TUNABLE DIODE LASER

T L Thatcher, M L Fischer, P N Price, W J Fisk, A J Gadgil, R G Sextro

Ernest Orlando Lawrence Berkeley National Laboratory, Berkeley, CA USA

ABSTRACT

Occupants of buildings can experience time and location dependent exposures to pollutants released transiently from indoor point sources, such as chemicals used in laboratories and chemical plants. We describe the design of an experiment to measure 30 path integrated gas concentrations in a large indoor space (7m × 9m × 11m) using a tunable diode laser, sampled at a rate of 30 paths every 6 seconds. The open path measurements can then be used to reconstruct a time dependent image of the evolving pollutant plume. To verify the reconstructed concentrations, the experimental design includes the rapid measurement of local samples using a short path (10 to 50 cm) tunable diode laser system with 30 points sampled over a six seconds interval.

INTRODUCTION

Exposures to transient indoor releases are strongly influenced by advection and dispersion of the pollutant in the indoor space. However, accurately measuring changing concentrations in a large indoor space requires a sampling method with a fine spatial and temporal resolution. Achieving this with conventional point sampling techniques involves a large number of sampling locations sampled at a high frequency. Even for a relatively sparse sample grid, this process presents a significant obstacle in terms of required equipment, sample management, and personnel time. A single experiment can easily generate hundreds of samples which need to be stored, managed, and analyzed. Open path infrared measurement followed by computed tomographic reconstruction has been proposed as a methodology for overcoming these obstacles [1]. To date, studies performed using steerable FTIR systems have been limited to steady state or slowly moving plumes due to the relatively long time required for a complete scan (6 or more minutes) [2]. We have designed a tunable diode laser (TDL) system using an optical multiplexer which will allow measurement of the entire array of 30 sample paths within a six second sample period which can then be used for computed tomography reconstructions. Since this type of reconstruction is a relatively new methodology, 30 localized samples will be collected to validate the reconstructed concentrations. The localized samples will be taken using short (10 to 50 cm) open path cells placed at strategic locations within the room. This system will also utilize a TDL source with an optical multiplexer, allowing concentration measurements at all 30 locations within a six second sample period.

METHODS

Experiments will be performed using methane as a tracer gas. Methane is a conservative tracer with a suitable absorption band in the range of conventional TDL systems. Below the

spectrum can be taken and the concentration of many gases can be determined from this spectrum. Otherwise, a narrow-band source such as a tunable diode laser can be used, in which case it must be tuned to the absorption line of a particular chemical of interest.
3. Given the path-integrated concentration along each path, one must solve the inverse problem: what spatial distribution of pollutants gave rise to the observed path integrals?

Optical tomographic methods will allow rapid measurements of pollutant concentrations without requiring that intrusive apparatus be placed throughout the interior of the room being studied, and without interfering with the natural airflow of the space. However, we still face substantial computational challenges in solving the inverse problem. In this paper we will discuss the experimental setup and the resulting computational challenges, and will describe our work to date in addressing these challenges.

In our planned experiments, we will use 30 telescopes and 30 infrared detectors. The output of a single tunable diode laser will be directed via a multiplexer and fiber-optic cables to each of the 30 telescopes in turn, so that path-integrated concentrations will be determined for 30 optical paths. The laser will be tuned to the absorption line of methane, which will be used as the tracer gas. This multiple source-detector system allows great flexibility in setting up the geometry, in contrast to previously investigated systems involving a single infrared source [3-6].

The system will take about 0.2 seconds to make a measurement along a ray; thus it will take about 6 seconds to measure all of the rays (see [7] for more information on the experimental apparatus). Since some of the anticipated experimental conditions will involve variation in concentrations over a 6 second period, we will almost certainly need to explicitly include the time variation in our tomographic models. However, in the present paper, we discuss only our investigations into algorithms and computational techniques to generate planar reconstructions from essentially stationary pollutant distributions. Methods of handling the time-dependent problem are still being developed, as are methods of performing 3-D reconstructions.

METHODS

In medical applications such as CAT scans, computed tomography is performed using methods based on pixels (or, in three-dimensional problems, volume elements commonly called 'voxels'). Unfortunately, pixel-based methods have so far not been found to be successful in gas concentration mapping. The problem is that the gas concentration mapping involves a very different realm of parameter space: medical imaging usually involves measuring path-integral data along thousands or tens of thousands of rays, whereas experimental constraints restrict gas mapping to a few dozen rays. If path integrals are measured along, say, 30 rays, then even a map based on a 6x6 grid of pixels will be very underdetermined: there may be a large or infinite number of pixel reconstructions that duplicate the path integrals perfectly. Standard pixel methods [1,2] such as those used in the medical field yield poor reconstructions with such data [3,4].

An alternative approach that has shown great promise in tomographic reconstruction of air pollutant profiles is Smooth Basis Function Minimization (SBFM) [4-6]. The idea of SBFM is to assume that the concentration distribution can be written as a superposition of a small number of smooth basis functions:

$$C(x,y) = \sum_i G(x,y;\gamma_i), \quad (1)$$

where i numbers the basis functions G, and γ represents the parameters for the basis function. For example, we might assume that the concentration in a plane can be written as a sum of i=2 Gaussian distributions, each described by a location (x,y), an amplitude A, a width in the u and v directions, and an angle between the u axis and the x axis. The tomographic inverse problem then becomes: find the sets of parameters for which the observed path integrals best match the path integrals under the predicted distribution $C(x,y)$. The usual approach is to search for the parameters for which the sum of squared residuals in the path integrals is minimized, though other measures of goodness of fit can also be used.

In analysis of both actual and simulated experimental data, SBFM has been found to produce good reconstructions for gas concentration distributions [5,6]. However, in contrast to standard pixel-based methods, there is no known prescription for finding the best-fit parameters. Starting with an initial guess at the parameters and using a technique such as the "steepest descents" method usually leads to a local, rather than global, minimum error. In the past, a computational technique known as simulated annealing has been used to attempt to find the global best fit, but this method (a type of monte carlo search of parameter space) requires a great deal of computer time. Thus it is not practical for real-time pollutant mapping, and indeed, for the type of time-dependent problem we ultimately wish to address, it is not clear that it is workable at all.

We have recently been investigating a hybrid approach: we first use standard pixel-based methods to generate a reconstruction, and use this reconstruction to obtain one or more "first guesses" at the Gaussian parameters. We then use this first guess as a start for a simulated annealing search, but the simulated annealing parameters (notably the "temperature") are set so that the search is restricted to an area of parameter space fairly close to the initial guess, greatly reducing the computational demands. After a short simulated annealing run, the steepest descent method is used to converge to the final answer.

As an example, we used a computational fluid dynamics (CFD) code to generate the pollutant distribution as a function of time for a particular release scenario. We considered the release of one cubic meter of diluted methane into a room (approximately 7.5 m on a side, with a high ceiling), with the release occurring directly in front of an air supply vent that is expelling air at about 2 m/s. The room dimensions are those of an experimental chamber that will be used for the experimental component of this work. For purposes of trying different computational algorithms and ray geometries, we will treat the CFD-generated distributions as the "true" pollutant distributions as a function of time.

In contrast to the actual experimental situation, we assumed that all of the path integrals were measured simultaneously, at t=6 s after the initial release. The calculated concentration in the release plane at that time is shown in the upper left plot of Figure 2. (The pollutant release occurred at t=0 near x=7.5, y=7.5; the plume has been blown almost all the way to the wall at x=0).

From these simulated concentrations, we calculated the ray integrals (the path-integrated concentrations) for the arrangement of 30 optical paths shown in Figure 1.

RESULTS

The lower plots in Figure 2 show pixel reconstructions based on the path integrals, using two standard reconstruction algorithms. Even with only 64 pixels, the problem is substantially underdetermined, as there are only 30 ray integrals. Both of the reconstructed maps differ substantially from the "actual" distribution. However, they do both place the bulk of the pollutant within the right part of the room, and they both generate about the right peak height at a location near the actual maximum.

From the first of the two pixel reconstructions, we obtained (by eye) rough guess starting parameters for a smooth basis function fit: two Gaussians distributions, located at (3,2) and (2,3), with width in both directions of 0.75. We then performed a simulated annealing fit to try to converge to a better solution, using a low initial "temperature" so as to prevent the parameters from wandering too far from the initial guesses. After several hundred simulated annealing iterations, we switched to a steepest descents fit to converge to a final fit (upper right plot in Figure 2). The final fit is excellent, though the estimated has a slightly lower peak height than the "true" distribution, and has a somewhat less pronounced asymmetry.

The total computer time taken to perform the reconstruction was a few minutes on a 300 MHz PC, running the Mathematica programming language. This is more than a factor of 10 improvement over our previous approach of performing the entire fit using simulated. The ability to obtain a useful initial guess of the distribution parameters using a pixel reconstruction allows us to skip most of the initial, "high-temperature" simulated annealing steps, and use of a steepest descent algorithm to do the final convergence similarly saves a great deal of computer time. Interestingly, even very small changes in the starting point for the steepest descent algorithm lead to different solutions: the goodness-of-fit function has many local minima. In practice, though, all such cases that we have found are very close to each other in parameter space (and apparently close to the global minimum), and generate nearly identical final concentration reconstructions, so as a practical matter these local minima do not cause a problem.

DISCUSSION

Even without further algorithmic improvements, our current system should allow excellent reconstruction of plumes that do not change very much during the 6 seconds or so that it takes to sample all of the rays. However, we are still searching for algorithmic improvements. We are also trying to evaluate which arrangements of optical paths lead to the best reconstructions.

A bigger challenge is to map rapidly moving plumes that both move and change shape substantially in a few seconds. That is a much more difficult problem, but it is one that we do think we can solve, again with smooth basis function minimization. As a simple example, consider again the plume shown in the upper left plot of Figure 2. This plume is moving fairly rapidly: just six seconds earlier, the pollutant was released at a point near (7.5,7.5). Since the time of release, the plume has moved and spread, and the peak concentration in the plane shown has decreased substantially as the pollutant has spread vertically. All of this can be modeled using time-dependent smooth basis functions:

$$C(x,y,t) = \sum_i G(x,y;\gamma_i(t)), \qquad (2)$$

For instance, we might model the concentration in the experiment with one or more Gaussian distributions that are moving, spreading, and changing in height, with all of these parameters varying linearly in time. This will add several more parameters to the minimization problem, and thus dramatically increase the computational challenge, but will not require a fundamentally different approach: the concept of a plume is built into SBFM. This contrasts with pixel-based methods, where it would be very difficult to specify constraints so that the reconstructions vary smoothly in time, let alone actually find a good fit subject to those constraints.

As we write this paper in early 1999, we are still awaiting delivery of our specially designed experimental apparatus, and we have barely scratched the surface as far as algorithmic development. Please contact us at Indoor Air '99 for an update on our research during the year.

REFERENCES

1. *Image Reconstruction from Projections,* 1979. G T Herman, ed. New York: Springer-Verlag.

2. Herman, GT, Lent, A, Rowland, SW, 1973. Art: Mathematics and applications. A report on the mathematical foundations and on the applicability to real data of the Algebraic Reconstruction Technique. *Journal of Theoretical Biology.* Vol. 42, pp 1-33.

3. Park, DY, Yost, MG, Levine, SP, 1997. Evaluation of virtual source beam configurations for rapid tomographic reconstruction of gas and vapor concentrations in workplaces. *Journal of the Air and Waste Management Association.* Vol 47, pp 582-591.

4. Drescher, AC, Gadgil, AJ, Price, PN, and Nazaroff, WW. 1996. Novel approaches for tomographic reconstruction of gas concentration and distributions in air: use of smooth basis functions and simulated annealing. *Atmospheric Environment.* Vol. 30, pp 929-940.

5. Drescher, AC, Park, DY, Yost, MG, et al. 1997. Stationary and time dependent tracer-gas concentrations measured by OP-FTIR remote sensing and SBFM computed tomography. *Atmospheric Environment.* Vol 31, pp 727-740.

6. Price, PN. 1998. Pollutant tomography using integrated concentration data from non-intersecting optical paths. *Atmospheric Environment.* In press.

7. Thatcher, TL, Fischer, ML, Price, PN, et al. 1999. Measuring dispersion of gases in a large scale indoor environment using an open path tunable diode laser. Indoor Air '99.

Code C was developed as a general-purpose code. It is currently the most used CFD code worldwide. Its mesh generator automatically creates a tetrahedral mesh and allows for semi-automated hexahedral meshing. Hybrid grids are also possible. Code C has the same full range of turbulence models available in Code B and also has LES capabilities. We were shown an example of a large auditorium modeled with Code C. The vendor has four technicians on staff to help users with HVAC applications. The code can model aerosol particles including inertial slip and gravitational settling. There is a range of options for wall boundary conditions such as reflection and escape. Deposition can also be modeled including the effects of surface reaction, and wall concentration. This is a significant strength of the code.

Code D is a general-purpose code used extensively in the automotive industry. The code has been optimized and widely used to simulate large and complex problems, and is the only code among the four that runs in a vectorized massively parallel mode. Code D has a semi-automated hexahedral mesh generator. There are quality checks for the mesh and an error estimator to help determine where local grid refinement is necessary. Code D does not contain an Algebraic or Reynolds stress turbulence model but does have a variety of two equation models as well as LES. There is a second order spatial discretization scheme offered in Code D that controls numerical diffusion. A major architectural firm has been using Code D for many years to satisfactorily model airflow in large spaces. The aerosol model includes gravitational settling. Code D has a easy-to-use framework for implementing the user defined subroutines.

Example Auditorium

Each of the venders was given the specifications of the auditorium to model. The room was modeled assuming symmetrical airflow about the vertical center plane of the room. There are two seating areas in the model, one on the ground and one in a small rear balcony. Heat sources representing people are arranged in rows. Exhaust vents are located on the floor near the heat sources. Mechanical ventilation provides 13°C supply air at the rate of 8 ACH. We specified the mesh resolution at approximately 500,000 elements. The vendors modeled only the airflow using a standard k-epsilon model. Although we tried to fully specify the problem, each vendor did something a little different making direct comparison of the results impossible. Two vendors directly solved the steady-state equations, one vendor used false transients to obtain a steady-state solution, while one vendor solved the time dependent equations with time-marching to try to reach the steady state solution. We examined the simulation predictions for "reasonableness," based on our engineering judgement.

RESULTS

Vendor A produced the first results. They modeled the entire room, rather than impose a symmetry boundary condition as suggested. They provided us with an animation of the results and an informative report including suggestions on how to better represent the inlet conditions. Their results seemed reasonable. Code A certainly meets the criterion of having a track record modeling airflows in buildings. However, it did not meet any of the other decision criteria and so we eliminated Code A.

The remaining three codes appeared to be comparably strong candidates. Each met most of the criteria. Ultimately our experience working with each of the vendors was as important to the decision process as the technical capabilities of the codes.

Vendor B provided a quick turn around and sent us converged steady state results. An examination of the results suggested a problem in the boundary conditions. Nothing was exiting through the ground floor exhaust grills, modeled as pressure boundary conditions. Simulations by all other vendors showed exhaust through these grills, as expected. There were also counter-intuitive distortions in the streamlines in the core region. At our request the vendor reviewed the results. They reported back that they had every confidence in their results. Our faith in Code B was inversely proportional to the vendor's confidence.

Vendor C made a faulty first attempt based on a misunderstanding of the boundary conditions. They subsequently presented us with a converged steady state solution. The vendor also ran the problem on a coarser mesh to demonstrate the grid independence of the solution. Vendor C solved the problem in two stages. In the first stage (300 iterations), they obtained a converged solution to the isothermal problem assuming only mechanical ventilation. The sum of the velocity residuals was then 10^{-3}. In the second stage (150 iterations), they turned on the heat sources until the sum of the velocity residuals reached a level of 10^{-2}. The flow solution seemed to make physical sense although we remained skeptical of claimed full convergence at the high level of the velocity residuals.

Vendor D reported trouble getting the problem to converge to a steady state solution. The vendor finally asserted that the flow in the room was steadily oscillating and that no time invariant solution existed. They sent us an animation showing an oscillation between two vortex structures, one in the balcony and one on the ground floor. The animation showed the heat building up on the floor and periodically injecting hot air into the room. These results also seemed reasonable. Vendor D performed a numerical experiment, halving the time step, to show that the period of the oscillation was independent of the time step. This led us to believe that the oscillation reflected the nature of the flow rather than a numerical artifact.

DISCUSSION

It was a close choice, but we finally chose Code D. The decision was based on apparent reasonableness of predicted air flow for the example auditorium, optimization of the code for massively parallel vectorized computing, willingness and ability of the vendor to work closely with our research staff, and features of the code allowing ease of user defined subroutines. We plan to use this last feature of Code D to implement our own detailed pollutant transport models, and overcome any deficits in the prepackaged pollutant models.

The true test of the commercial CFD code will come when predictions are compared to our experimental results [7]. Preliminary CFD predictions, modeling a methane pulse release in our experimental facility, are presented in our paper on computed tomography reconstructions [8].

ACKNOWLEDGMENTS

This work was funded through the U.S. Department of Energy, Contract No. DE-AC03-76SF00098.

REFERENCES

1. Chen, Q. 1997. Computational Fluid Dynamics for HVAC: Successes and Failures. *ASHRAE Transactions.* Vol. 103 (1), pp 178-187.

2. Baker, A J, Kelso, R M, Gordon, E B, et al. 1997. Computational Fluid Dynamics: A Two-Edged Sword. *ASHRAE Journal.* Vol. 39 (8), pp 51-58.

3. Nazaroff, W W, Gadgil, A J, and Weschler, C J. 1993. Critique of the Use of Deposition Velocity in Modeling Indoor Air Quality. In *Modeling Indoor Air Quality and Exposure* (ed. Nagda, N L). STP 1205, ASTM. pp 81-104.

4. Nicas, M. 1996. Estimating Exposure Intensity in an Imperfectly Mixed Room. *American Industrial Hygiene Association Journal.* Vol. 57, pp 542-550.

5. Behar, J V. 1996. Modeling Indoor Air Concentrations Near Emission Sources in Imperfectly Mixed Rooms. *Journal of the Air and Waste Management Association.* Vol. 46, pp 861-868.

6. Emmerich, S J. 1997. Use of Computational Fluid Dynamics to Analyze Indoor Air Quality Issues, NISTIR 5997. National Inst. of Standards and Technology. Gaithersburg, MD, USA. flame.cfr.nist.gov/bfrlpubs/build97/art016.html.

7. Thatcher, T L, Fischer M L, Price P N, et al. 1999. Measuring Dispersion of Gases in a Large Scale Indoor Environment Using an Open Path Tunable Diode Laser. To be published in the *Proceeding of the 8th International Conference on Indoor Air Quality and Climate*. Edinburgh August 1999.

8. Price, P N, Fischer, M L, Finlayson E U, et al. 1999. Recent Advances in Mapping Gas Concentrations with Optical Remote Sensing. To be published in the *Proceeding of the 8th International Conference on Indoor Air Quality and Climate.* Edinburgh, UK. August 1999.

9. Murakami, S, Kato, S, Ooka, R. 1994. Comparison of Numerical Predictions of Horizontal Nonisothermal Jet in a Room with Three Turbulence Models – k-ε EVM, ASM and DSM. *ASHRAE Transactions.* Vol. 100 (2), pp 697-704.

10. Chen, Q, Chao, N-T. 1996. Prediction of Buoyant Plume and Displacement Ventilation with Different Turbulence Models. *Proceedings of the 7th International Conference on Indoor Air Quality and Climate – Indoor Air '96,* Vol. 1, pp 787-792.

11. Nielsen, P V. 1998. The Selection of Turbulence Models for Prediction of Room Airflow. *ASHRAE Transactions.* Vol. 104 (1B), pp 1119-1127.

12. Grummon, A D. 1997. Resource Guide FEA/CFD Software. *Desktop Engineering.* Vol. 4 (1), pp 46-50.

13. Freitas, C J. 1995. Perspective: Selected Benchmarks from Commercial CFD Codes. *J. of Fluid Engineering, Transactions of the ASME.* Vol. 117, pp 208-218.